# Sedimentological and diagenetic controls on the reservoir quality of marginal marine sandstones buried to moderate depths and temperatures: Brent Province, UK North Sea

Auwalu Y. Lawan[a,b], Richard H. Worden[a*], James E.P Utley[a], Stephen F. Crowley[a]

[a]Department of Earth, Ocean and Ecological Sciences, University of Liverpool, Liverpool, L69 3GP, UK

[b]Department of Geology, Bayero University, Kano State, Nigeria.

* Corresponding author: r.worden@liv.ac.uk

In press with Marine and Petroleum Geology

Accepted 22nd March 2021, available online 8th March 2021

**Abstract**

A study of the Brent Group sandstones, in well 211/13-A33 in the Thistle Field, northern North Sea, UK, from a sequence of shoreface, foreshore, delta plain and finally barrier shoreline depositional environments, was undertaken with the aim of contrasting the roles of depositional and diagenetic processes on reservoir quality. These subarkosic and sublitharenite sandstones were buried to ~9,000 ft TVDSS and have experienced a maximum burial temperature of about 95°C. This study utilised wireline and core analysis data, with core samples studied using petrography, XRD, SEM-CL, and SEM-EDS. The dominant diagenetic cements are kaolinite and siderite, with minor quantities of pyrite, chlorite, illite, K-feldspar, calcite and quartz cement. A common sequence of diagenetic events occurred in sandstones from all four depositional environments. The dominant reservoir quality controlling factors are depth-controlled mechanical compaction and variable kaolinite growth, with grain size being an important secondary control. The shoreface sandstones have the highest degree of compactional porosity-loss because they have the greatest quantity of detrital ductile grains. Quartz cement is a minor phase in all formations because these sandstones have only just exceeded the temperature threshold for quartz cement growth. Siderite is found in all formations but with the greatest quantity found in the shoreface and delta plain sandstones, since these environments were most enriched in detrital iron minerals such as biotite and chlorite. The shoreface sandstones host stratigraphically-localised, pore-occluding calcite cement that has compartmentalised the reservoir. Overall, the foreshore and delta plain sandstones have the best reservoir quality because they have (i) few ductile grains resulting in low degrees of compaction, (ii) low quantities of pore-filling cement

and (iii) they tend to be medium-grained. In contrast, the shoreface sandstones and barrier shoreline sandstones have poorer reservoir quality as they have (i) moderate to large quantities of ductile grains, (ii) moderate quantities of pore-filling cement and (iii) they tend to be fine- or very fine-grained. Detrital sand mineralogy and grain size vary as a function of depositional environment and these have subsequently played a major role in linking diagenesis and reservoir quality to depositional environment.

Key words: Sandstone reservoir quality, Sandstone diagenesis, Mechanical compaction, Kaolinite cement, Siderite cement, Detrital mineralogy, Calcite-cemented layers, Secondary porosity.

## 1. Introduction

There has been much recent focus on the understanding of reservoir quality (porosity and permeability) in sandstones buried to depths and temperatures at which quartz cement dominates, i.e., significantly greater than approximately 100°C (Ajdukiewicz and Lander, 2010; Worden et al., 2018a). This has taken the form of studies of the prediction of quartz growth (Lander and Walderhaug, 1999; Walderhaug et al., 2000) and the efficacy of various processes that inhibit quartz growth such as chlorite (Ehrenberg, 1993b; Worden et al., 2020), microcrystalline quartz grain coatings (Aase et al., 1996a) or early oil emplacement (Worden et al., 2018a; Worden et al., 2018b). There has been somewhat less attention given to sandstones at intermediate depths and temperatures (by which we mean approximately 50 to < 100°C) although the new imperative of carbon capture and storage (CCS) has presented an additional driver to better understand the properties of less deeply buried sandstones, since they are likely to be the initial targets for CCS in mature petroleum provinces (Alcalde et al., 2019).

Both primary facies and secondary diagenetic processes can significantly affect sandstone reservoir quality (Girard et al., 2002) and thus both can have important impacts on the economic viability of a petroleum reservoir and how it would function as a CCS host. Understanding whether depositional processes or diagenetic processes dominate reservoir quality impacts the prediction of porosity and permeability, leads to increased accuracy in volumetric reserve estimation (e.g., stock tank oil initially in place: STOIIP), or CCS capacity, and enables forecasting of well production or fluid injection rates. The accurate understanding and prediction of reservoir quality is therefore key to obtain predictable well flow-rates and injection-rates throughout the lifetime of a petroleum field, or CCS site (Alcalde et al., 2019; Sneider, 1990). To understand and predict porosity and permeability, it is important to understand the sediment's composition and texture, and what, why, how and when diagenetic changes took place within a reservoir (Ehrenberg, 1990; Girard et al., 2002; Worden et al., 2018a). The

aim of this paper is to determine whether and how the specific environments of deposition, in marginal marine to delta-top settings, control reservoir quality in relatively high porosity and high permeability rocks buried to intermediate depths and temperatures.

The fundamental controls on sandstone reservoir quality can be broadly grouped into four categories: (i) clastic sediment supply (the sediment factory), (ii) eogenetic (near-surface, relatively low temperature), (iii) mesogenetic (typically assumed to be > 70°C) and (iv) telogenetic (uplift or unconformity-related) (Worden et al., 2018a). The clastic factory is influenced by a combination of the outcrop geology in the sediment's source terrain, climate, relief, the sediment's transport path length, and the local generation of autochtonous carbonate (e.g., marine carbonate production or calcrete).

Eodiagenesis, also known as early and shallow diagenesis, includes all processes that occur at, or near to, the surface of the Earth, or where the chemistry of the interstitial waters is controlled mainly by the overlying depositional environment (Berner, 1980; Chapelle, 2001; Worden et al., 2018a; Worden and Burley, 2003). Specifically, this is the regime where the influence of the original depositional pore water dominates, and so includes post-depositional weathering and soil development in continental depositional settings, and bacterially-mediated redox reactions in marine environments (Worden and Burley, 2003). The term sandstone eodiagenesis has been used to imply different conditions with some confining eodiagenesis to sediment within a few metres of the Earth's surface (Worden and Burley, 2003). However, eodiagenesis can include "open system" (possibly involving material flux) systems that extend down to about 2,000 m and about 60-70°C, before compactional porosity-loss becomes dominant and leads to lower permeability in both sandstones and neighbouring lithologies (Morad et al., 2000; Worden et al., 2018a; Worden and Burley, 2003). Eodiagenesis involves a range of processes including redox reactions, microbial-sediment and animal-sediment (bioturbation) interactions, the growth of new low-temperature minerals, and much of the initial stages of mechanical compaction (Worden et al., 2018a).

Mesodiagenesis, also known as burial diagenesis, includes all the diagenetic processes that occur once the sediment has passed from the influence of the depositional environment through to the earliest stages of low-grade metamorphism (Worden and Burley, 2003). Mesogenetic processes include compaction, grain replacement, grain dissolution, matrix and eogenetic clay replacement, carbonate cement alteration and growth, the later stages of mechanical compaction, chemical compaction, and quartz cementation. Mesogenetic processes tend to be 'closed system' (i.e., largely closed to material flux, with the exception of highly soluble species such a Na, K and $CO_2$), and occur > 2,000 m and in excess of 70°C (Worden et al., 2018a). The Middle Jurassic sandstones in the Thistle Field did not

undergo early uplift (Nadir and Hay, 1978; Williams and Milne, 1991) and so there is no need to consider telodiagenesis in this context (Worden et al., 2018a).

The objectives of this study were to address the roles of depositional processes and diagenesis on reservoir quality in marginal-marine sandstones buried to between 8,742 ft and 9213 ft true vertical depth and with a maximum temperature of about 90°C. The example studied is from Mid Jurassic Brent Group sediments from the Thistle Field in the Northern North Sea Basin. To achieve this, we used a multidisciplinary approach integrating wireline data, sedimentary core logging, burial history re-construction, porosity-permeability data, and a range of petrographic techniques, quantitative mineralogy via scanning electron microscopy techniques, and X-ray diffraction (XRD). To understand whether depositional sub-environment influences reservoir quality, it is essential to link sedimentary data to petrographic data to define the precise sub-environment for each petrographic or core analysis data-point; this has led to the need for facies analysis of each sample ahead of quantitative reservoir quality analysis. The specific research questions here addressed include:

1. For these marginal marine to delta-top sediments, do sandstones that were deposited in different sub-environments have different reservoir quality?

2. What was the sequence of post-depositional diagenetic processes that have affected these sandstones?

3. How have diagenetic processes influenced reservoir quality?

4. What are the origins of the diagenetic cements that affect reservoir quality?

5. Is there any difference in the diagenetic evolution of sediments deposited in different marginal marine to delta-top sub-environments?

**2. Geological Background**

The Thistle Field is located in the East Shetland Basin (Ratley and Hayward, 1993) (Fig. 1) and covers an area of about 16 $km^2$ (Williams and Milne, 1991). The Thistle Field has a Middle Jurassic succession of clastic reservoirs known as the Brent Group, that was deposited in a regressive and then transgressive marine deltaic sequence (Bayat and Tehrani, 1985; Nadir, 1981; Nadir and Hay, 1978; Reynolds, 1995; Williams and Milne, 1991). Relative sea-level changes controlled the distribution and evolution of the Brent Group and post-depositional structural movements in the Viking Graben created the trapping geometries in the Brent Province (Yielding et al., 1992). The Brent Group has been divided into five formations that can be correlated regionally, in stratigraphic order these are

the Broom, Rannoch, Etive, Ness and Tarbert Formations (Fig.2) (Budding and Inglin, 1981; Deegan and Scull, 1977; Ratley and Hayward, 1993).

Petroleum geochemical analysis revealed that the Kimmeridge Clay Formation, with its high sapropelic kerogen content, is the source rock for the Thistle petroleum and, by analogy to other reservoirs in the Brent province, migration probably took place from the early Cenozoic, with filling in the middle to later Cenozoic (Scotchman et al., 1989). The initial estimate of oil in place in Thistle was 794 MMBBL with an ultimate recovery of 396 MMBBL. Oil production started in 1978 with initial daily output averaging 50,000 BOPD. Production has continued to decline over the years, and current production is approximately 15,000 BOPD (EnQuest, 2018).

The Broom Formation represents a regressive-transgressive delta fan complex (Reynolds, 1995; Richards, 1992). The succeeding Rannoch, Etive and Ness Formations represent a linked delta-front and delta top depositional system (Fig. 2) (Cannon et al., 1992). The Rannoch, Etive and Ness Formations are pre-rift deposits, representing components of a northwards-building delta, that formed during transient doming of the North Sea (Underhill, 2003). The Rannoch Formation consists of an upward-coarsening delta-front to lower shoreface succession typically evolving from mudstone to very fine- or fine-grained sandstone (Cannon et al., 1992; Reynolds, 1995; Richards and Brown, 1986). Rannoch Formation sandstones are typically parallel laminated and hummocky cross-stratified with abundant mica concentrated along laminae (Cannon et al., 1992; Reynolds, 1995; Richards and Brown, 1986). The Etive Formation is a fine- to medium-grained sandstone deposited in an upper shoreface to tidal-channel setting, that is mostly poorly-laminated to massive (Cannon et al., 1992; Reynolds, 1995; Richards and Brown, 1986). The Ness Formation consists of a heterolithic, delta-top, fluvial sequence of interbedded sandstones, mudstone and coals (Cannon et al., 1992; Reynolds, 1995). The overlying Tarbert Formation represents the uppermost part of the Brent Group and comprises a transgressive barrier shoreline sandstone that records the onset of syn-rift deposition and the subsequent drowning of the Brent delta (Fig. 2) (Cannon et al., 1992; Reynolds, 1995). The Tarbert Formation consists of grey to brown, relatively massive, fine to medium-grained sandstone with subordinate thin siltstone, mudstone and localised coal intraclasts inherited from the earlier Ness Formation sediments (Cannon et al., 1992).

Extensive exploration, appraisal and development drilling in the Brent Province, over the last four decades, has led to the development of a rich, extensive and sometimes controversial literature on the diagenesis of the Brent Group reservoirs, to be addressed in the Discussion (Aase et al., 1996b; Ashcroft and Ridgway, 1996; Bjørlykke et al., 1992; Blackbourn, 1984; Cassagnabère et al., 1999; Chuhan et al., 2000; Ehrenberg, 1993a; Ehrenberg and Jakobsen, 2001; Giles et al., 1992; Girard et al.,

2002; Harris, 1992; Huggett et al., 1997; Jahren and Ramm, 2000; Lundegard, 1994; Macaulay et al., 1998; Marcussen et al., 2010a; Marcussen et al., 2010b; McAulay et al., 1994; McAulay et al., 1993; Morad et al., 1990; Morton, 1992; Nedkvitne and Bjørlykke, 1992; Prosser et al., 1993; Ramm, 2000; Ramm and Bjørlykke, 1994; Sanjuan et al., 2003; Scotchman, 1990; Walderhaug et al., 2000; Went et al., 2013; Wilkinson et al., 2000; Worden et al., 2019; Ziegler et al., 2001).

## 3. Methods and materials

### 3.1 Wireline and conventional core analysis data

Wireline data and conventional core analysis data for well 211/18a-A33 were provided by EnQuest PLC. The well reported here was drilled in late 1979 and early 1980, as an oil producing well. The Rannoch, Etive, Ness and Tarbert Formation sandstones are present as thick successions, but the basal and mudstone-dominated Broom Formation is no more than a few feet in thickness, and is not part of this study of sandstone reservoir quality and diagenesis. The well was deviated. The top of the uppermost sandy unit (Tarbert Formation) has a measured depth of 10,222 ft and a true vertical depth of 8,472 ft. The base of the lowermost sandy unit (Rannoch Formation) has a measured depth of 10,767 ft and a true vertical depth of 9,177 ft. Samples will be identified by reference to their measured depths (ft-md). Continuous core was collected, with minor breaks, from 10,257 to 10,822 ft-md, including the whole of the regressive and transgressive cycle represented by the Rannoch through to Tarbert Formations.

Core plugs were originally (in 1980) taken every 12 inches (approximately 30 cm). Helium porosity and horizontal and vertical permeability were measured, immediately after the well was drilled, by Redwood Corex using industry-standard methods.

Downhole wireline log data reported include calliper, bulk density, sonic (interval transit time), gamma ray, deep resistivity, and neutron porosity. The sonic log tool failed for the upper part of the cored sequence; compressional sonic data are only available at depths > 10,455 (ft-md).

The proportion of shale was derived using normalised gamma log data and the Vshale calculation:

$$Vshale = \frac{\mathrm{GR}_{log} - \mathrm{GR}_{min}}{GR_{max} - \mathrm{GR}_{min}}$$

(Equation 1)

Where $GR_{max}$ is the maximum gamma value for the reservoir, $GR_{log}$ is the measured gamma value for the depth of interest and $GR_{min}$ is the minimum gamma value for the reservoir. Vshale reveals the total quantity of radioactive minerals; this is often treated as being the same as the total quantity of clay minerals since these are typically dominated by radioactive potassium-bearing illite (Rider and Kennedy, 2011). Strictly speaking, Vshale does not represent the total quantity "shale" since kaolinite and chlorite are not radioactive. Mica is an important detrital component in the Rannoch Formation (Moss, 1992), mica is potassium-rich (and thus radioactive) so its presence leads to locally elevated Vshale values for this stratigraphic interval.

The reported core depths did not initially match the measured (log) depths due to core slippage, core rubbling, etc. Core depths were depth-shifted to log depth, on a core-by-core basis, by matching core analysis porosity to density log-derived porosity (Rider and Kennedy, 2011) and by matching known depths of shale-rich horizons (from sedimentary logging) in core to spikes in the gamma log. Core shifts varied from 8' to 13'.

### 3.2 Sedimentary core logging

Detailed sedimentary logging was undertaken from 10,803 to 10,256 ft-md depth with a total thickness of 547 ft, equivalent to 435.3 ft true vertical thickness. The sedimentary logs recorded grain size, primary sedimentary structures, ichnofabrics, and visible signs of cementation. A condensed sedimentary log was produced at a scale of 1:120 to allow comparison between wireline and sedimentary logs, helping core-to-log shift corrections. Finally, a condensed sedimentary log at a scale of 1:600 was prepared to highlight the sedimentary evolution in conjunction with wireline log and core analysis data (Fig. 3).

A largely process-based (i.e., textural) classification of sedimentary facies was adopted, following the method defined by Farrell et al. (2012). The scheme is independent of composition and geologic environment and is closely allied to process-sedimentology. The classification scheme was modified to add a category for highly carbonate cemented beds. Facies codes and their descriptions are presented in Table 1. Twelve discrete lithofacies were identified.

### 3.3 Optical microscopy and SEM

To allow petrographic data to be related to petrophysical data, 40 core samples were taken directly adjacent to, and in the same bed as, the core plug points; we chose this approach as we did not have access to the core plugs. The 40 petrographic polished thin sections samples cover the range of

lithofacies. In addition, SEM stub samples were made from representative samples of all depositional environments. Polished sections were impregnated with blue resin to highlight porosity during optical petrography.

All samples were examined and point counted using optical light microscopy using an Olympus BX51 microscope (Emery and Robinson, 1993). Backscattered scanning electron microscopy (BSEM) was carried out using a Hitachi TM3000 table-top SEM at an accelerating voltage of 15 kV and a working distance of 17.5 mm. To help differentiate quartz grains and quartz cement, SEM-CL imaging was undertaken using a Philips XL30 at 10 kV by integrating the signals from 16 discrete frames using a slow scanning raster; this took about 8 minutes for each image.

Modal analysis was performed on the 40 sandstone thin sections in order to quantify the various detrital and diagenetic phases (Van der Plas and Tobi, 1965). Compositional point counting of 300 points per sample was undertaken using a PETROG System developed by Conwy Valley System Ltd (CVS), UK. Textural analysis was performed on 200 grains per sample using the PETROG system.

**3.4 Scanning electron microscopy-energy dispersive spectroscopy (SEM-EDS)**

Quantitative evaluation of mineral proportions and mineral-based petrographic imaging were undertaken using SEM-EDS, which consists of an automated, spatially-resolved petrography system, based within a scanning electron microscope, using energy-dispersive X-ray spectroscopy detectors and an extensive mineral database (Armitage et al., 2010; Pirrie et al., 2004). SEM-EDS analyses give quantitative mineral proportions, grain and pore space morphology and distribution, to a minimum resolution of ~1 µm (the smallest beam-sample interaction volume width). SEM-EDS cannot identify or quantify microporosity and it struggles to quantify any mineral grain that is smaller than about 1 or 2 µm. The SEM-EDS instrument used in this study was an FEI WellSite QEMSCAN at the University of Liverpool, using a tungsten-filament, operating at 15 kV, equipped with two Bruker EDS detectors (Wooldridge et al., 2018).

**3.5 Vitrinite reflectance analysis**

Seven coal-bearing Brent samples were collected from different intervals, three from the Ness and Etive Formations, and two from the Rannoch Formation, and analysed for vitrinite reflectance as an input to the burial history reconstruction. Sample preparation and analysis was conducted by Egs-ploration® Maennedorf, Switzerland. Whole rock sample preparation for analysis in incident white light was performed on crushed (0.55 mm) whole rocks following the guidelines set out in the

International Organization for Standardization publications ISO 7404-2, ISO 7404-3 and ISO 7404-5. Crushed particles were cold-set into an epoxy resin block and sequentially ground then polished using decreasing abrasives and polishing powders using an automated Buehler Ecomet 3®, Automet 2® head, polishing system and isopropanol as a lubricant. The reflectance of vitrinite particles was determined in a dark-room using a Zeiss Standard Universal research microscope-photometer system (UMSP-30) equipped with a 12 V, 100 W tungsten-halogen lamp, a 40-power Epiplan oil immersion objective, filtered 546 nm non-polarized incident light and Zeiss immersion oil with a refractive index of 1.517 at 23°C. Reflectance measurements (% $R_o$) were recorded on randomly-oriented particles. A Zeiss triple glass standard with reflectances of 0.506 %, 1.025 % and 1.817 % was used in addition to McCrone® yttrium-aluminum-garnet (0.917 %), spinel (0.413 %) and cubic zirconium (3.256 %) mineral standards for photometer calibration and reflectance determination.

### 3.6 Burial history modelling

Burial history modelling was performed using BasinMod®, provided by Platte River Associates. The stratigraphic data used are based on the whole stratigraphy of the area from Lower Jurassic Cook Formation to Uppermost Middle Miocene- to Quaternary-Nordland Group.

For modelling purposes, lithology mixes were constructed based on the geological and biostratigraphical reports in the substantial literature in the Mid-Jurassic Brent Group and for the whole of the North Sea stratigraphy (Mitchener et al., 1992; Reynolds, 1995; Richards, 1992). Thermal maturity data (i.e., the new vitrinite reflectance data) and bottom hole temperature values were included to help constrain the thermal history of the well. Compaction was modelled using an effective stress fluid flow model to simulate the extent of overburden-induced porosity-loss though time.

## 4 Results

### 4.1 Brent core sedimentary logs, sedimentary facies and depositional environments

Output from sedimentary core logging and facies analysis is summarized in Figure 3A and Table 1. The various formations of the Brent Group have been discriminated based on sedimentological characteristics. Images of key lithofacies, facies codes and description of the twelve facies are given in Figures 4A to 4L and Table 1. The 12 facies described in Table 1, and shown in Figures 3A and 4, are bioturbated muddy sandstone (mSbiot); planar, hummocky and swaley cross-bedded sandstone (Sx-1); trough cross-bedded sandstone (Sx-2); flaser bedded sandstone (Sf); rippled laminated sandstone

(Sr-lam); bioturbated sandstone (Sbiot); massive silty sandstone (zSm); carbonate cemented silty sandstone (zScem); finely laminated siltstone (Zlam); bioturbated silty mudstone (zMbiot); massive mudstone (Mm); coal (P). Five facies associations are also listed in Table 1 including fan delta, shoreface, foreshore, delta plain and barrier shoreline. Following the seminal work by Daws (1992) and Richards (1992), the Brent Group sediments have here been grouped into four depositional environments: shoreface, foreshore, delta plain and barrier shoreline, which represent regressive and then transgressive depositional conditions. The shoreface sediments represent the Rannoch Formation; the foreshore sediments represent the Etive Formation, the delta plain sediments represent the Ness Formation, and the barrier shoreline sediment represents the Tarbert Formation.

**4.2 Wireline logs analysis and comparison to sedimentary log**

A Vshale log, representing the relative proportions of radioactive clay minerals (i.e., illite and possibly smectite), has been plotted in Figure 3B. We have also plotted a density-neutron crossover diagram, following wireline log conventions (Rider and Kennedy, 2011), in which reservoir and non-reservoir are depicted (Fig. 3C). For the shoreface (Etive Formation) and the Delta plain (Ness Formation), there is excellent agreement between the identified fine-grained (shaley) sections of core and high Vshale and non-reservoir from the density-neutron crossover diagram (Figs. 3A to C). Similarly, for the shoreface (Etive Formation) and the Delta plain (Ness Formation), there is excellent agreement between the identified reservoir sandstone sections of core and low Vshale and reservoir from the density-neutron crossover plot.

The shoreface sandstones of the Rannoch Formation have a much higher baseline Vshale measurement than the overlying foreshore, delta plain and barrier shoreline sandstones suggesting that the shoreface sandstones are more clay- or mica-rich than the other sandstones (Fig. 3B). The density-neutron cross-over area is narrower, suggesting that the reservoir quality is somewhat poorer, for the shoreface sandstones than the other sandstones. There are at least four noteworthy exceptions to the agreement between the Vshale and density-neutron crossover in the shoreface sandstones at the base of the succession (between 10,600 and 10,750 ft), where there are tight (high density, low neutron) intervals that have no detectable Vshale increase. The low porosity intervals in the shoreface sandstones must be due to the presence of pore-filling cement, instead of the presence of clay minerals. In core, the low porosity sandstones in the shoreface sandstones are represented by carbonate cemented silty sandstone (zScem, Fig. 4H).

### 4.3 Core analysis porosity and permeability

Core analysis porosity and horizontal permeability data are presented in Figures 3D and E, compared in Figure 5A and displayed as a function of depositional environment in Figures 5B and 5C. Core analysis porosity data range from 2.4 to 31.5 %, Fig. 5B). Core analysis horizontal permeability data range from 0.04 to 6,000 mD (Fig. 5C).

The core analysis data (Figs. 3D and E) match well with the sedimentary log (Fig. 3A) and the Vshale (Fig. 3B) and density-neutron cross-over diagrams (Fig. 3C). The high porosity and permeability tend to equate to low Vshale and net reservoir on the density-neutron cross-over diagram. However, very low porosity and permeability values at four intervals in the shoreface sandstones, in facies zScem, do not equate to high Vshale values and result from pore-filling cement rather than shale. All other low porosity and permeability layers match with shale horizons in the sedimentary log and high Vshale and non-reservoir in the density-neutron cross-over plot.

The shoreface sediments of the Rannoch Formation progressively increase in porosity and permeability up-section, which matches the subtly increasing grain size (Fig. 3A) and the decreasing density log signal (Fig. 3C). The highest porosity and permeability values in the foreshore, delta plain and barrier shoreline sandstones are broadly similar, approaching 30% porosity and well over 1,000 mD.

Based on the whole collection of core plugs, including sandstone and non-reservoir facies rocks, the foreshore and barrier shoreline sediments have the highest porosity and permeability values (Fig. 5). The shoreface sediments have poorer reservoir quality than the foreshore and barrier shoreline sediments, partly related to the high Vshale and partly related to highly cemented intervals (both influences evident in the wireline logs (Fig. 3). The delta plain sediments have sections with poor reservoir quality due to the presence of bioturbated muddy siltstones with their high Vshale values also evident in the wireline logs (Fig. 3).

### 4.4 SEM-EDS mineralogy

The SEM-EDS-derived mineral proportions of the 40 polished sections of sandstone are presented in Table 2 and illustrated in Figure 6. SEM-EDS reveals total mineral proportions and cannot discriminate between different forms of the same mineral, for example quartz cement from quartz grains. Differences in locations of minerals within the rock fabric will be examined in the sections reporting on modal analysis.

### *4.4.1 Framework minerals*

Quartz is the dominant mineral in these sandstones, with important but subordinate quantities of K-feldspar and plagioclase (Figs. 6A to C). Quartz is found in lowest proportions in shoreface and barrier shoreline sandstones with significantly higher proportions in the foreshore and delta plain sandstones. Both K-feldspar and plagioclase are least abundant in the foreshore and delta plain sandstones and most abundant in the shoreface and barrier shoreline sandstones (Figs. 6B and C). This reveals that there were fundamentally different types of sands deposited in different sedimentary environments. This mutual exclusivity of quartz and feldspar has led to a spectrum of sandstones with a large range of mineralogical maturity values.

### *4.4.2 Mica minerals*

Micas are dominated by muscovite but there are significant quantities of biotite (Figs. 6D and E). Both micas are found in highest quantities in shoreface sandstones with low to negligible quantities in the foreshore and delta plain sandstones and minor but significant quantities in barrier shoreline sandstones.

### *4.4.3 Clay minerals*

Clay minerals are represented by kaolinite, illite and chlorite (Figs. 6F to H). Kaolinite is the dominant clay mineral in all sedimentary environments. Smectite is effectively absent from these rocks. All clay minerals are found in greatest quantities in shoreface sandstones with lowest quantities in the foreshore and delta plain sandstones. Barrier shoreline sandstones have intermediate quantities of clay minerals.

### *4.4.4 Pyrite*

Pyrite is ubiquitous but present in small quantities in most depositional environments (Fig. 6I). The greatest quantity of pyrite is found in barrier shoreline sandstones.

### *4.4.5 Carbonate minerals*

The dominant carbonate mineral found in reservoir sandstones is siderite. Siderite is mostly present in small quantities (Fig. 6J). The shoreface sandstones have the greatest quantity, on average (nearly 1 %), but the delta plain sandstones have localised concentrations of > 17 % siderite.

Note that the wholly calcite cemented sandstones with porosity approaching 0 % (zScem, Figs. 3 and 4H) were not the focus of this study as the calcite has led to negligible porosity and the rock is non-reservoir. For most of the Brent reservoir sandstones studied here, calcite is not a reservoir quality issue as revealed by Figure 6K, but its presence leads to stratigraphically-controlled flow barriers, as evident in Figure 3. Dolomite concentration is also represented (Fig. 6L); the y-axis reveals small quantities that mimic the relative distribution of calcite but that do not influence reservoir quality.

## 4.5 Detrital composition and rock fabric

In general terms, the sandstones studied here are predominantly moderately well-sorted (Fig. 7A) and very fine- to medium-grained (Fig. 7B). Grains are sub-rounded (Fig. 8), and sandstones are classed as subarkoses and sublitharenites (Fig. 9), using the McBride (1963) classification scheme, and including detrital mica as a lithic grain.

### *4.5.1 Sorting*

All sandstones are well- or moderately well-sorted (Figs. 7A and 8). There is relatively little difference between the four depositional environments. Any systematic differences in reservoir quality are therefore unlikely to be related to variations in sorting.

### *4.5.2 Grain size*

In contrast to sorting, there are significant variations in the median grain size for the four depositional environments (Figs. 7B and 8). The shoreface sandstones are very fine-grained with a median grain size of 0.09 mm. In contrast the foreshore sandstones straddle the fine- to medium-grain size with a median of 0.24 mm. The delta plain sandstones are fine-grained with a median grain size of 0.19 mm and display the widest range of grain sizes. The barrier shoreline sandstones are very fine-grained with a median grain size of 0.11 mm. The variation of grain sizes found in the various depositional environments are likely to be responsible for reservoir quality differences.

### *4.5.3 Quartz-feldspar-lithic (QFL) sandstone classification*

Point count data reveal significant differences in the composition of framework grains from the four depositional environments. The shoreface sandstones predominantly sit in the sub-lithic field since abundant detrital micas have here been classed as lithic grains (Fig. 9A). Given the mica population first identified using SEM-EDS (Figs. 6D and E), this is not so surprising. In contrast, the foreshore sandstones and the barrier shoreline sandstones sit in the subarkose field (Figs. 9B and D). The delta plain sandstones straddle the subarkose and sublithic sandstone fields (Fig. 9C). It can be anticipated that the differences in QFL classification will have an impact on reservoir quality.

### *4.5.4 Rigid framework grain populations (quartz and feldspars)*

As will be shown, there is very little quartz cement in these sandstones so that most of the quartz is present as sand grains. The SEM-EDS data revealed the dominance of quartz in these sandstones, and the point counting subsequently revealed that quartz grains are predominantly monocrystalline (Fig. 7D) with much lower proportions of polycrystalline quartz grains (Fig. 7E).

### *4.5.5 Ductile and lithic grain populations*

The only significant ductile grains in these sediments are detrital muscovite, biotite and possibly chlorite, as previously quantified using SEM-EDS (Figs. 6D to 6F). There are significant variations between the four depositional environments with a far greater quantity of ductile grains in the shoreface sandstones than the other three environments (Figs. 6D-E and 9). Lithic grains are mainly altered and degraded undifferentiated sedimentary clasts and metamorphic rock fragments. They are generally present in small quantities that do not vary significantly between the four depositional environments (Fig. 7F).4.6 Diagenetic mineralogy and textures.

## 4.6 Diagenetic components

Both SEM-EDS and point counting revealed that sandstones from the four depositional environments contain a common set of diagenetic, as well as detrital, minerals so that the detrital minerals and the secondary effects of diagenetic change will be described in turn. In approximate order of abundance, the cements are kaolinite, siderite, pyrite, chlorite, calcite, feldspar cements, with only trace quantities of illite, dolomite and quartz cement. The quantities and morphologies of the mineral cements differ between sedimentary environments. Mineral cements, grain-replacement, grain deformation,

secondary (new) pores and the overall paragenetic sequence are illustrated in light optical images in Figure 10, BSEM images in Figure 11, SEM-EDS images in Figures 12 and 13 and CL and SEM images in Figure 14.

### *4.6.1 Kaolinite cement*

Kaolinite is the most abundant diagenetic mineral (Fig. 6G) and it occurs in four morphologies: (1) large platy crystallites with a relics of muscovite precursor (Fig. 10B), (2) vermicular crystallites that typically occur in primary and secondary oversized pores related to the dissolution of feldspar (Fig. 10C), (3) pseudomorphic replacement of detrital muscovite and biotite grains resulting in expansion of the mica lamellae (Figs. 10B and 11F), (4) collections of blocky crystals, each about 5 μm, that occupy oversized pores (Fig. 11F). All types of kaolinite morphologies are present in all parts of the Brent Group, except blocky kaolinite crystals were not observed in shoreface sandstone (Appendix 1).

### *4.6.2 Siderite cement*

Siderite is the second most abundant cement after kaolinite. Siderite occurs as: (1) coarsely-crystalline rhombic and lozenge-shaped crystals sitting in primary pores (Figs. 8B, 10B), (2) disseminated, micro rhombic crystals associated with the alteration of biotite (Figs. 11A, B and D), and (3) aggregates of microcrystalline rhombs (Figs. 10C, 12, 13A, B and C). The alteration of biotite to siderite is common in the shoreface sandstones, with discrete siderite rhombs growing within delaminated detrital biotite (Figs. 11A, B and D). Siderite is locally abundant in the delta plain sandstones reaching up to 17% (Figs. 6J and 13A) where it occurs as aggregates of lozenge-shaped, microcrystalline rhombs that typically fill large pores between loosely packed framework grains. In the foreshore and barrier shoreline sandstones, siderite occurs predominantly as coarsely crystalline, lozenge-shaped rhombs in primary pores (Fig. 13A).

### *4.6.3 Pyrite cement*

Pyrite is present in sandstones from all depositional environments (Fig. 6I), occurring as: (1) disseminated early diagenetic framboids which occur throughout the pore network (Figs. 11B and E), (2) disseminated euhedral crystals within the pore network (Fig. 11B), and (3) pervasive poikilotopic masses which locally enclose packed framework grains (Fig. 13D). Pyrite is not restricted to a subset of depositional environments and all three pyrite morphologies were observed in all sedimentary environments (Appendix 1).

### *4.6.4 Chlorite (replacive)*

Small quantities of authigenic chlorite occur in all sedimentary environments (Fig. 6F). Biotite is locally replaced by chlorite in shoreface, delta plain, and barrier shoreline sandstones. Grain replacive chlorite is largely absent in the shoreface sandstone. No grain-coating chlorite was observed. SEM-EDS revealed that the chlorite is typically associated with pore-filling kaolinite and siderite (Figs. 12 A-D, 13 A-B).

### *4.6.5 Calcite and dolomite cement*

Trace quantities of calcite cement are found in sandstones from most depositional environments (and see Fig. 6K) but has no role in controlling reservoir quality due to the small volumes. However, four pervasively calcite-cemented intervals are present in shoreface sandstone (Figs. 3A, 4A and 11C) that lead to the sandstone being a barrier to flow rather than part of the reservoir system. Very small quantities of dolomite are present (Fig. 6L), that follow the calcite distribution pattern.

### *4.6.6 K-feldspar cement*

K-feldspar cement occurs as overgrowths on detrital K-feldspar grains. K-feldspar cement is present as an authigenic mineral throughout the Brent Group. It ranges from 0 to 1 % of the rock volume (Fig. 7G). The thickness of feldspar overgrowths varies but reaches up to 15 µm (Figs. 10F, 11E), K-feldspar cement locally grows as discrete rhombic outgrowths that result from the crystallographic complexity of the feldspar mineral system (Worden and Rushton, 1992).

### *4.6.7 Illite cement*

Modal analysis shows that illite cement is a minor clay mineral (Fig. 6H) and is typically associated with pore-filling kaolinite (Fig. 13 C) and mica grain replacement (Figs. 12 A and B, 13 B) in all depositional environments except in foreshore sandstones.

### *4.6.8 Quartz cement*

Quartz cement was observed throughout the Brent Group, but it represents a relatively minor component in these sandstone reservoirs (Fig. 7 H), with averages less than 0.22 % in all depositional

environments (Appendix 1). Quartz cement occurs as minor and incomplete syntaxial overgrowths on detrital quartz grains, with a thickness range from 5 to 15 μm (Fig. 14A-H).

In summary, analysis of diagenetic components of these Brent Group sandstone reveals that barrier shoreline and shoreface sandstones contain the greatest quantity of diagenetic kaolinite and siderite (Appendix 1). Barrier shoreline sandstones contain the greatest quantity of diagenetic pyrite followed by foreshore sandstones while delta plain sandstones have the lowest quantity. Diagenetic calcite (except for tightly cemented layers in shoreface sandstone), pore-filling chlorite, illite, K-feldspar and quartz all constitute minor (< 1 %) diagenetic phases.

### 4.7 Burial history models

The thermal-history of the well from the Lower Jurassic to the present is represented in Figure 15. The temperature history is a function of variable heat flow and variable subsidence with heat flow being modelled to increase during periods of rifting. The maximum temperature modelled for this well is 95°C. The new vitrinite reflectance data from the Brent Group at 10,762ft, 10,761ft, 10,500.2ft, and 10,317.5ft, are 0.66%$R_0$, 0.59%$R_0$, 0.54%$R_0$, 0.59%$R_0$, 0.51%$R_0$, and 0.49%$R_0$ respectively corresponding to temperatures equivalent to the onset of oil generation. The present temperature is 95°C is most likely close to the maximum temperature that this well has experienced.

## 5. Discussion

### 5.1 Paragenetic sequence

Observations of the textural relationships of the various mineral cements, using light optics, SEM, BSEM and SEM-EDS, have allowed us to interpret the order of mineral growth, also known as the paragenetic sequence (Fig. 16). All diagenetic phases (kaolinite, siderite, pyrite, chlorite, calcite, feldspar cement, and trace amounts of illite and quartz cement) were observed in all four depositional environments although the quantities and morphologies differ.

The common presence of long, concavo-convex surfaces and locally sutured contacts grain-contacts (Fig. 11A) indicates that the sandstone has been subjected to moderate to high degrees of mechanical compaction. Mica flakes that were deformed during mechanical compaction are present in all sandstones from all four depositional environments (Figs. 8A, 10B, 11B, 11D, 12B, 12B, 13B and C).

Diagenetic pyrite is present in sandstones from all depositional environments (Fig. 6I). Precipitation of framboidal pyrite (Fig. 11E) was the first recorded diagenetic mineral phase in sandstones from all

depositional environments. In contrast, poikilotopic pore-filling pyrite represents a late diagenetic phase (Fig. 11B), which is present in small quantities in sandstones from all depositional environments.

Calcite precipitation, strongly localised to stratigraphically-restricted cemented layers (Figs. 3A, 4H), occurred before kaolinite precipitation (Fig. 11C). Calcite tends to be either absent or totally pore-filling (Fig. 3A, 3C, 3D, 3E) and it leads to rocks that are non-reservoir. The origin of stratigraphically-restricted calcite in Brent Group and equivalent sandstones has been discussed many times (Lundegard, 1994; Morad and De Ros, 1994; Prosser et al., 1993; Worden et al., 2019) and will not be discussed further here.

Biotite and feldspar dissolution (Figs. 8 A, 8B and 8C) also seem to represent relatively early diagenetic events because they have been replaced by the eogenetic minerals, siderite, and kaolinite respectively (Figs. 8A, 8B, 8C, 10B, 12A, and 12B). The breakdown and dissolution of biotite is spatially associated with precipitation of siderite in between broken-apart biotite 001-flakes (Figs. 11A, 11B, 11D) but some siderite crystals occur in large clusters (Fig. 12B-D) suggesting that siderite growth may have started during eodiagenesis and continued into the mesogenetic realm. The breakdown and dissolution of feldspar grains is spatially associated with precipitation of kaolinite leading to clusters of kaolinite that are the same size as sand grains (Figs. 11A, 11D, 11F). Some clusters of kaolinite seem to have been deformed, acting as ductile “grains” (Fig. 10B) suggesting that at least some kaolinite replacement of feldspar occurred before mechanical compaction was complete (i.e., before grain stabilisation).

K-feldspar cement overgrowths on feldspar grains represents a later diagenetic event as shown by the absence of this cement at K-feldspar grain-grain contacts (Figs. 10F and 11E). Traces of K-feldspar cement are present in sandstones from all depositional environments, but the greatest quantity was found in foreshore and delta plain sandstones (Fig. 7G). Textural relationship indicates that feldspar overgrowth post-dated mechanical compaction (Fig. 11E). Some K-feldspar cements have undergone subsequent dissolution whereas the detrital substrate seems to have remained intact suggesting a complex relationship between K-feldspar crystallography, strained cement crystals and evolving pore-water geochemistry (Worden and Rushton, 1992).

Small amounts of authigenic pore-filling chlorite and grain replacive chlorite occur in sandstones (Figs. 12A, 12B, 12D, 13A-B) from all depositional environments within the Brent Group (Fig. 6F). Chlorite is most abundant in biotite-rich sandstones (Fig. 6D), suggesting a genetic relationship.

Authigenic illite is a minor diagenetic phase (Fig. 6H) and was only identified using the SEM-EDS (Fig. 6H); illite mainly appears to be an alteration product of diagenetic kaolinite (Figs. 12A-B, 13B, 13C-E). Fibrous pore-filling illite was not observed in any samples.

Authigenic quartz overgrowths are a minor phase observed in sandstones from all four environments of deposition (Fig. 7H). Most of the syntaxial quartz overgrowth are within the size range of 5-15 μm (Fig. 14A-H). Numerous long intergranular concavo-convex contacts between individual quartz grains, and some suture contacts, were observed (Figs. 11A, 12D). Application of the thermal history model (Fig. 15) linked to an empirically-derived kinetic quartz growth model (Walderhaug, 1994a) shows that the expected maximum volume of quartz cement is in the range 2.5% to 3.5%. The range is a function of grain size and the proportion of detrital quartz in the various sandstones (Fig. 9). The small observed volume of quartz cement (Fig. 7H) is thus a function of the subdued thermal history of this well as opposed to inhibition of quartz cement by, for example, grain coating microquartz (Worden et al., 2012), grain coating chlorite (Worden et al., 2020), or early oil emplacement (Worden et al., 2018b).

Sandstones from all depositional environments have similar paragenetic sequences as all contain the same types of the diagenetic phases and only differ in terms of the quantities. The overall paragenetic sequence is presented in Figure 16.

**5.2 Sources of mineral cements**

***5.2.1 Processes that led to kaolinite cement***

Kaolinite is the most abundant cement in sandstones from all the four depositional environments, with the shoreface sandstones having the greatest quantity (Fig. 6G). Kaolinite is spatially associated with partly dissolved feldspar grains (Figs. 8A-D, and 12A-C) and there are good and significant correlations between the quantity of kaolinite and the quantities of K-feldspar and plagioclase (Table 3). Based on these lines of evidence, it is likely that kaolinite formed because of the alteration of detrital feldspar (Bauluz et al., 2008; Harris, 1992; Marfil et al., 2003). Stoichiometric breakdown reactions for K-feldspar and plagioclase to kaolinite may be described:

$2KAlSi_3O_8 + 2H^+ + H_2O \Rightarrow Al_2Si_2O_5(OH)_4 + 4SiO_2 + K^+$

K-feldspar kaolinite silica

(Equation 2)

$[(2/(1+X)](Ca_XNa_{1-X})Al_{1+X}Si_{3-X}O_8 + 2H^+ + H2O \Rightarrow$

plagioclase

$$Al_2Si_2O_5(OH)_4 + [(4\text{-}4X).2/(1+X)]SiO_2 + [(1\text{-}X).2/(1+X)]Na^+ + [X.2/(1+X)]Ca^{2+}$$

kaolinite quartz

(Equation 3)

Where X is proportion of calcium replacing sodium in the detrital plagioclase. Feldspar breakdown reactions require protons (i.e., acidic pore waters) and release metals into the aqueous medium.

Note that there is also a strong association between the quantity of muscovite and the quantity of kaolinite (Fig. 17A, Table 3). This might suggest that muscovite breakdown during diagenesis was another source of kaolinite (Morad, 1990), although some have presented evidence, from Carboniferous clastic rocks, that muscovite does not breakdown to kaolinite (Crowley, 1991). A stoichiometric breakdown reaction for muscovite to kaolinite may be described:

$$2KAl_3Si_3O_{10}(OH)_2 + 6H^+ + 3H_2O \Rightarrow 3Al_2Si_2O_5(OH)_4 + 6K^+$$

muscovite kaolinite

(Equation 4)

Like the feldspar alteration reactions (equations 2 and 3), the theoretical breakdown of muscovite to kaolinite also requires protons (i.e., acidic pore waters) and releases metals into the aqueous medium. The potential sources of acidic formation waters, especially in the early stages of clastic diagenesis, have been discussed at length; acid waters may be related to meteoric water influx, e.g. during sea level lowstands (Morad et al., 2010) or inversion events (Osborne et al., 1994). Acidic formation waters are most likely linked to microbial and thermal organic breakdown reactions during eo- and meso-diagenesis (Worden and Burley, 2003) in the dominant fine-grained clastic fill of basins resulting in large volumes of $CO_2$ (Andresen et al., 1994) as well as more exotic organic acids (Barth and Riis, 1992).

The fate of the released potassium can include increasing $K^+$ concentration in formation water, growth of K-feldspar overgrowths (Figs. 11B, (11E), and incorporation into associated mudstones during the illitisation of smectite (Gier et al., 2018). The fate of the released sodium is probably limited to increasing $Na^+$ concentration in the formation water as there are few Na-bearing diagenetic minerals and Thistle formation waters have relatively low salinity at roughly half seawater concentration of sodium and chloride (Warren and Smalley, 1994). If the detrital plagioclase had an anorthite component, the calcium released during the formation of kaolinite was probably incorporated into the calcite-cemented layers in the delta front- lower shoreface sandstones (Worden et al., 2019).

The greater quantity of kaolinite in the shoreface sandstones compared to other depositional environment, may be due to the greater quantities of reactant aluminosilicate minerals such as K-

feldspar, plagioclase and muscovite (Fig. 6B, 6C, 6E) (Bjørlykke and Brendsdal, 1986; Hurst and Irwin, 1982). The relics of dissolved feldspar, with little infilling secondary cement (Fig. 10A), testify to the relative lateness of some of the feldspar dissolution.

### *5.2.2 Siderite cement sources*

Siderite ($FeCO_3$) is the second most abundant diagenetic cement. The shoreface and barrier shoreline sandstones have the highest median values, but the highest local concentrations are found in the delta plain sandstone (Fig. 6J). Siderite has been reported to be common in Brent-equivalent sandstones (Kantorowicz, 1985).

Siderite is typically precipitated in low redox/reducing conditions, where there is a supply of iron, where carbonate concentration is high and where sulphide concentration is low (Matsumoto and Iijima, 1981; Mozley, 1989; Mozley and Wersin, 1992). In situations where sulphide concentration is high, Fe-sulphide minerals tend to develop at the expense of siderite. Where there is a supply of iron but both sulphide and bicarbonate concentrations are low, Fe-silicate minerals, such as berthierine, will tend to form (Worden et al., 2020). In these sandstones, siderite is intimately associated with altered detrital biotite (Figs. 10B, 11A, 11B, 11D) suggesting that the short-range supply of iron from the decomposing mica is a key control on siderite growth (Bjørlykke and Brendsdal, 1986). A stoichiometric breakdown reaction for Fe-biotite to siderite and, in this case, kaolinite, may be written:

$$2KFe_3AlSi_3O_{10}(OH)_2 + 6H_2CO_3 + 2H^+ \Rightarrow 6FeCO_3 + Al_2Si_2O_5(OH)_4 + 4SiO_2 + 7H_2O + 2K^+$$

Fe-biotite carbonate siderite kaolinite silica

Equation 5

The aqueous carbonate was probably supplied by organic sources undergoing bacterial breakdown, but such processes must have happened in low salinity and non-marine (low sulphate concentration) pore waters since otherwise Fe-sulphide minerals would have developed (see 5.2.3). The presence of low salinity water may have been due to (1) onshore water table-driven flux of groundwater through these sand-dominated deltaic sediments or (2) the transient fall in relative sea level which exposed these marginal marine sediments to meteoric water influx (Morad et al., 2010).

### *5.2.3 Pyrite cement sources*

Framboidal pyrite is present in all samples from the four depositional environments (Appendix A, Figs 11B, 11E, 12D, 13D); this type of pyrite is typically assumed to be the result of colonies of sulphate-reducing bacteria acting where organic matter, available iron and aqueous sulphate coincide (Berner,

1984; Wilkin et al., 1996). The most likely source of the iron was detrital biotite, which, even after alteration, still represents up to several percent of the rock by volume. However, the Brent river may also have fed Fe-oxyhydroxides into the depositional environment (Worden et al., 2020). The Brent delta top sediments had lush vegetation, as indicated by the presence of coaly horizons, so there was likely no shortage of organic substrate. The greater volume of siderite than pyrite in the whole sedimentary Brent system (Figs. 6I and 6J) suggests that access to aqueous sulphide was relatively limited during eodiagenesis. The barrier shoreline sandstones contain the greatest quantity of pyrite (Fig. 6I) suggesting that inundation by sulphate-rich seawater may have been locally important for the formation of this mineral.

Formation of late diagenetic pyrite (Fig. 11B) entailed continued alteration of biotite in the presence of reduced sulphur sources, such as $H_2S$ or aqueous sulphide. The presence of late stage $H_2S$ in sedimentary systems is not unusual with the sulphide either coming from thermal breakdown of source rocks or oils, or via thermochemical sulphate reduction (Worden and Smalley, 2001; Worden et al., 2003). The former seems more likely in the Brent sediments because formation waters have negligible aqueous sulphide (Warren and Smalley, 1994).

#### *5.2.4 Chlorite cement sources*

Chlorite is present in small quantities throughout these Brent sediments; it is most enriched in the micaceous shoreface sediment (Fig. 6F). The chlorite identified by SEM-EDS includes detrital chlorite or chlorite that has partly replaced detrital biotite (Figs. 12A, and 12B), and detrital lithic grains (Fig. 12B). The development of replacive chlorite could have occurred at a range of locations including the weathering zone in the hinterland, in soils, in transient fluvial sediment accumulations or during in-situ eodiagenesis.

Significantly, no grain-coating chlorite was observed in sediments from any of the depositional environments even though the sediments are relatively iron-rich, as revealed by the quantities of detrital Fe-rich biotite, siderite and pyrite (Figs. 6D, 6I and 6J). Other parts of the North Sea Basin have Fe-rich Lower and Middle Jurassic deltaic sediments that are characterised by abundant, grain-coating Fe-rich chlorite (Jahren et al., 1998; Martinius et al., 2005; Skarpeid et al., 2017) and rather less siderite than is present in the Brent sediments (Ashcroft and Ridgway, 1996; Wilkinson et al., 2000). Brent delta sediments contain abundant plant remains and thin coal seams (Fig. 4L) (Powell, 2010; Ruau et al., 1996) which resulted from accumulation of the remains of lush vegetation on the coastal plain. It is likely that partial decomposition of the delta-top vegetation led to bicarbonate-enriched

groundwater explaining why siderite is dominant and both grain-coating and pore-filling chlorite are absent despite the Fe-enrichment of primary Brent sediments (Worden et al., 2020).

### *5.2.5 Illite cement sources*

Illite is a minor diagenetic phase (Fig. 6H) which has locally replaced muscovite (Fig.12 A-B), detrital lithics grains and pseudomatrix (Fig. 13B-C). Illite abundance follows the abundance of muscovite and kaolinite (Figs. 6E, 6G, 6H) suggesting genetic relationships (Table 3). Only replacive illite was found (Figs. 12A and 13C) with an absence of fibrous illite, as can be found in some deeper North Sea reservoirs (Matthews et al., 1994). At temperatures significantly greater than 100°C, i.e., higher than the 90°C for the Brent sandstones in the Thistle Field at the present day, kaolinite reacts with K-feldspar to produce abundant illite and quartz cement (Bjorkum and Gjelsvik, 1988; Bjørlykke, 1980; Bjørlykke and Aagaard, 1992; Ehrenberg and Nadeau, 1989; Ramm and Ryseth, 1996). The coexistence of kaolinite and K-feldspar suggests that the Brent Group in the Thistle Field is at its maximum temperature (i.e., there has been no uplift or cooling).

### *5.2.6 K-feldspar cement sources*

K-feldspar overgrowths occur as individual euhedral crystals dispersed over the surface of detrital feldspar grains (Fig. 11B, 11E). The diagenetic feldspar has a different extinction angle that the substrate when observed in cross-polarised light. This is due to the difference in crystallography of high temperature detrital (monoclinic) and low temperature diagenetic (triclinic) K-feldspar (Worden and Rushton, 1992). The boundary between the detrital and diagenetic feldspar will be site of strain due to the different lattice parameters; this may have led to local dissolution of K-feldspar cement (Fig. 11E). Diagenetic K-feldspar may be the product of dissolution of the unstable high temperature detrital feldspar and local recrystallisation of the more stable low temperature feldspar (Ali and Turner, 1982; Deros et al., 1994; Glover and Hosemann, 1970; Worden and Rushton, 1992).

### *5.2.7 Quartz cement sources*

Minor quartz overgrowths, present in sandstones from all environments of deposition (Figs. 11B, 14A-H), occur as thin and discontinuous euhedral and syntaxial crystals. The small volume of quartz cement can be attributed to the temperature being at, or about, a maximum of 90°C (Fig. 15); quartz cement growth is a kinetically controlled process that can be shown to need temperatures, in Mesozoic sediments, in excess of 100°C for quartz cement to be abundant (Walderhaug, 1994a, b).

Intergranular concavo-convex contacts and suture contacts (Figs. 11A and 12D) between quartz grains seem to suggest that incipient pressure solution has occurred and was a source for quartz cement (Fig. 14A-H) (Girard et al., 2001; Worden and Barclay, 2000). Alteration of feldspars and micas into clay minerals (Equations 2 to 5) may also have been a source of silica (McKinley et al., 2003; Worden and Morad, 2003), this typically occurs at temperatures significantly lower than for quartz cement derived from pressure solution (Worden and Morad, 2000).

### 5.3 Reservoir quality

#### *5.3.1 Primary depositional controls on reservoir quality*

Reservoir quality varies as a function of depositional environment (Figs. 3 and 5). Primary depositional factors that influence reservoir quality are grain size, grain morphology, sorting and clay or matrix content in the sands (Bjørlykke et al., 1992; Daws, 1992; Gier et al., 2008; Giles et al., 1992; Hamlin et al., 1996; Olaussen et al., 1984). Sorting is similar for sandstones from all depositional environments (Fig. 7A) but grain size varies considerably with the foreshore sandstones and delta plain sandstones being significantly coarser grained than sandstones from the shoreface and barrier shoreline sandstones (Fig. 7B).

The trough cross-bedded (Sx-2, Fig. 4C) and flaser bedded (Sf, Fig. 4D) sandstones from foreshore and delta plain environments have the best reservoir quality (Figs. 5 and 18). The fundamental reason for this is because sandstones from these environments have the highest detrital (and total) quartz concentrations and are coarsest grained (Figs. 6A, 7D, 7E) which are functions of the palaeohydraulic energy inherent to those environments compared to foreshore and barrier shoreline environments.

In contrast, the planar, hummocky and swaley cross-bedded sandstones (Sx-1, Fig. 4B) from the shoreface environment are fine to very fine-grained (Fig. 7B) and have the greatest quantity of mica (Figs. 6D and 6E) have the lowest reservoir quality characteristics (Figs. 5 and 18). The shoreface sandstone exhibits a coarsening upward sequence (Figs. 3A and 18B), with reductions in the quantities of mica and clay matrix (Fig. 18F) and a corresponding increase in reservoir quality (especially permeability) up the succession (Fig. 18B). Micas and clay minerals were re-worked and winnowed out from the upper shoreface and transported out to sea and redeposited in the lower shoreface.

We have directly compared porosity and permeability to grain size and sorting, split by depositional environment to assess the roles of textural variables (Fig. 19). Finer grained sandstones tend to have lower porosity (Fig. 19A) and permeability (Fig. 19C) than coarser grained sandstones. There appears

to be no simple relationship between sorting and porosity (Fig. 19B) or permeability (Fig. 19D); this seems to be the result of sandstones from different depositional environments having a limited range of sorting coefficients.

There is a crude split between fair and excellent reservoir quality as a function of grain size and depositional environment (Fig. 20A). The finer grained sandstones, especially from the shoreface environment, tend to have lower permeability values than coarser grained sandstones (and see Fig. 19C). The relationship between permeability and grain size is well established with finer grained sandstones leading to narrower pore throats and thus smaller capillaries for fluids to pass through (Beard and Weyl, 1973; Cade et al., 1994; Swanson, 1981). However, there is no simple relationship between porosity and grain size (and see Fig. 19A to support this) since the porosity of packed spheres has been shown to be independent of grain size (Beard and Weyl, 1973). We have already shown that there is no relationship between sorting and porosity (Fig. 19B) so there must be another control at play. In the following section we will show that this is due to greater compaction in the shoreface sandstones compared to sandstones from other environments with the degree of compaction being controlled by the greater quantity of ductile mica minerals (see Fig. 18F).

We have graded all core analysis porosity and permeability data separately for the four depositional environments as a function of wireline log-derived Vshale (equation 1, Fig. 3) to illustrate the effects of the radioactive clay content on reservoir quality (Fig. 21). The highest porosity and permeability samples tend to have the lowest Vshale, suggesting an absence of biotite, muscovite and illite in the best reservoir quality rocks. The very high Vshale samples tend to have low porosity and permeability suggesting an abundance of biotite, muscovite and illite. The lowest porosity and permeability samples are from the calcite cemented layers in the shoreface sandstones and these have lower Vshale than the rest of the shoreface sandstones suggesting either that the growth of calcite occurred only in the cleanest sandstones, or that calcite growth led to dissolution of clay minerals. The shoreface samples tend to have relatively high Vshale for a given porosity, compared to other depositional environments, as illustrated by the high volume of muscovite and biotite in shoreface sandstones (Fig 18F). However, the relationship between Vshale and reservoir quality is not simple with some low Vshale samples having relatively low porosity and permeability; this is probably a consequence of non-radioactive (and thus gamma-ray invisible) kaolinite having a major effect on reservoir quality (Figs. 17B, 20B).

### *5.3.2 Diagenetic controls on reservoir quality 1: compaction*

Mechanical compaction leads to volume-reduction due to applied effective stress and occurs by grain repacking and rearrangement, ductile grain deformation and brittle grain fracture from the due to progressive burial (Worden et al., 2018a; Worden and Burley, 2003). The extent of these processes is addressed below. If chemical compaction (pressure solution) has occurred in these sandstones, it is a minor process due to the limited thermal stress experienced by these sandstones (i.e., temperature < 100°C, Fig. 15). Chemical compaction has had little overall impact on reservoir quality and will not be addressed further.

Houseknecht (1987) presented a method to assess the relative extents of both compaction and cementation based on the measurement of intergranular volume and an assumed initial porosity value. Intergranular volume (IGV) represents the addition of porosity and pore-filling cement, both measured using optical point counting. The assumed initial porosity and the intergranular volume are used to define the compactional porosity-loss (COPL), and cementation porosity-loss (CEPL). We have displayed sandstones from the four depositional environments on separate diagrams in Figures 22A-D which show that reservoir quality has been controlled by both cementation and compaction. The stratigraphic distributions of compactional and cementation porosity-loss (COPL and CEPL) are displayed in Figures 18D and 18E.

Shoreface sandstones have the highest degree of compactional porosity-loss (mean 30.2 %) followed by foreshore sandstones (mean 21.5 %), delta plain sandstones (mean 16.0 %), and barrier shoreline sandstones (mean 16.1 %) (Fig. 18D). Overall, the shoreface sandstones are anomalous in terms of the amount of compaction. The difference in the degree of compaction between the shoreface and other sandstones cannot be explained by any sort of differential compaction as a function of depth as the ~450 ft maximum difference in depth between the shoreface and other sandstone has a negligible effect on the degree of mechanical compaction in rocks at ~9,000 ft (Paxton et al., 2002). The difference in the extent of compaction can, however, be explained by reference to the elevated quantity of micas (muscovite and biotite) in the shoreface sandstones compared to the other three depositional environments (Figs. 6D, 6E, 12A, 12B, 18F). Micas are weak minerals that undergo ductile compaction and grain breakage, thus facilitating greater vertical strain than rigid minerals such as quartz. The higher degree of compactional porosity-loss in the shoreface sandstones compared to the other depositional environments explains why these sandstones have lower porosity and at least partly explain why they have lower permeability (Fig. 20A), noting that the finer grain size of shoreface sandstones also contributes to their lower permeability (Fig. 19C).

### *5.3.3 Diagenetic controls on reservoir quality 2: cementation*

As well as compaction, diagenetic cements also exert controls on reservoir quality. The growth of pore-filling cement explains why porosity values are lower than they would be had only compaction occurred (Bloch and Helmold, 1995; Gier et al., 2008; Luo et al., 2009; Meadows and Beach, 1993; Tamar-Agha, 2009; Vinchon et al., 1996; Worden and Burley, 2003). Both early and late diagenetic cement can have an impact on the reservoir quality of sandstones (Gier et al., 2008; Higgs et al., 2007; Worden and Burley, 2003).

Kaolinite cement represents the most volumetrically significant pore-filling cement (Fig. 6G). Comparison of the quantities of kaolinite and porosity reveals a strong inverse correlation (Fig. 17B, $R^2$ = 0.85) confirming that kaolinite is a major diagenetic control on porosity in Brent Group sandstones. Kaolinite has the highest concentrations in the shoreface sandstones (Fig. 6G, 17B). Core analysis porosity plotted versus permeability further illustrate the roles of kaolinite and depositional environment on reservoir quality (Fig. 20B). The more kaolinite-rich sandstones, especially from the shoreface environment, tend to have lower porosity and permeability values than kaolinite-poor sandstones (Fig. 20B). The relationship between porosity, permeability and pore-filling cement, such as kaolinite, is well established, with more cement leading to narrower pore throats and thus smaller capillaries for fluids to pass through (Cade et al., 1994; Swanson, 1981). The quantity of authigenic kaolinite directly correlates with the quantity of detrital muscovite (Fig. 17A) so that the extent of reduction of porosity and permeability during diagenesis (i.e., by kaolinite growth) is a result of depositional processes concentrating reactive detrital grains in shoreface environments, such as mica and feldspar, that led to preferential kaolinite growth during diagenesis (Equations 2 to 5).

Siderite represents the second most volumetrically significant pore-filling cement (Fig. 6J). Siderite can lead to anomalously low permeability (Figs. 12A-D, 13A, 18F and 20B).

Pervasive calcite cement layers in the shoreface sandstone create impermeable zones and thereby stratigraphically compartmentalise the shoreface sandstones reservoirs (Figs. 3A-E and 5). Calcite cement is not a reservoir quality issue since it is either totally pore-filling (Fig. 11C) or present in such low quantities that it has a negligible effect on reservoir quality (Fig. 6K).

Pyrite and smectite constitute minor cements in all the samples analysed, representing the four depositional environments (Table 2). Pyrite and smectite do not exert significant effects on reservoir quality of these sandstones. Pearson correlation analysis (Table 3) of pyrite and smectite with porosity and permeability suggest statistically non-significant relationships.

### *5.3.4 Implications for shallower (cooler) and deeper (hotter) Brent Group reservoirs*

We have compared data from numerous Brent Group reservoirs, in the Northern North Sea, in terms of depth, permeability and temperature, with data taken directly from the Millennium Atlas (Husmo et al., 2003). The subject of this study, the Thistle Field, sits centrally within the ranges of depth, temperature, and permeability. Deeper reservoirs tend to be hotter and tend to have lower permeability, as expected, and vice versa. Based on the data presented in this study, the Thistle Field represents a moderately compacted sandstone with, except for kaolinite, relatively little development of pore-filling cement, such as quartz, illite or dolomite, that are typical of greater depths of burial (Giles et al., 1992). Shallower Brent Group sandstones tend to have relatively high permeability, probably because they have experienced lower effective stress and thus have undergone less compaction and perhaps less kaolinite growth. Deeper and hotter Brent Group sandstones tend to have lower permeability as they have undergone kinetically-controlled growth of quartz, illite and, possibly, dolomite cements, and pressure solution, at temperatures significantly greater than 100°C (Bjørlykke et al., 1992). The lack of a simple straight-line relationship in the data, and specifically the wide range of permeability values for a given depth of burial in Figure 23, is probably the result of locally variable initial sand composition in terms of the initial amounts of detrital mica, matrix and feldspars, different quantities of pore-occluding calcite cement, the possibility of localised uplift and cooling and reservoir-specific variable thermal histories and effective stress histories. Figure 23 shows that regional overviews of reservoir quality are useful but each geographic site, each reservoir, must be examined to make specific predictions of porosity and permeability.

## 6 Conclusions

1. Brent Group sediments, from continuous core through a wide series of depositional environments (in stratigraphic order: shoreface, foreshore, delta plain and barrier shoreline) in the Thistle Field well, 211/18a-33A, buried to 9,178 ft TVDSS, are at their maximum burial temperature of 95°C today. They are predominantly very fine to medium grained, subarkoses to sublitharenites.

2. Reservoir quality is best in delta plain sandstone followed by foreshore, barrier shoreline, and shoreface sandstones. This trend is largely controlled by primary grain size amd depositional composition of the sediment; mica and feldspar concentrations control subsequent eogenetic and mesogenetic processes of compaction and cementation.

3. Reservoir quality was strongly by controlled by compaction. Compactional porosity-loss decreases stratigraphically, up the succession, associated with decreasing quantities of detrital mica and diagenetic kaolinite. The role of ductile mica and clay minerals suggests that variable extents of mechanical compaction had a major secondary control on reservoir quality.

4. Grain size exerts a subordinate controls on the reservoir quality of the sandstones, with the highest permeabilities associated with the coarsest grained sandstones.

5. Reservoir quality was also controlled by cementation. The main diagenetic phases include kaolinite and siderite, with minor quantities of pyrite, calcite, chlorite, K-feldspar, and quartz cement. Oil emplacement was relatively late compared to the cementation events and has not had a detectable effect on sandstone diagenesis of these Brent Group sandstones.

6. The shoreface sandstones are locally characterised by five intervals of pervasive poikilotopic calcite cementation that formed impermeable barriers and stratigraphically compartmentalised the reservoir.

7. The regressive and transgressive sandstones of the shoreface, foreshore, delta plain and barrier shoreline succession have a similar paragenetic sequence that only differs in terms of the quantities and morphologies of cements. Early diagenetic events include mechanical compaction, framboidal pyrite precipitation, biotite dissolution, feldspar dissolution, siderite precipitation, early calcite precipitation, and early kaolinite precipitation. Later diagenetic events include minor pressure solution, K-feldspar overgrowth, chlorite, illite, late pyrite precipitation, and quartz overgrowth.

8. Quartz, K-feldspar and illite cements constitute, at most, minor amounts. The minor quantity of these kinetically-controlled cements can be attributed to the relatively low maximum burial temperature ($< 95^0$C) for a limited period of time (approximately 20 Myrs).

9. Pearson correlation analysis revealed a significant negative correlation between reservoir quality and some detrital and authigenic minerals. Greater quantities of K-feldspar, plagioclase, biotite, and muscovite, are associated with greater quantities of diagenetic kaolinite, siderite and illite. This implies a genetic relationship between the detrital minerals and their authigenic products that reflects the controlling effects of the clastic factory, depositional sorting and winnowing as well as eogenetic, and mesogenetic processes.

10. Siderite is the most abundant Fe-mineral in the Brent Group; it is associated with detrital biotite replacement and therefore reflects the importance of original sediment composition

and provenance of the sediments. Minor amounts of grain-replacive and pore-filling chlorite have been found, although these rocks, like other reported examples of Middle Jurassic Brent Group sandstones, do not contain grain-coating chlorite, probably because iron was preferentially locked up in siderite and minor pyrite at, or soon after, deposition.

11. The primary control on the variable reservoir quality, observed in this study, is the depositional clastic factory which determined the QFL-grain type, grain size and sorting. Secondary controls are eogenetic and mesogenetic processes such as grain rearrangement, ductile compaction, grain replacement and kaolinite and siderite growth, that collectively controlled the reduction of depositional porosity and permeability.

**Acknowledgements**

We would like to thank the Nigerian government's Petroleum Technology Development Fund for providing funding for this research project. We would also like to thank Thermo-Fisher-FEI Company (Hillsboro, Oregon) for loan of the SEM-EDS QEMSCAN equipment and associated software and Dr Alan Butcher for offering excellent analytical and geological advice throughout the loan period of the QEMSCAN. We would also like to thank reviewer Stuart Archer for providing much needed advice and guidance on the representation of the data and suggesting the addition of two useful figures.

**Figure captions**

Figure**.** 1 Regional and Location map of the case study showing the Thistle Field highlighted in black, after Williams and Milne (1991).

Figure. 2 General Stratigraphy of the Brent Thistle Field. Brent Group succession highlighted in red. Modified after Brown and Richards (1989).

Figure 3. Brent Thistle well 211/18a-A33 (A) Summary sedimentary log for all formations, lithofacies shown by colour, grain size and dominant sedimentary structure (SF = Shoreface, FS = Foreshore, DP = Delta Plain, BS = Barrier Shoreline) (B) Wireline log-derived Vshale (equation 1). (C) Wireline log-derived neutron-density cross-over. (D) Core porosity. (E) Core permeability. Sandstone permeability and porosity increase up-section in the shoreface sandstones of the Rannoch Fm. and its tight carbonate cemented intervals plus the highly variable porosity and permeability of the foreshore(Etive Fm.) and delta plain (Ness Fm.) sandstone and the decreasing permeability and porosity up-section in the barrier shoreline sandstones (Tarbert Fm.).

Figure 4. A-L Core photographs of the sedimentary facies from the Brent Group sandstones, with descriptions and interpretations of the facies given in Table 1. Twelve lithofacies were discriminated base on lithology, grain size, sedimentary structures, and bioturbation.

Figure 5. Core porosity and horizontal permeability data split by depositional environments. Shoreface (SF) sandstones are present in the Rannoch Formation. Foreshore (FS) sandstones are present in the Etive Formation. Delta Plain (DP) sandstones are found in the Ness Formation. Barrier Shoreline (BS) sandstones are present in the Tarbert Formation. Shoreface sandstones and delta plain sandstones have highly variable reservoir quality. (A) Core porosity versus horizontal permeability revealing significant differences in reservoir quality of the four depositional environments. (B) Boxplot of core porosity data, where "n" is the number of samples and "m" is the median value. Each boxplot shows the median and upper and lower quartile (> and < 25 % of the median); the whiskers reveal the maximum and minimum values. Outliers are defined as > 1.5 times the upper or lower quartile. The shoreface sandstones have much lower porosity than the other three environments. The delta plain sandstones show the greatest spread of the data. (C) Boxplot of horizontal permeability data, broadly showing the same variation of properties as the porosity data in part B.

Figure 6. SEM-EDS minerals proportions in Brent Group sandstones split by depositional environment, where SF are Shoreface sandstones (Rannoch Formation), FS are Foreshore sandstones (Etive Formation), DP are delta plain sandstones (Ness Formation, and BS are barrier shoreline sandstones (Tarbert Formation). Part A shows the count size for all environments in all parts of this figure (m represents the median in all figures). (A) Quartz varies significantly between depositional environments with the greatest volume found in the foreshore and delta plain sandstones. (B) K-feldspar varies significantly between depositional environments with the smallest volume found in the foreshore and delta plain sandstones. (C) Plagioclase varies significantly between depositional environments with the smallest volume found in the foreshore and delta plain sandstones. (D) Muscovite is present in greater volumes in shoreface sandstones than all other depositional environments. (E) Biotite is found in greater volumes in shoreface sandstones than all other depositional environments. (F) Chlorite is found in greater volumes in shoreface sandstones than all other depositional environments. (G) Kaolinite is found in greater volumes in shoreface sandstones than all other depositional environments. (H) Illite is found in greater volumes in shoreface sandstones than all other depositional environments. (I) Pyrite is present in low volumes in most samples in most depositional environments. (J) Siderite is found in intermediate quantities in most samples in most depositional environments. One outlier is a delta plain sandstones with about 17 % siderite. (K) Calcite is present at low concentrations in most samples but is present in greatest

quantities in the shoreface sandstones. (I) Dolomite is negligible in all samples but is also present in greatest quantities in the shoreface sandstones.

Figure 7. Selected optical point count data on texture, intergranular porosity, grain type and quartz and K-feldspar cement with sandstones split by depositional environment. SF are shoreface sandstones of the Rannoch Formation; FS are foreshore sandstones of the Etive Formation; DP are delta plain sandstones of the Ness Formation; BS are barrier shoreline sandstones of the Tarbert Formation. Part A shows the count size for all environments in all parts of this figure (m represents the median value of all boxplots). (A) Sorting does not seem to vary significantly between depositional environments. (B) Grain size varies significantly between depositional environments with shoreface and barrier shoreline sandstones significantly finer grained than the foreshore and delta plain sandstones. (C) Intergranular mesoporosity, broadly matching the core analysis porosity (Fig. 5B). (D) Point count detrital monocrystalline quartz showing some significant differences between depositional environments. (E) Point count detrital polycrystalline quartz showing significant differences between depositional environments. (F) Point count detrital rock fragments revealing low quantities and little difference between depositional environments. (G) Point count K-feldspar cement showing low quantities, with most in foreshore and delta plain depositional environments. (H) Point count quartz cement showing negligible quantities and no significant differences between depositional environments.

Figure 8. Plane polarised photomicrographs illustrating variation in texture in different depositional environments of the Brent Group. (A) Fine grained shoreface (SF) sandstone with muscovite (Mu), biotite ( Bt ), K feldspar ( Ksp ), sideritised biotite (Sd-Bt ) (10712 ft-md). (B) Foreshore (FS) sandstone showing dissolved K feldspar (Ksp), kaolinite cement (ka), siderite (sid ) (10541 ft-md). (C) Delta plain (DP) medium grained sandstone with quartz (Qz) and localised secondary porosity due to feldspar grain dissolution (10425 ft-md. (D) Barrier shoreline (BS) fine to medium grained sandstone with secondary porosity and siderite cement (Sid) (10259 ft-md).

Figure 9. Ternary sandstone compositional diagram; (A) shoreface sandstones of the Rannoch Formation; (B) foreshore sandstones of the Etive Formation; (C) delta plain sandstones of the Ness Formation; (D) barrier shoreline sandstones of the Tarbert Formation, using the diagram of McBride (1963). All foreshore, delta plain and barrier shoreline sandstones plot within the subarkose field with the exception of only two samples from Ness Formation that plots in the quartz arenite field. Most foreshore samples are sublitharenites due to the presence of detrital mica.

Figure 10. Plane polarised images summarising the key detrital reservoir quality controls. (A and B) Shoreface, very fine sandstone with abundant detrital mica flakes deformed around more competent

quartz grains (Qz) and biotite (Bt) partly replaced by siderite (Sd) in A (10705 ft-md). Note the abundant pore-filling kaolinite (Ka) and the bent muscovite (Mu) flakes and the splayed biotite grains (Bt) in B (10712 ft-md). (C and D) Foreshore, medium grained sandstone with aggregates of lozenge shaped pore-filling siderite (Sd) in C, and abundant pore-filling kaolinite (Ka) in D (10521 ft-md). (E and F) Delta plain, medium grained sandstone with pore-filling siderite (Sd) (10425 ft-md). Note the clean fluvial sandstone in F with feldspar overgrowth (Koc) (depth 10443 ft-md). (F and G) Barrier shoreline, medium grained sandstone with open pores (depth 10259ft-md)

Figure 11. Photomicrographs illustrating the key reservoir quality controls of the very fine-grained micaceous shoreface sandstones of the foreshore sandstones of the Rannoch Formation. (A) BSEM image showing feldspar dissolution; a common diagenetic feature in these shoreface sandstones. Also note the grains compaction and the splayed biotite (Bt) with siderite (Sd) within the flakes (10754ft-md). (B) BSEM image showing framboidal pyrite (Pf), pore-filling pyrite (Ppf), lozenge-shape siderite (Sd) within the flakes of replacive biotite grains and syntaxial quartz overgrowths (10566 ft-md). (C) BSEM image of pervasive carbonate cemented interval in the shoreface sandstones of the Rannoch Formation, note the poikilotopic calcite (Cc) cement with floating quartz (Qz) grains (10711.42 ft-md). (D) BSEM image depicting the compaction of the detrital grains with grain contacts and deformed mica grains (10754 ft-md). (E) BSEM image showing pore-filling framboidal pyrite (Pf) clay matrix and feldspar cement growth (Koc) (10517ft-md). (F) BSEM image illustrating the major reservoir quality controlling, pore-filling kaolinite (Ka) (10673ft-md) .

Figure 12. SEM-EDS images illustrating the key reservoir quality controls. (A) Image of pore-filling kaolinite in the fine-grained shoreface sandstone. Note the grains compaction and the splayed biotite with siderite within the flakes (10566 ft-md). (B and C) Images showing the very fine grained shoreface sandstone with chlorite replacing biotite grain (Bt) and abundant pore-filling kaolinite within the pores. Note the siderite (Sd) sits within the flakes of biotite (Bt) (10754 ft-md) g pore-filling kaolinite; a common porosity occluding cement in the moderately well sorted foreshore sandstone. Also note the plagioclase grain enclosed by kaolinite (Ka) (10521 ft-md) (D) Image showing the lozenge-shape pore-filling siderite in foreshore sandstone (10485 ft-md). Colour key to SEM-EDS images shown to the right of the image.

Figure 13. SEM-EDS images illustrating further key reservoir quality controls. (A) Abundant pore-filling siderite; a common porosity occluding cement in the bioturbated delta plain sandstones (10337 ft-md). (B) Pore-filling kaolinite in channel-fill delta plain sandstones (10425 ft-md). (C) Abundant pore-filling siderite and kaolinite; a common porosity-occluding cement in the fine-grained, barrier

shoreline sandstones (10257 ft-md). (D) Medium grained sandstone with sparse pore-filling kaolinite in the barrier shoreline sandstones (10274 ft-md). Key to SEM-EDS images shown in Figure 12.

Figure 14. SEM-CL and SEI images of polished thin sections and stubs showing evidence of relatively small quantity of authigenic quartz cement in the Brent Group (SF: shoreface sandstones of the Rannoch Fm., UFS: foreshore sandstones of the Etive Fm., DP: delta plain sandstones of the Ness Fm., BS: barrier shoreline sandstones of the Tarbert Fm. (A and B) CL and SEM images of minor quartz and K-feldspar cement (10614 ft-md). (C and D) CL and SEM images of minor quartz cement (Qoc) and K-feldspar dissolution (10451 ft-md) (E and F) CL and SEM images of minor quartz cement and vermicular kaolinite (10377 ft-md). (G and H) CL and SEM images of minor quartz cement (Qoc) and abundant K-feldspar cement (10257 ft-md).

Figure 15. Burial history diagrams of a well 211/18a-A33 modelled using BasinMod® software package. Plot of temperature (°C) and age of the whole drilled succession. Vitrinite reflectance data collected from the five coaly intervals of the Brent Group succession were used to constrain the model. The Brent Group burial history is highlighted in grey. Note the relatively shallow and slow burial during the Middle Jurassic to Early Cretaceous and then rapid burial during the Late Cretaceous and Tertiary.

Figure 16. Overall paragenetic sequence common for all depositional environments (and formations) represented by the Brent Group, highlighted with porosity destruction processes (red) and porosity enhancement processes (blue). The various processes have been split between early and late by the black line, Early are eogenetic processes; late are Mesogenetic processes. Evidence of the paragenetic sequence from the petrographic observation are as follows: mechanical compaction (Figs. 10B and G, 11A and 12A), framboidal pyrite (Fig. 11B and E, 12D and 13D), biotite dissolution (Fig. 11A, 12A and B), feldspar dissolution (Figs. 8B, C and D, 11A) siderite precipitation, early (Figs. 8A, 11 A-C, 12 A-B) and late (Fig. 8B and D, 10C-E and G, 12C and D, 13 A-B) , calcite precipitation; early (Fig. 11 C) and late (Figs. 12B and 13C), kaolinite precipitation (Figs.10B, 11C and F, 12A-C, 13 B), K-feldspar overgrowth (Fig. 11E), chlorite precipitation (Figs. 12A-B and 13A-B) , illite replacement (Figs.12A-B, 13B-C), pore-filling pyrite (Figs. 11B, 12D, 13D) chemical compaction (Figs. 11A, 14C), quartz overgrowth (Figs. 11B, 14A-H).

Figure 17. Comparison of kaolinite to porosity and muscovite, with all data derived from SEM-EDS analysis. Sandstones have been split into different depositional environments; SF: shoreface sandstones (Rannoch), FS: foreshore (Etive), DP: delta plain (Ness) and BS: barrier shoreline (Tarbert). (A) Kaolinite versus muscovite showing good positive correlation suggesting that kaolinite may have been sourced from muscovite. (B) Kaolinite versus porosity showing good negative correlation of

increasing kaolinite content with decreasing porosity indicating that kaolinite is a major control on reservoir quality.

Figure 18. Bar diagrams with a display of reservoir quality parameters versus depth (n=40) from the shoreface (Rannoch), foreshore (Etive), delta plain (Ness) and barrier shoreline (Tarbert) sandstones. Note the variation of the various reservoir quality parameters with depth; a general trend of porosity, permeability and grain size decrease with depth and the percentage of compactional porosity loss (COPL) increase with depth indicating that compactional processes dominated porosity loss in the sandstones. Sample from delta plain sandstone at depth 10337ft marked by (*) cannot have CEPL and COPL due to the presence of pore-filling siderite and abundant grain replacive siderite that are hard to differentiate.

Figure 19. Plots of reservoir properties, defined using point counting, split by different depositional environments; SF: shoreface (Rannoch), FS: foreshore (Etive), DP: delta plain (Ness) and BS: barrier shoreline (Tarbert) sandstones: (A) core permeability versus mean grain size, (B) core permeability versus sorting (Trask) (C) core porosity versus mean grain size, (D) core porosity versus sorting (Trask). Note the plots indicate that grain size control the reservoir quality of the sandstones with the best reservoir quality in delta plain and foreshore sandstones and worst in shoreface and barrier shoreline sandstones. Sorting does not seem to have any effect on the reservoir quality.

Figure 20. Comparison of porosity to permeability with data divided by the two main reservoir quality controls and split into different depositional environments; SF: shoreface sandstones (Rannoch), FS: foreshore (Etive), DP: delta plain (Ness) and BS: barrier shoreline(Tarbert). The symbols in these diagrams are all the same shape to facilitate better comparison of the fourth variables: kaolinite and grain size; the data points have also been sized according to SEM-EDS-derived kaolinite content. (A) Grain size exerts a significant control on reservoir quality of the Brent sandstones with finer grain size equating to lower core analysis porosity and permeability. (B) Kaolinite also exerts a significant control on reservoir quality of the Brent sandstones with more kaolinite equating to lower core analysis porosity and permeability. The samples arrowed (i) and (ii) in parts A and B are anomalous. Sample (i) is foreshore sandstones that is unusually matrix rich (See Appendix A, Etive Formation sample 10521ft (DD). Sample (ii) is a delta plain sandstone that contains an anomalous quantity of siderite (16%) that has blocked pore throats but left pores relatively open thus diminishing permeability more than porosity (See Figure 13A).

Figure 21. Plot of core analysis porosity and permeability with the data split by depositional environment (parts A to D) and coloured by the wireline log-derived Vshale (equation 1) for each core analysis plug point. Small red symbols equate to low Vshale. Large blue symbols equate to high

Vshale. (A) Shoreface sandstones tend not to have the lowest Vshale values found in the three other depositional environments, although the very low-porosity, highly calcite-cemented samples (marked), have low Vshale (radioactive, K-rich clay-mineral content). There is a subtle decrease in Vshale as porosity increases, which is a common pattern for all four environments. (B) The foreshore sandstones tend to have high porosity and permeability and low Vshale. (C) Delta plain samples have a wide range of reservoir quality commensurate with the log data (Fig. 3) and the wide range of Vshale values; Vshale increases as porosity decreases but there is no simple relationship between the ranges of permeability for a given porosity and Vshale. (D) The barrier shoreline samples broadly resemble the foreshore samples in terms of porosity, permeability and Vshale.

Figure 22. Plots of intergranular volume (IGV) versus volume of cement (Houseknecht, 1988) from the four depositional environments. (A) Shoreface sandstones (Rannoch Fm), (B) Foreshore sandstones (Etive Fm), (C) Delta plain sandstones (Ness Fm.) and (D) Barrier shoreline sandstones (Tarbert Fm.). The plot shows that the porosity-loss is due to both compaction and cementation. Samples from the pervasively calcite cemented intervals of the shoreface sandstone (part A) are anomalous compared to the other sandstones. The lower intergranular porosity (and core analysis porosity) of the shoreface sandstones is a result of more compaction-dominated porosity-loss compared to the other sandstones.

Figure 23. Plot of field-average permeability for Brent Group sandstones from the northern North Sea area versus depth to the crest of each field, with symbols graded by the temperature of the reservoir; all data taken from Figure 10.21 from the Millennium Atlas (Husmo et al., 2003). The Thistle Field, the subject of this study, is present in the middle of the ranges of depth, temperature and permeability. Deeper reservoirs are hotter, as expected, and tend to have lower permeability, and vice versa. The Thistle Field represents a moderately compacted sandstone with relatively little development of pore-filling cement. Shallower Brent Group sandstones tend to have higher permeability as they are less compacted and probably have less kaolinite. Deeper Brent Group sandstones tend to have lower permeability as they undergo kinetically-controlled growth of quartz, illite and, possibly, dolomite cements at temperatures significantly in excess of 100°C. The spread in the data is the result of locally variable initial sand composition, unknown degrees of localised uplift and cooling, variable thermal histories and effective stress histories,

**Table captions**

Table. 1 Brent Thistle well 211/18a-A33 sedimentary facies details description tabulated with facies code, descriptions of grain size, structures/bioturbation, interpreted depositional environment of the

Brent sandstones. The facies were arranged by; (a) broad group sandstone facies and (b) silty-sandstone, siltstones, mudstone and coal.

Table 2. SEM-EDS normalised mineralogy data for the 40 sandstone samples selected from the Rannoch, Etive, Ness and Tarbert Formations from the Brent Group from well 211/18a-A33.

Table 3. Pearson's Correlation Coefficient matrix calculated from the SEM-EDS mineral map and background data. For P=values <0.05[x], the correlation is statistically significant. P values of P<0.01[xx] and P<0.001[xxx] represent very and extremely significant correlations.

Appendix 1. Point count data for the 40 sandstone samples selected from the Rannoch, Etive, Ness and Tarbert Formations from the Brent Group from well 211/18a-A33. (proposed to be an online resource)

**References**


Aase, N. E., Bjørkum, P. A., and Nadeau, P. H., 1996a, The effect of grain-coating microquartz on preservation of reservoir porosity: American Association of Petroleum Geologists Bulletin, v. 80, no. 10, p. 1654-1673.

Aase, N. E., Bjørkum, P. A., and Nadeau, P. H., 1996b, The effect of grain-coating microquartz on preservation of reservoir porosity: AAPG bulletin, v. 80, no. 10, p. 1654-1673.

Ajdukiewicz, J. M., and Lander, R. H., 2010, Sandstone reservoir quality prediction: The state of the art: American Association of Petroleum Geologists Bulletin, v. 94, no. 8, p. 1083-1091.

Alcalde, J., Heinemann, N., Mabon, L., Worden, R. H., Maver, M., Robertson, H., Ghanbari, S., Swennenhuis, F., Mann, I., Walker, T., Gomersal, S., Allen, M. J., Bond, C. E., Haszeldine, R. S., James, A., Mackay, E. J., de Coninck, H., Faulkner, D. R., and Murphy, S., 2019, Developing full-chain industrial carbon capture and storage in a resource- and infrastructure-rich hydrocarbon province: Journal of Cleaner Production, v. 233, p. 963-971.

Ali, A. D., and Turner, P. J., 1982, Authigenic K-feldspar in the Bromsgrove Sandstone Formation (Triassic) of central England: Journal of Sedimentary Petrology, v. 52, p. 187-197.

Andresen, B., Throndsen, T., Barth, T., and Bolstad, J., 1994, Thermal generation of carbon dioxide and organic acids from different source rocks: Organic Geochemistry, v. 21, no. 12, p. 1229-1242.

Armitage, P. J., Worden, R. H., Faulkner, D. R., Aplin, A. C., Butcher, A. R., and Iliffe, J., 2010, Diagenetic and sedimentary controls on porosity in Lower Carboniferous fine-grained lithologies, Krechba field, Algeria: A petrological study of a caprock to a carbon capture site: Marine and Petroleum Geology, v. 27, no. 7, p. 1395-1410.

Ashcroft, W. A., and Ridgway, M. S., 1996, Early discordant diagenesis in the Brent Group, Murchison Field, UK North Sea, detected in high values of seismic-derived acoustic impedance: Petroleum Geoscience, v. 2, no. 1, p. 75-81.

Barth, T., and Riis, M., 1992, Interactions between organic-acid anions in formation waters and reservoir mineral phases: Organic Geochemistry, v. 19, no. 4-6, p. 455-482.

Bauluz, B., Mayayo, M. J., Yuste, A., and Lopez, J. M. G., 2008, Genesis of kaolinite from Albian sedimentary deposits of the Iberian Range (NE Spain): analysis by XRD, SEM and TEM: Clay Minerals, v. 43, no. 3, p. 459-475.

Bayat, M. G., and Tehrani, D. H., 1985, The Thistle Field - Analysis Of Its Past Performance And Optimisation Of Its Future Development, Offshore Europe: Aberdeen, United Kingdom, Society of Petroleum Engineers, p. 27.

Beard, D. C., and Weyl, P. K., 1973, Influence of texture on porosity and permeability of unconsolidated sand: American Association of Petroleum Geologists Bulletin, v. 57, p. 349-369.

Berner, R. A., 1980, Early diagenesis, a theoretical approach., Princeton, Princeton University Press.

Berner, R. A., 1984, Sedimentary pyrite formation - an update: Geochimica et Cosmochimica Acta, v. 48, no. 4, p. 605-615.

Bjorkum, P. A., and Gjelsvik, N., 1988, An isochemical model for formation of authigenic kaolinite, K-feldspar and illite in sediments: Journal of Sedimentary Research, v. 58, no. 3, p. 506-511.

Bjørlykke, K., 1980, Clastic diagenesis and basin evolution: Revista del Instituto de Investigaciones Geológicas. Diputación Provincial, Universidad de Barcelona, v. 34, p. 21-44.

Bjørlykke, K., and Aagaard, P., 1992, Clay minerals in the North Sea: In: Origin, diagenesis and petrophysics of clay minerals in sandstones (eds. Houseknecht, D.W. and Pittman, E.D.) SEPM Special Publication, v. 47, p. 65-80.

Bjørlykke, K., and Brendsdal, A., 1986, Diagenesis of the Brent Sandstone in the Statfjord Field, North Sea: Roles of organic matter in sediment diagenesis, p. 157-167.

Bjørlykke, K., Nedkvitne, T., Ramm, M., and Saigal, G., 1992, Diagenetic processes in the Brent Group (Middle Jurassic) reservoirs of the North Sea: an overview, *in* Morton, A. C., Haszeldine, R. S., Giles, M. R., and Brown, S., eds., Geology of the Brent Group. Special Publication, Volume 61: London, The Geological Society, p. 263-287.

Blackbourn, G. A., 1984, Diagenetic history and reservoir quality of a Brent sand sequence: Clay Minerals, v. 19, no. 3, p. 377-389.

Bloch, S., and Helmold, K. P., 1995, Approaches to predicting reservoir quality in sandstones: American Association of Petroleum Geologists Bulletin, v. 79, no. 1, p. 97-115.

Brown, S., and Richards, P. C., 1989, Facies and development of the mid-Jurassic Brent delta near the northern limit of its progradation, UK North Sea, *in* Whateley, M. K. G., and Pickering, K. T., eds., Deltas: Sites and Traps for Fossil Fuels, Volume 41: London, The Geological Society, p. 253-267.

Budding, M. C., and Inglin, H. F., 1981, A reservoir geological model of the Brent sands in Southern Cormorant, *in* Illing, L. V., and Hobson, G. D., eds., Petroleum Geology of the Continental Shelf of North-West Europe: London, Heyden, p. 326-334.

Cade, C. A., Evans, I. J., and Bryant, S. L., 1994, Analysis of permeability controls - a new approach: Clay Minerals, v. 29, no. 4, p. 491-501.

Cannon, S. J. C., Giles, M. R., Whitaker, M. F., Please, P. M., and Martin, S. V., 1992, A regional assessment of the Brent Group, UK sector, North Sea, *in* Morton, A. C., Haszeldine, R. S., Giles, M. R., and Brown, S., eds., Geology of the Brent Group. Special Publication, Volume 61: London, Geological Society, p. 81-107.

Cassagnabère, A., Iden, I., Johansen, H., Lacharpagne, J., and Beaufort, D., Kaolinite and dickite in Frøy and Rind sandstone hydrocarbon reservoirs of the Brent Formation (Norwegian Continental Shelf), *in* Proceedings Clays for our Future: Proceedings of the 11th International Clay Conference1999, ICC97 Organizing Committee, Ottawa, p. 97-102.

Chapelle, F., 2001, Ground-water microbiology and geochemistry, John Wiley & Sons.

Chuhan, F. A., Bjørlykke, K., and Lowrey, C., 2000, The role of provenance in illitization of deeply buried reservoir sandstones from Haltenbanken and north Viking Graben, offshore Norway: Marine and Petroleum Geology, v. 17, no. 6, p. 673-689.

Crowley, S. F., 1991, Diagenetic modification of detrital muscovite - an example from the Great Limestone Cyclothem (Carboniferous) of Co Durham, UK: Clay Minerals, v. 26, no. 1, p. 91-103.

Daws, J. A., 1992, Sedimentology, diagenesis and reservoir characterisation of the Brent Group in the North Viking Graben-East Shetland Basin, northern North Sea [PhD: Aberdeen.

Deegan, C. E., and Scull, B. J., 1977, A standard lithostratigraphic nomenclature for the Central and Northern North Sea: Report of the Institute of Geological Sciences.

Deros, L. F., Sgarbi, G. N. C., and Morad, S., 1994, Multiple authigenesis of K-feldspar in sandstones - evidence from te Cretaceous Areado Formation, Sao Fransisco Basin, Central Brazil: Journal of Sedimentary Research Section a-Sedimentary Petrology and Processes, v. 64, no. 4, p. 778-787.

Ehrenberg, S., 1993a, Preservation of anomalously high porosity in deeply buried sandstones by grain-coating chlorite: examples from the Norwegian continental shelf: AAPG Bulletin, v. 77, no. 7, p. 1260-1286.

Ehrenberg, S., and Jakobsen, K., 2001, Plagioclase dissolution related to biodegradation of oil in Brent Group sandstones (Middle Jurassic) of Gullfaks Field, northern North Sea: Sedimentology, v. 48, no. 4, p. 703-721.

Ehrenberg, S. N., 1990, Relationship between diagenesis and reservoir quality in sandstones of the Garn Formation, Haltenbanken, mid-Norwegian continental shelf: American Association of Petroleum Geologists Bulletin, v. 74, no. 10, p. 1538-1558.

-, 1993b, Preservation of anomalously high-porosity in deeply buried sandstones by grain coating chlorite - examples from the Norwegian continental shelf: American Association of Petroleum Geologists Bulletin, v. 77, no. 7, p. 1260-1286.

Ehrenberg, S. N., and Nadeau, P. H., 1989, Formation of diagenetic illite in sandstones of the Garn Formation, Haltenbanken area, mid-Norwegian continental shelf: Clay Minerals, v. 24, no. 2, p. 233-253.

Emery, D., and Robinson, A. G., 1993, Inorganic geochemistry: application to petroleum geology, Oxford, Blackwell, 254 p.:

EnQuest, 2018, Results for the year ended 31 December 2017 and 2018 outlook

Farrell, K. M., Harris, W. B., Mallinson, D. J., Culver, S. J., Riggs, S. R., Pierson, J., Self-Trail, J. M., and Lautier, J. C., 2012, Standardizing texture and facies codes for a process-based classification of clastic sediment and rock: Journal of Sedimentary Research, v. 82, no. 6, p. 364-378.

Gier, S., Worden, R. H., Johns, W. D., and Kurzweil, H., 2008, Diagenesis and reservoir quality of Miocene sandstones in the Vienna Basin, Austria: Marine and Petroleum Geology, v. 25, no. 8, p. 681-695.

Gier, S., Worden, R. H., and Krois, P., 2018, Comparing clay mineral diagenesis in interbedded sandstones and mudstones, Vienna Basin, Austria, *in* Armitage, P. J., Butcher, A., Churchill, J., Csoma, A., Hollis, C., Lander, R. H., Omma, J., and Worden, R. H., eds., Reservoir Quality of Clastic and Carbonate Rocks: Analysis, Modelling and Prediction. Special Publication, Volume 435: London, Geological Society, p. 389-404.

Giles, M. R., Stevenson, S., Martin, S. V., Cannon, S. J. C., Hamilton, P. J., Marshall, J. D., and Samways, G. M., 1992, The reservoir properties and diagenesis of the Brent Group: a regional perspective, *in* Morton, A. C., Haszeldine, R. S., Giles, M. R., and Brown, S., eds., Geology of the Brent Group, Volume 61: London, The Geological Society, p. 289-327.

Girard, J. P., Munz, I. A., Johansen, H., Hill, S., and Canham, A., 2001, Conditions and timing of quartz cementation in Brent reservoirs, Hild Field, North Sea: constraints from fluid inclusions and SIMS oxygen isotope microanalysis: Chemical Geology, v. 176, no. 1-4, p. 73-92.

Girard, J. P., Munz, I. A., Johansen, H., Lacharpagne, J. C., and Sommer, F., 2002, Diagenesis of the Hild Brent sandstones, northern North Sea: Isotopic evidence for the prevailing influence of deep basinal water: Journal of Sedimentary Research, v. 72, no. 6, p. 746-759.

Glover, J., and Hosemann, P., 1970, Optical data on some authigenic feldspars from Western Australia: Mineralogical Magazine, v. 37, no. 289, p. 588-592.

Hamlin, H. S., Dutton, S. P., Seggie, R. J., and Tyler, N., 1996, Depositional controls on reservoir properties in a braid-delta sandstone, Tirrawarra oil field, South Australia: American Association of Petroleum Geologists Bulletin, v. 80, no. 2, p. 139-156.

Harris, N. B., 1992, Burial diagenesis of Brent sandstones: a study of Statfjord, Hutton and Lyell fields, *in* Morton, A. C., Haszeldine, R. S., Giles, M. R., and Brown, S., eds., Geology of the Brent Group. Special Publication, Volume 61: London, Geological Society, p. 351-375.

Higgs, K. E., Zwingmann, H., Reyes, A. G., and Funnell, R. H., 2007, Diagenesis, porosity evolution, and petroleum emplacement in tight gas reservoirs, Taranaki Basin, New Zealand: Journal of Sedimentary Research, v. 77, no. 11-12, p. 1003-1025.

Houseknecht, D. W., 1987, Assessing the relative importance of compaction processes and cementation to reduction of porosity in sandstones: American Association of Petroleum Geologists Bulletin, v. 71, no. 6, p. 633-642.

-, 1988, Intergranular pressure solution in four quartzose sanstones: Journal of Sedimentary Petrology, v. 58, no. 2, p. 228-246.

Huggett, J., Ashcroft, W. A., and Ridgway, M. S., 1997, Discussion on early discordant diagenesis in the Brent Group, Murchison Field, UK North Sea, detected in high values of seismic-derived acoustic impedance: Petroleum Geoscience, v. 3, no. 1, p. 95-96.

Hurst, A., and Irwin, H., 1982, Geological modelling of clay diagenesis in sandstones: Clay minerals, v. 17, no. 1, p. 5-22.

Husmo, T., Hamar, G. P., Hoiland, O., Johennessen, E. P., Romuld, A., Spencer, A. M., and Titterton, R., 2003, Lower and Middle Jurassic, *in* Evans, D., and Graham, C. G., eds., The Millenium Atlas: petroleum geology of the central and northern North Sea: London, The Geological Society, p. 129-155.

Jahren, J., Olsen, E., and Bjørlykke, K., 1998, Chlorite coatings in deeply buried sandstones - Examples from the Norwegian continental shelf, Water-Rock Interaction, 321-324 p.:

Jahren, J., and Ramm, M., 2000, The porosity-preserving effects of microcrystalline quartz coatings in arenitic sandstones: Examples from the Norwegian continental shelf, *in* Worden, R. H., and Morad, S., eds., Spcial publication-international association of sedimentologists, Volume 29: Oxford, Blackwells.

Kantorowicz, J. D., 1985, The petrology and diagenesis of Middle Jurassic clastic sediments, Ravenscar Group, Yorkshire: Sedimentology, v. 32, no. 6, p. 833-853.

Lander, R. H., and Walderhaug, O., 1999, Predicting porosity through simulating sandstone compaction and quartz cementation: American Association of Petroleum Geologists Bulletin, v. 83, no. 3, p. 433-449.

Lundegard, P. D., 1994, Mixing zone origin of C-13-depleted calcite cement - Oseberg Formation Sandstones (Middle Jurassic), Veslefrikk Field, Norway: Geochimica et Cosmochimica Acta, v. 58, no. 12, p. 2661-2675.

Luo, J. L., Morad, S., Salem, A., Ketzer, J. M., Lei, X. L., Guo, D. Y., and Hlal, O., 2009, Impact of diagenesis on reservoir quality evolution in fluvial and lacustrine-deltaic sandstones: evidence from Jurassic and Triassic sandstones from the Ordos Basin, China: Journal of Petroleum Geology, v. 32, no. 1, p. 79-102.

Macaulay, C. I., Fallick, A., McLaughlin, O. M., Haszeldine, R. S., and Pearson, M. J., 1998, The significance of $\delta^{13}C$ of carbonate cement in reservoir sandstones; a regional perspective from the Jurassic of the Northern North Sea, *in* Morad, S., ed., Carbonate cementation in sandstones. Special Publication of the International Association of Sedimentologists, Volume 26: Oxford, Blackwells, p. 395-408.

Marcussen, O., Maast, T. E., Mondol, N. H., Jahren, J., and Bjørlykke, K., 2010a, Changes in physical properties of a reservoir sandstone as a function of burial depth - The Etive Formation, northern North Sea: Marine and Petroleum Geology, v. 27, no. 8, p. 1725-1735.

Marcussen, Ø., Maast, T. E., Mondol, N. H., Jahren, J., and Bjørlykke, K., 2010b, Changes in physical properties of a reservoir sandstone as a function of burial depth–The Etive Formation, northern North Sea: Marine and Petroleum Geology, v. 27, no. 8, p. 1725-1735.

Marfil, R., Delgado, A., Rossi, C., Iglesia, A. L., and Ramseyer, K., 2003, Origin and diagenetic evolution of kaolin in reservoir sandstones and associated shales of the Jurassic and Cretaceous, Salam Field, Western Desert (Egypt): Clay Mineral Cement in Sandstones, p. 319-342.

Martinius, A. W., Ringrose, P. S., Brostrom, C., Elfenbein, C., Naess, A., and Ringas, J. E., 2005, Reservoir challenges of heterolithic tidal sandstone reservoirs in the Halten Terrace, mid-Norway: Petroleum Geoscience, v. 11, no. 1, p. 3-16.

Matsumoto, R., and Iijima, A., 1981, Origin and diagenetic evolution of Ca–Mg–Fe carbonates in some coalfields of Japan: Sedimentology, v. 28, no. 2, p. 239-259.

Matthews, J. C., Velde, B., and Johansen, H., 1994, Significance of K-Ar ages of authigenic illitic clay minerals in sandstones and shales from the North Sea: Clay Minerals, v. 29, no. 3, p. 379-389.

McAulay, G. E., Burley, S. D., Fallick, A. E., and Kusznir, N. J., 1994, Palaeohydrodynamic fluid flow regimes during diagenesis of the Brent Group in the Hutton-NW Hutton reservoirs - constraints from oxygen isotope studies of authigenic kaolinite and reverse flexural modelling: Clay Minerals, v. 29, no. 4, p. 609-626.

McAulay, G. E., Burley, S. D., and Johnes, L. H., 1993, Silicate mineral authigenesis in the Hutton and NW Hutton fields - implications for subsurface porosity development, *in* Parker, J. R., ed., Petroleum Geology of Northwest Europe: Proceedings of the 4th Conference: Bath, Geological Soc Publishing House, p. 1377-1394.

McBride, E. F., 1963, A classification of common sandstones: Journal of Sedimentary Petrology, v. 33, p. 664-669.

McKinley, J. M., Worden, R. H., and Ruffell, A. H., 2003, Smectite in sandstones: A review of the controls on occurrence and behaviour during diagenesis, *in* Worden, R. H., and Morad, S., eds.,

Clay mineral cements in sandstones, Special Publication of the International Association of Sedimentologists, Volume 34: Oxford, Blackwells, p. 109-128.

Meadows, N. S., and Beach, A., 1993, Controls on reservoir quality in the Triassic Sherwood Sandstone of the Irish Sea, *in* Parker, J. R., ed., Petroleum Geology of Northwest Europe: Proceedings of the 4th Conference, p. 823-833.

Mitchener, B. C., Lawrence, D. A., Partington, M. A., Bowman, M. B. J., and Gluyas, J., 1992, Brent Group: sequence stratigraphy and regional implications, *in* Morton, A. C., Haszeldine, R. S., Giles, M. R., and Brown, S., eds., Geology of the Brent Group. Special Publication, Volume 61: London, Geological Society, p. 45-80.

Morad, S., 1990, Mica alteration reactions in Jurassic reservoir sandstones from the Haltenbanken area, offshore Norway: Clays and Clay Minerals, v. 38, no. 6, p. 584-590.

Morad, S., Al-Ramadan, K., Ketzer, J. M., and De Ros, L. F., 2010, The impact of diagenesis on the heterogeneity of sandstone reservoirs: A review of the role of depositional facies and sequence stratigraphy: American Association of Petroleum Geologists Bulletin, v. 94, no. 8, p. 1267-1309.

Morad, S., Bergan, M., Knarud, R., and Nystuen, J. P., 1990, Albitization of detrital plagioclase in Triassic reservoir sandstones from the Snorre Field, Norwegian North Sea: Journal of Sedimentary Research, v. 60, no. 3, p. 411-425.

Morad, S., and De Ros, L. F., 1994, Geochemistry and diagenesis of stratabound calcite cement layers within the Rannoch Formation of the Brent Group, Murchison Field, North Viking Graben (Northern North Sea) - Comment: Sedimentary Geology, v. 93, no. 1-2, p. 135-141.

Morad, S., Ketzer, J. M., and De Ros, L. F., 2000, Spatial and temporal distribution of diagenetic alterations in siliciclastic rocks: implications for mass transfer in sedimentary basins: Sedimentology, v. 47, p. 95-120.

Morton, A. C., 1992, Provenance of Brent Group sandstones: heavy mineral constraints, *in* Morton, A. C., Haszeldine, R. S., Giles, M. R., and Brown, S., eds., Geology of the Brent Group. Special Publication, Volume 61: London, Geological Society, p. 227-244.

Moss, B., 1992, The petrophysical characteristics of the Brent sandstones, *in* Morton, A. C., Haszeldine, R. S., Giles, M. R., and Brown, S., eds., Geology of the Brent Group. Special Publication, Volume 61: London, Geological Society, p. 471-496.

Mozley, P. S., 1989, Complex compositional zonation in concretionary siderite - implications for geochemical studies: Journal of Sedimentary Petrology, v. 59, no. 5, p. 815-818.

Mozley, P. S., and Wersin, P., 1992, Isotopic composition of siderite as an indicator of depositional environment: Geology, v. 20, no. 9, p. 817-820.

Nadir, F., 1981, Thistle field development: Journal of Petroleum Technology, v. 33, no. 10, p. 1,828-821,834.

Nadir, F. T., and Hay, J. T., 1978, Geological and reservoir modelling of the Thistle field, SPE European Petroleum Conference, Society of Petroleum Engineers, p. 233-237.

Nedkvitne, T., and Bjørlykke, K., 1992, Secondary porosity in the Brent Group (Middle Jurassic), Huldra Field, North Sea: implication for predicting lateral continuity of sandstones?: Journal of Sedimentary Petrology, v. 62, no. 1, p. 23-34.

Olaussen, S., Dalland, A., Gloppen, T., and Johannessen, E., 1984, Depositional environment and diagenesis of Jurassic reservoir sandstones in the eastern part of Troms I area, Petroleum Geology of the North European Margin, Springer, p. 61-79.

Osborne, M., Haszeldine, R. S., and Fallick, A. E., 1994, Variations in kaolinite morphology with growth temperature in isotopically mixed pore-fluids, Brent Group, UK North Sea: Clay Minerals, v. 29, no. 4, p. 591-608.

Paxton, S. T., Szabo, J. O., Ajdukiewicz, J. M., and Klimentidis, R. E., 2002, Construction of an intergranular volume compaction curve for evaluating and predicting compaction and porosity loss in rigid-grain sandstone reservoirs: American Association of Petroleum Geologists Bulletin, v. 86, no. 12, p. 2047-2067.

Pirrie, D., Butcher, A. R., Power, M. R., Gottlieb, P., and Miller, G. L., 2004, Rapid quantitative mineral and phase analysis using automated scanning electron microscopy (QemSCAN): Potential applications in forensic geoscience, *in* Pye, K., and Croft, D. J., eds., Forensic Geoscience: Principles, Techniques and Applications, Volume 232: Bath, Geological Society, p. 123-136.

Powell, J. H., 2010, Jurassic sedimentation in the Cleveland Basin: a review: Proceedings of the Yorkshire Geological Society, v. 58, p. 21-72.

Prosser, D. J., Daws, J. A., Fallick, A. E., and Williams, B. P. J., 1993, Geochemistry and diagenesis of stratabound calcite cement layers within the Rannoch Formation of the Brent Group, Murchison Field, North Viking Graben (Northern North Sea): Sedimentary Geology, v. 87, no. 3-4, p. 139-164.

Ramm, M., 2000, Reservoir quality and its relationship to facies and provenance in Middle to Upper Jurassic sequences, northeastern North Sea: Clay Minerals, v. 35, no. 1, p. 77-94.

Ramm, M., and Bjørlykke, K., 1994, Porosity/depth trends in reservoir sandstones: Assessing the quantitative effects of varying pore-pressure, temperature history and mineralogy, Norwegian Shelf data: Clay minerals, v. 29, no. 4, p. 475-490.

Ramm, M., and Ryseth, A. E., 1996, Reservoir quality and burial diagenesis in the Statfjord Formation, North Sea: Petroleum Geoscience, v. 2, no. 4, p. 313-324.

Ratley, R. P., and Hayward, A. B., 1993, Sequence stratigraphy of a failed rift system: the Middle Jurassic to Early Cretaceous basin evolution of the Central and Northern North sea, *in* Parker, J. R., ed., 4th Geological society london: london, p. 215-249.

Reynolds, A. D., 1995, Sedimentology and sequence stratigraphy of the thistle field, northern north sea, *in* Steel, R. J., Felt, V. L., Johannessen, E. P., and Mathieu, C., eds., Norwegian Petroleum Society Special Publications, Volume 5, Elsevier, p. 257-271.

Richards, P. C., 1992, An introduction to the Brent Group: a literature review, *in* Morton, A. C., Haszeldine, R. S., Giles, M. R., and Brown, S., eds., Geology of the Brent Group. Special Publication, Volume 61: London, Geological Society, p. 15-26.

Richards, P. C., and Brown, S., 1986, Shoreface storm deposits in the Rannoch Formation (Middle Jurassic), North-West Hutton Oil-Field: Scottish Journal of Geology, v. 22, p. 367-375.

Rider, M., and Kennedy, M. J., 2011, The geological interpretation of well logs, Cambridge, UK, Rider-French Consulting.

Ruau, O., Pradier, B., Landais, P., and Gardette, J. L., 1996, Influence of the conditions of deposition on the chemistry and the reflectance variations of the Brent coals: Organic Geochemistry, v. 25, no. 5-7, p. 325-339.

Sanjuan, B., Girard, J. P., Lanini, S., Bourguinon, A., and Brosse, E., 2003, Geochemical modelling of diagenetic illite and quartz cement formation in Brent sandstone reservoirs: example of the Hild Field, Norwegian North Sea, *in* Worden, R. H., and Morad, S., eds., Clay Mineral Cements in Sandstones. Special Publication of the International Association of Sedimentologists, Volume 34: Oxford, Blackwells, p. 425-452.

Scotchman, I. C., 1990, Diagenetic quartzarenite and destruction of secondary porosity - an example from the Middle Jurassic Brent Sandstone of Northwest Europe - comment: Geology, v. 18, no. 8, p. 799-799.

Scotchman, I. C., Johnes, L. H., and Miller, R. S., 1989, Clay diagenesis and oil migration in Brent Group sandstones of NW Hutton Field, UK North-Sea: Clay Minerals, v. 24, no. 2, p. 339-374.

Skarpeid, S. S., Churchill, J. M., Hilton, J. P. J., Izatt, C. N., and Poole, M. T., The Knarr Field: a new development at the northern edge of the North Sea, *in* Proceedings Geological Society, London, Petroleum Geology Conference series2017, Volume 8, Geological Society of London, p. PGC8. 23.

Sneider, R. M., 1990, Introduction: Reservoir description of sandstones, *in* Barwis, J. H., McPherson, J. G., and Studlick, J. R. J., eds., Sandstone petroleum reservoirs: New York, Springer-Verlag, p. 1-3.

Swanson, B. F., 1981, A simple correlation between permeabilities and mercury capillary pressures: Journal of Petroleum Technology, v. 33, no. 12, p. 2498-2504.

Tamar-Agha, M. Y., 2009, The influence of cementation on the reservoir quality of the Risha Sandstone Member (Upper Ordovician), Risha Gas field, NE Jordan: Journal of Petroleum Geology, v. 32, no. 2, p. 193-208.

Underhill, J. R., 2003, The tectonic and stratigraphic framework of the United Kingdom's oil and gas fields, *in* Gluyas, J., and Hichens, H. M., eds., United Kingdom Oil and Gas Fields, Commemorative Millenium Volume, Memoir 20: London, The Geological Society, p. 17-59.

Van der Plas, L., and Tobi, A., 1965, A chart for judging the reliability of point counting results: American Journal of Science, v. 263, no. 1, p. 87-90.

Vinchon, C., Giot, D., OrsagSperber, F., Arbey, F., Thibieroz, J., Cros, P., Jeannette, D., and Sizun, J. P., 1996, Changes in reservoir quality determined from the diagenetic evolution of Triassic and Lower Lias sedimentary successions (Balazuc borehole, Ardeche, France): Marine and Petroleum Geology, v. 13, no. 6, p. 685-694.

Walderhaug, O., 1994a, Precipitation rates for quartz cement in sandstones determined by fluid inclusion microthermometry and temperature history modelling: Journal of Sedimentary Research Section a-Sedimentary Petrology and Processes, v. 64, no. 2, p. 324-333.

-, 1994b, Temperatures of quartz cementation in Jurassic sandstones from the Norwegian continental shelf - evidence from fluid inclusions: Journal of Sedimentary Research Section a-Sedimentary Petrology and Processes, v. 64, no. 2, p. 311-323.

Walderhaug, O., Lander, R. H., Bjørkum, P. A., Oelkers, E. H., Bjørlykke, K., and Nadeau, P. H., 2000, Modelling quartz cementation and porosity in reservoir sandstones: examples from the Norwegian continental shelf, *in* Worden, R. H., and Morad, S., eds., Quartz cementation in sandstones, Special Publication of the International Association of Sedimentologists, Volume 29: Oxford, Blackwells, p. 39-50.

Warren, E. A., and Smalley, P. C., 1994, North Sea formation water atlas, London, UK, Geological Society, Geological Society of London Memoir, 208 p.:

Went, D. J., Hamilton, R. V., Platt, N. H., and Underhill, J. R., 2013, Role of forced regression in controlling Brent Group reservoir architecture and prospectivity in the northern North Sea: Petroleum Geoscience, v. 19, no. 4, p. 307-328.

Wilkin, R. T., Barnes, H. L., and Brantley, S. L., 1996, The size distribution of framboidal pyrite in modern sediments: An indicator of redox conditions: Geochimica Et Cosmochimica Acta, v. 60, no. 20, p. 3897-3912.

Wilkinson, M., Haszeldine, R., Fallick, A., and Osborne, M., 2000, Siderite zonation within the Brent Group: microbial influence or aquifer flow?: Clay Minerals, v. 35, no. 1, p. 107-118.

Williams, R. R., and Milne, A. D., 1991, The Thistle Field, Blocks 211/18a and 211/19, UK North Sea, *in* Abbotts, I. L., ed., United Kingdom Oil and Gas Fields 25 Years Commemorative Volume, Volume 14: London, The Geological Society, p. 199-207.

Wooldridge, L. J., Worden, R. H., Griffiths, J., and Utley, J. E. P., 2018, The origin of clay-coated sand grains and sediment heterogeneity in tidal flats: Sedimentary Geology, v. 373, p. 191-209.

Worden, R. H., Armitage, P. J., Butcher, A., Churchill, J., Csoma, A., Hollis, C., Lander, R. H., and Omma, J., 2018a, Petroleum reservoir quality prediction: overview and contrasting approaches from sandstone and carbonate communities, *in* Armitage, P. J., Butcher, A., Churchill, J., Csoma, A., Hollis, C., Lander, R. H., Omma, J., and Worden, R. H., eds., Reservoir Quality of Clastic and Carbonate Rocks: Analysis, Modelling and Prediction. Special Publication, Volume 435: London, Geological Society, p. 1-31.

Worden, R. H., and Barclay, S. A., 2000, Internally-sourced quartz cement due to externally-derived CO2 in sub-arkosic sandstones, North Sea: Journal of Geochemical Exploration, v. 69, p. 645-649.

Worden, R. H., Bukar, M., and Shell, P., 2018b, The effect of oil emplacement on quartz cementation in a deeply buried sandstone reservoir: American Association of Petroleum Geologists Bulletin, v. 102, p. 49-75.

Worden, R. H., and Burley, S. D., 2003, Sandstone diagenesis: the evolution from sand to stone, *in* Burley, S. D., and Worden, R. H., eds., Sandstone diagenesis, recent and ancient. International Association of Sedimentologists Reprint Series, Volume 4, p. 3-44.

Worden, R. H., French, M. W., and Mariani, E., 2012, Amorphous silica nanofilms result in growth of misoriented microcrystalline quartz cement maintaining porosity in deeply buried sandstones: Geology, v. 40, no. 2, p. 179-182.

Worden, R. H., Griffiths, J., Wooldridge, L. J., Utley, J. E. P., Lawan, A. Y., Muhammed, D. D., Simon, N., and Armitage, P. J., 2020, Chlorite in sandstones: Earth Science-Reviews, v. 204, p. 103105.

Worden, R. H., and Morad, S., 2000, Quartz cementation in sandstones: a review of the key controversies *in* Worden, R. H., ed., Quartz cementation in sandstones.Special Publication of the International Association of Sedimentologists, Volume 29: Oxford, Blackwells, p. 1-20.

Worden, R. H., and Morad, S., 2003, Clay minerals in sandstones: controls on formation, distribution and evolution, *in* Worden, R. H., and Morad, S., eds., Clay mineral cements in sandstones. Special Publication of the International Association of Sedimentologists, Volume 34: Oxford, Blackwells, p. 3-41.

Worden, R. H., Morrall, G., Kelly, S., Mc Ardle, P., and Barshep, D. V., 2019, A renewed look at calcite cement in marine-deltaic sandstones: the Brent Reservoir, Heather Field, Northern North Sea, UK, *in* Dowey, P. J., Osborne, M. J., and Volk, H., eds., Application of Analytical Techniques to Petroleum Systems. Special Publication, Volume 484: London, Geological Society.

Worden, R. H., and Rushton, J. C., 1992, Diagenetic K-feldspar textures: a TEM study and model for diagenetic feldspar growth: Journal of Sedimentary Petrology, v. 62, no. 5, p. 779-789.

Worden, R. H., and Smalley, P. C., 2001, $H_2S$ in North Sea oil fields: importance of thermochemical sulphate reduction in clastic reservoirs, *in* Cidu, R., ed., Water-Rock Interaction 2001: Lisse, Balkema, p. 659-662.

Worden, R. H., Smalley, P. C., and Barclay, S. A., 2003, $H_2S$ and diagenetic pyrite in North Sea sandstones: due to TSR or organic sulphur compound cracking?: Journal of Geochemical Exploration, v. 78-9, p. 487-491.

Yielding, G., Badley, M. E., and Roberts, A. M., 1992, The structural evolution of the Brent Province: Geological Society, London, Special Publications, v. 61, no. 1, p. 27-43.

Ziegler, K., Coleman, M. L., and Howarth, R. J., 2001, Palaeohydrodynamics of fluids in the Brent Group (Oseberg Field, Norwegian North Sea) from chemical and isotopic compositions of formation waters: Applied Geochemistry, v. 16, no. 6, p. 609-632.

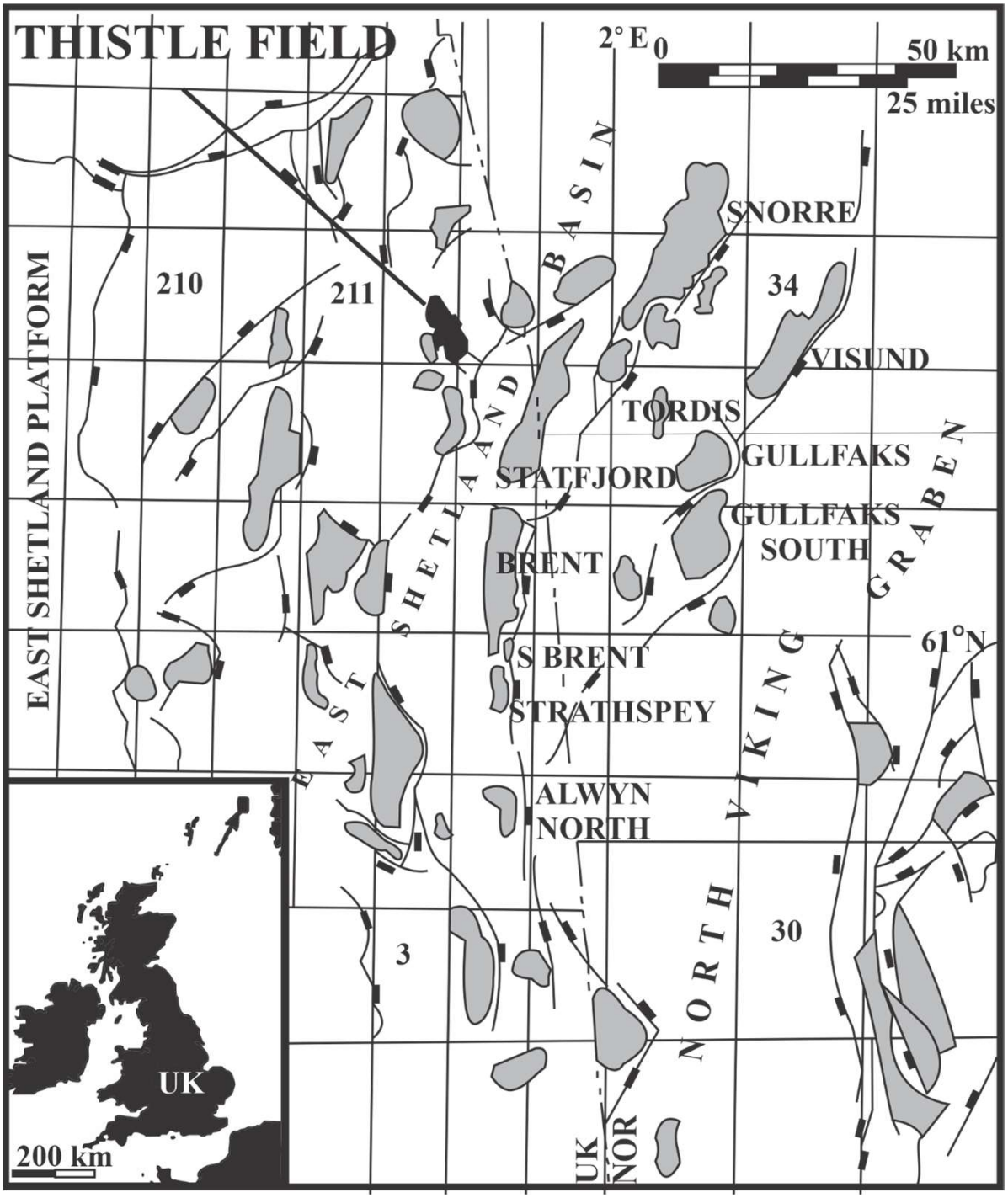
THISTLE FIELD
2° E
0
50 km
25 miles
SNORRE
34
VISUND
TORDIS
GULLFAKS
STATFJORD
GULLFAKS SOUTH
BRENT
S BRENT
STRATHSPEY
ALWYN NORTH
61°N
30
3
210
211
EAST SHETLAND BASIN
EAST SHETLAND PLATFORM
VIKING GRABEN
NORTH
UK
NOR
UK
200 km

Figure 1

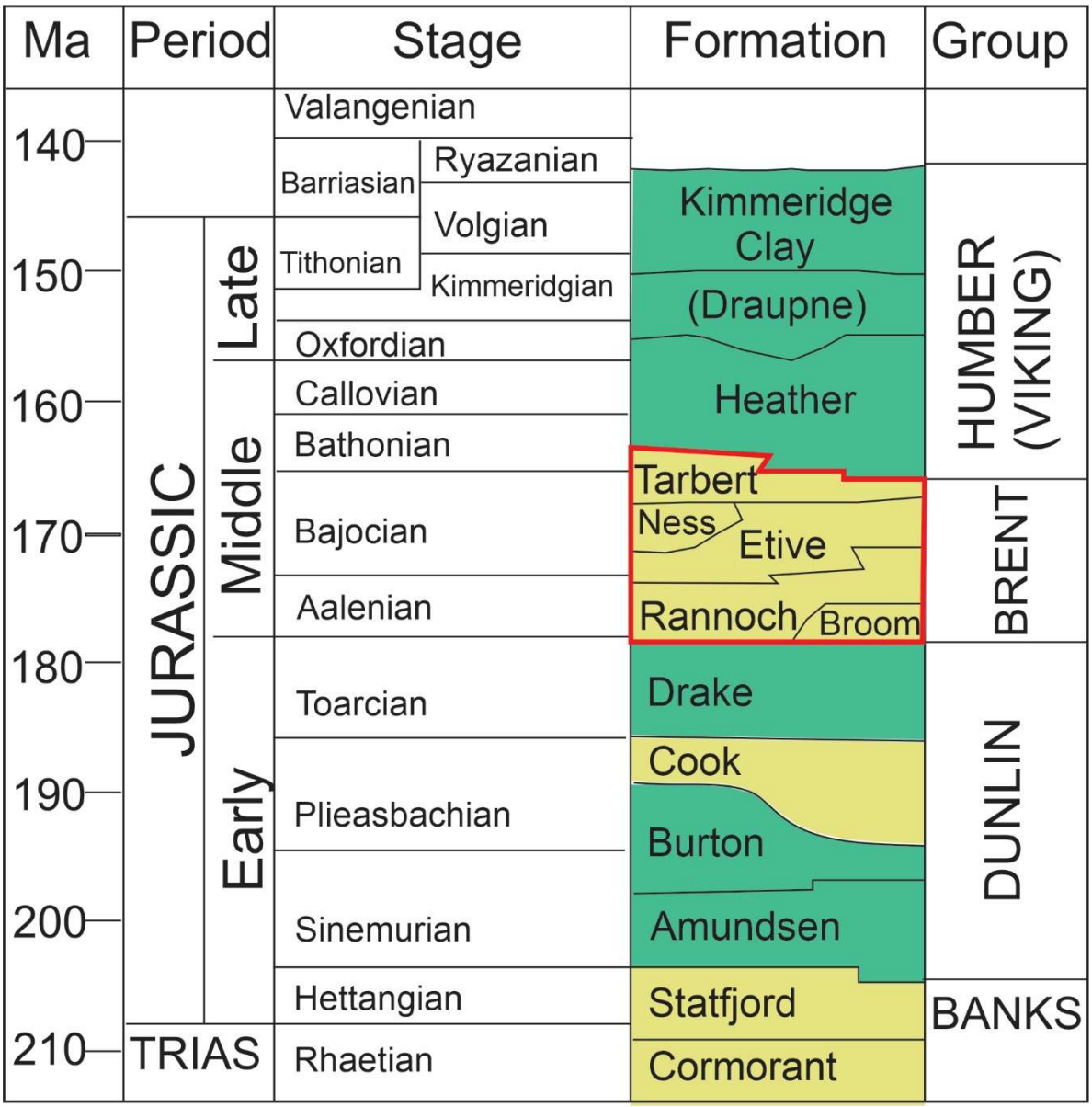
Ma
Period
Stage
Formation
Group
140
150
160
170
180
190
200
210
JURASSIC
Late
Middle
Early
TRIAS
Valangenian
Barriasian
Ryazanian
Volgian
Tithonian
Kimmeridgian
Oxfordian
Callovian
Bathonian
Bajocian
Aalenian
Toarcian
Plieasbachian
Sinemurian
Hettangian
Rhaetian
Kimmeridge Clay
(Draupne)
Heather
Tarbert
Ness
Etive
Rannoch
Broom
Drake
Cook
Burton
Amundsen
Statfjord
Cormorant
HUMBER (VIKING)
BRENT
DUNLIN
BANKS

Figure 2

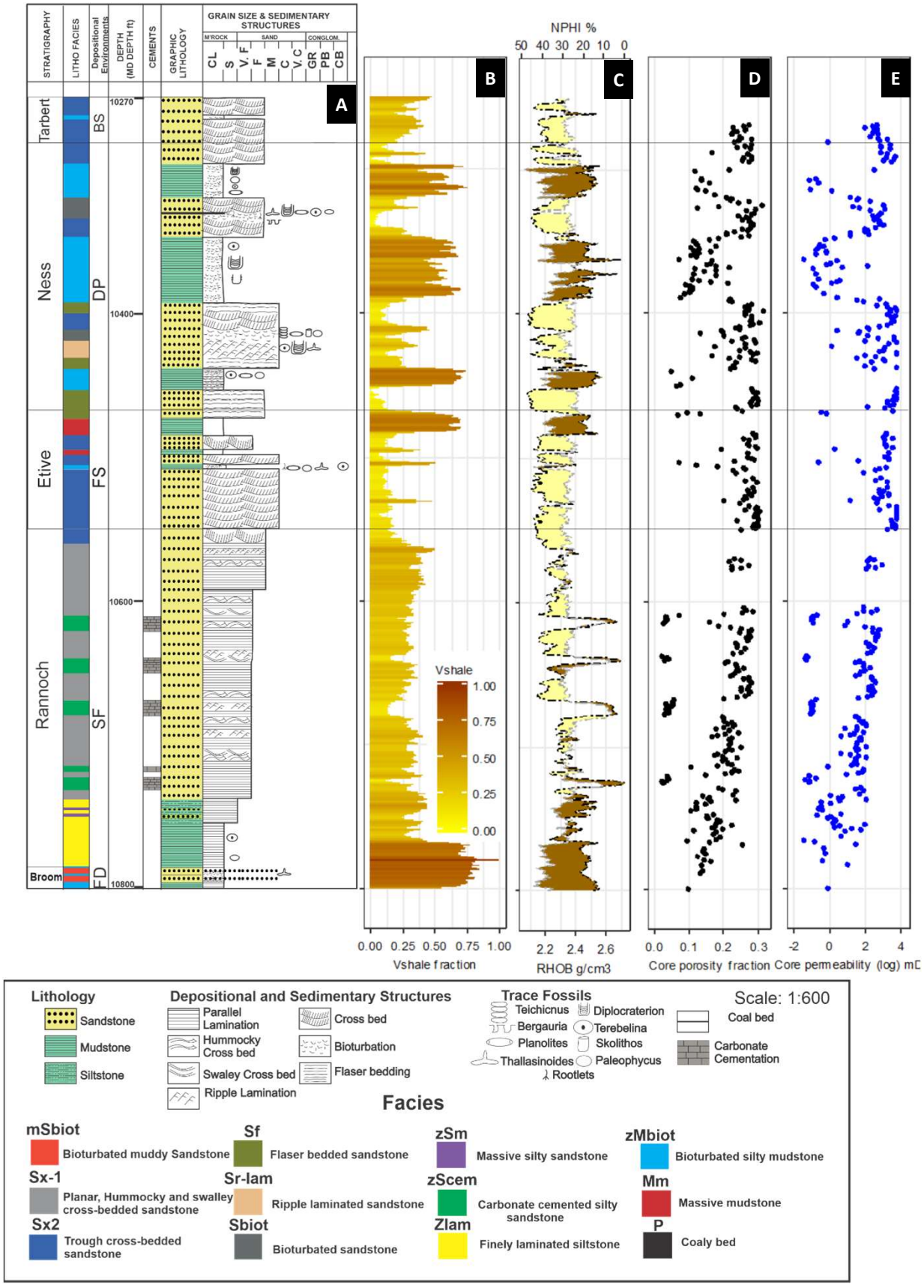
STRATIGRAPHY
LITHO FACIES
Depositional Environments
DEPTH (MD DEPTH ft)
CEMENTS
GRAPHIC LITHOLOGY
GRAIN SIZE & SEDIMENTARY STRUCTURES
M'ROCK
SAND
CONGLOM.
CL
S
V. F
F
M
C
V. C
GR
PB
CB
A
Tarbert
Ness
Etive
Rannoch
Broom
BS
DP
FS
SF
FD
10270
10400
10600
10800
B
C
D
E
NPHI %
50 40 30 20 10 0
Vshale
1.00
0.75
0.50
0.25
0.00
0.00 0.25 0.50 0.75 1.00
Vshale fraction
2.2 2.4 2.6
RHOB g/cm3
0.0 0.1 0.2 0.3
Core porosity fraction
-2 0 2 4
Core permeability (log) mD
Lithology
Sandstone
Mudstone
Siltstone
Depositional and Sedimentary Structures
Parallel Lamination
Hummocky Cross bed
Swaley Cross bed
Ripple Lamination
Cross bed
Bioturbation
Flaser bedding
Trace Fossils
Teichicnus
Bergauria
Planolites
Thallasinoides
Rootlets
Diplocraterion
Terebelina
Skolithos
Paleophycus
Coal bed
Carbonate Cementation
Scale: 1:600
Facies
mSbiot
Bioturbated muddy Sandstone
Sx-1
Planar, Hummocky and swalley cross-bedded sandstone
Sx2
Trough cross-bedded sandstone
Sf
Flaser bedded sandstone
Sr-lam
Ripple laminated sandstone
Sbiot
Bioturbated sandstone
zSm
Massive silty sandstone
zScem
Carbonate cemented silty sandstone
Zlam
Finely laminated siltstone
zMbiot
Bioturbated silty mudstone
Mm
Massive mudstone
P
Coaly bed

Figure 3

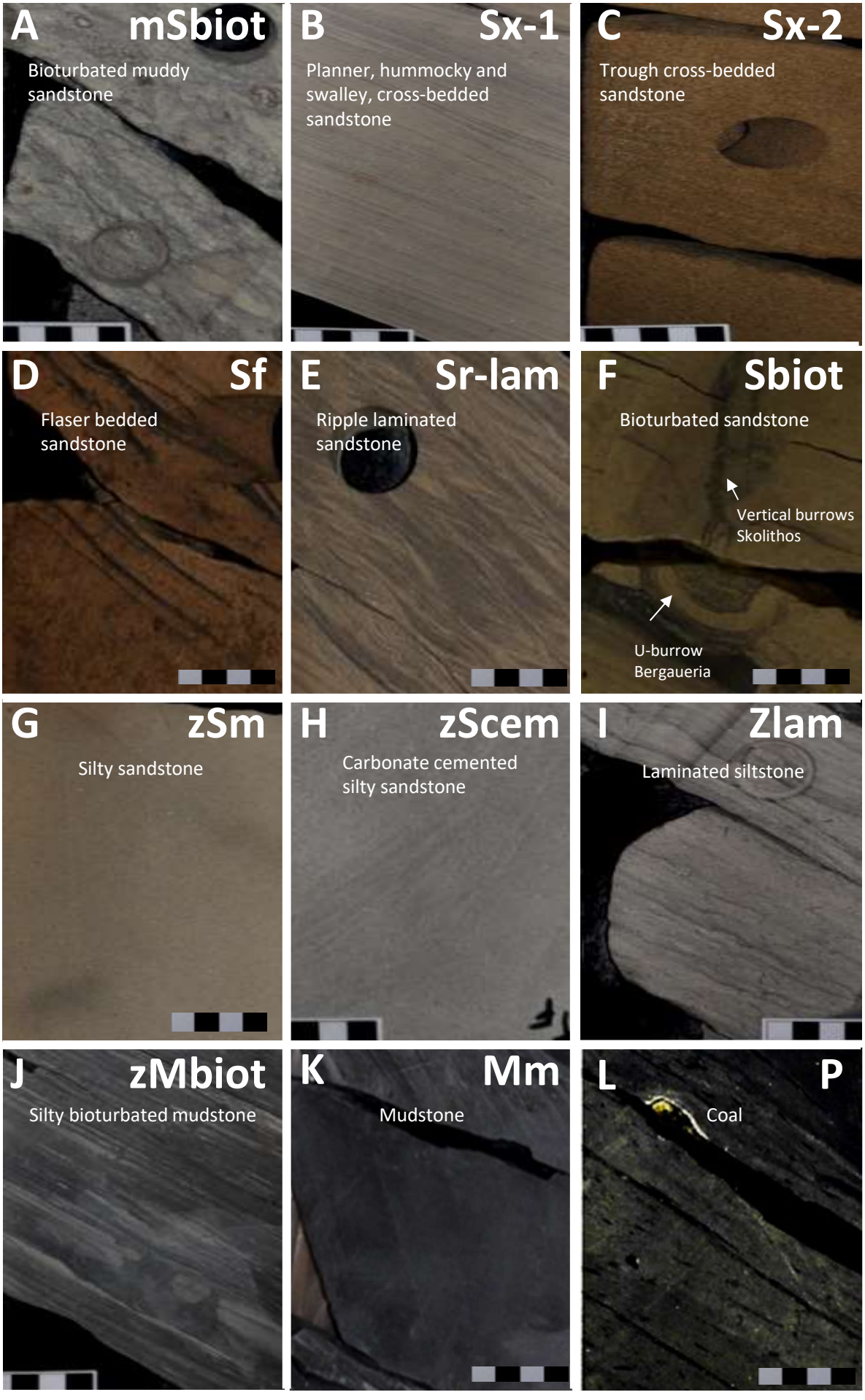
A
mSbiot
Bioturbated muddy sandstone
B
Sx-1
Planner, hummocky and swalley, cross-bedded sandstone
C
Sx-2
Trough cross-bedded sandstone
D
Sf
Flaser bedded sandstone
E
Sr-lam
Ripple laminated sandstone
F
Sbiot
Bioturbated sandstone
Vertical burrows
Skolithos
U-burrow
Bergaueria
G
zSm
Silty sandstone
H
zScem
Carbonate cemented silty sandstone
I
Zlam
Laminated siltstone
J
zMbiot
Silty bioturbated mudstone
K
Mm
Mudstone
L
P
Coal

Figure 4

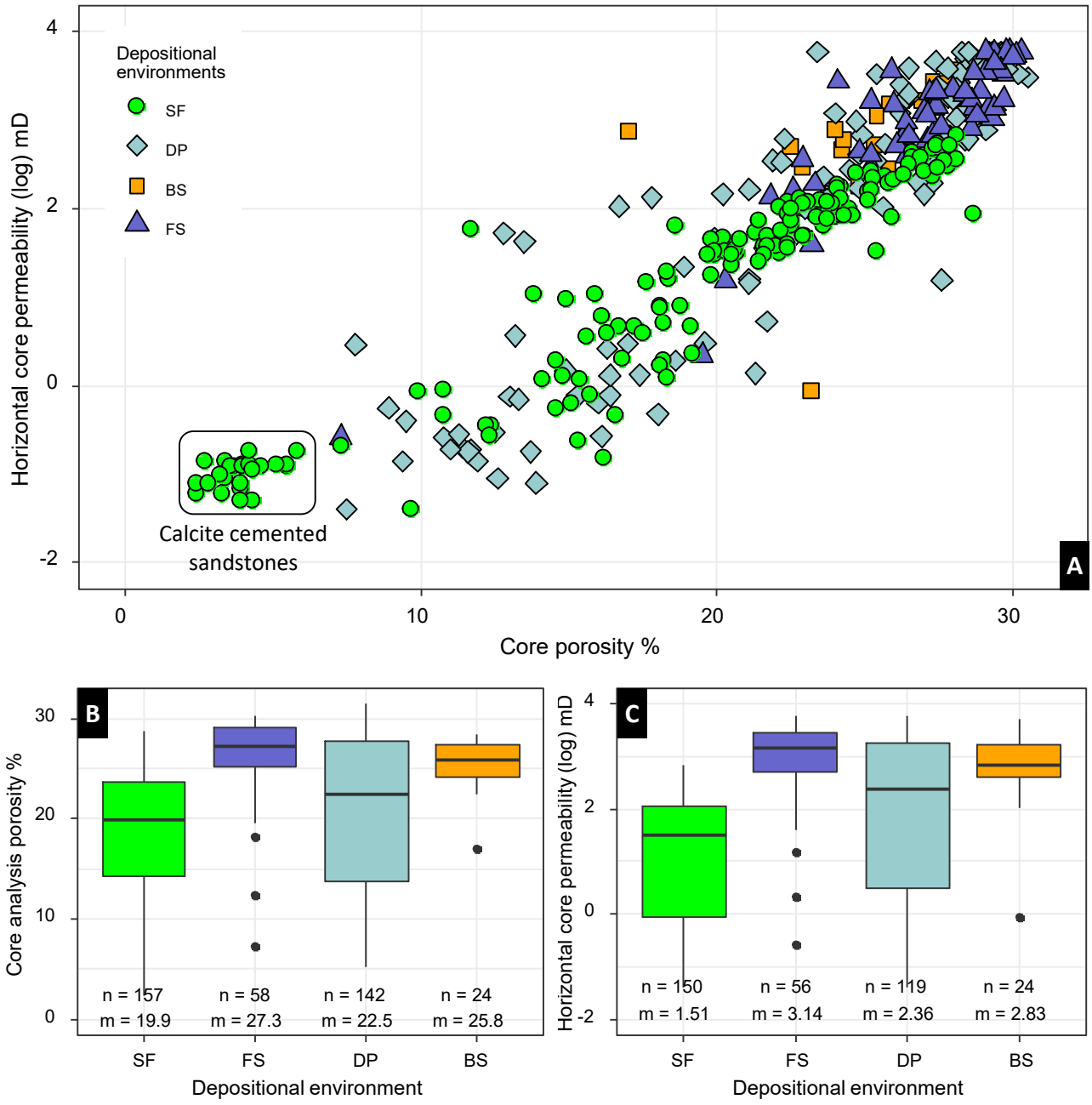
Depositional environments
SF
DP
BS
FS
Horizontal core permeability (log) mD
Core porosity %
Calcite cemented sandstones
A
B
Core analysis porosity %
n = 157
m = 19.9
n = 58
m = 27.3
n = 142
m = 22.5
n = 24
m = 25.8
SF
FS
DP
BS
Depositional environment
C
Horizontal core permeability (log) mD
n = 150
m = 1.51
n = 56
m = 3.14
n = 119
m = 2.36
n = 24
m = 2.83
SF
FS
DP
BS
Depositional environment

Figure 5

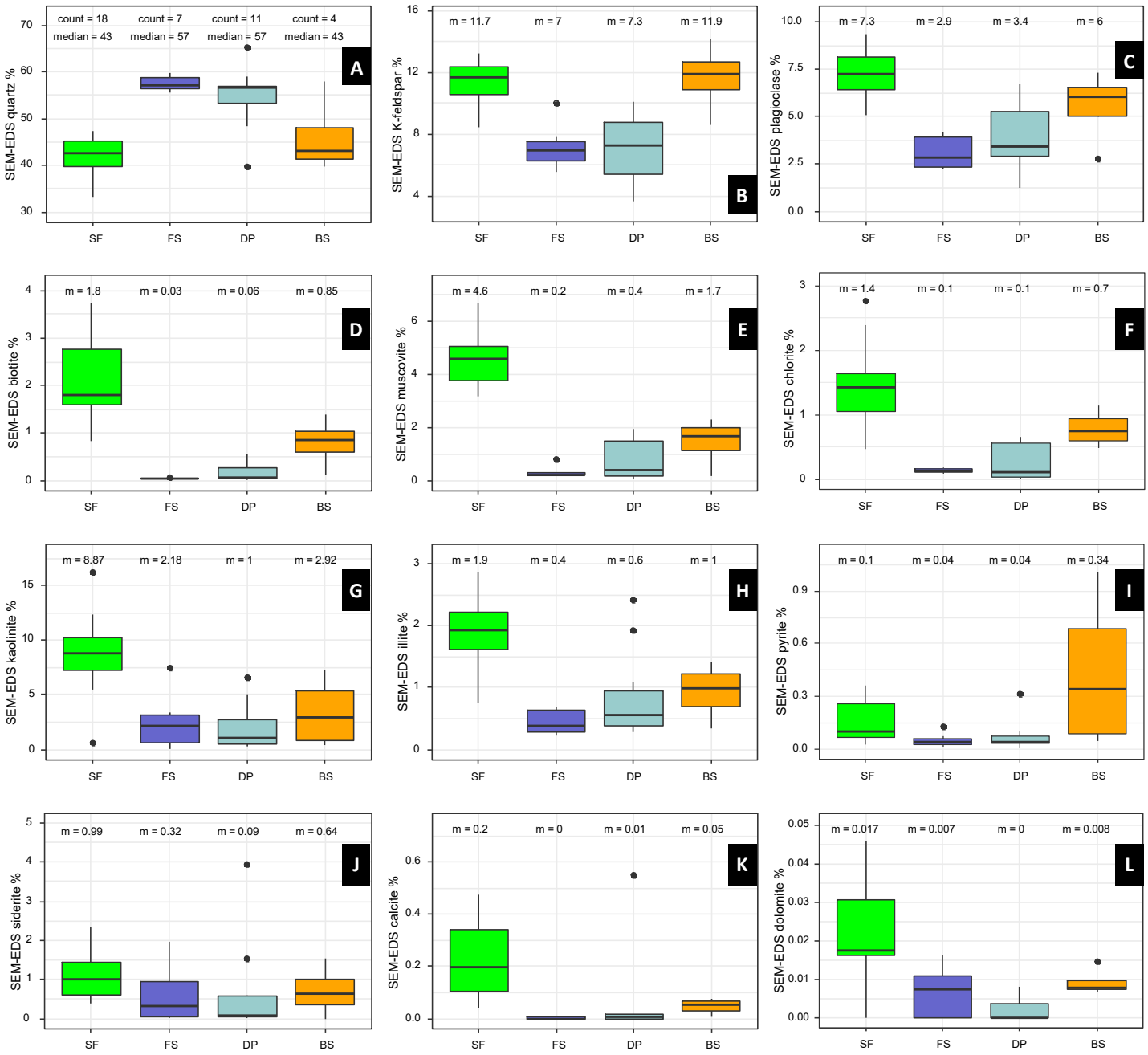
count = 18
median = 43
count = 7
median = 57
count = 11
median = 57
count = 4
median = 43
A
SEM-EDS quartz %
m = 11.7
m = 7
m = 7.3
m = 11.9
B
SEM-EDS K-feldspar %
m = 7.3
m = 2.9
m = 3.4
m = 6
C
SEM-EDS plagioclase %
m = 1.8
m = 0.03
m = 0.06
m = 0.85
D
SEM-EDS biotite %
m = 4.6
m = 0.2
m = 0.4
m = 1.7
E
SEM-EDS muscovite %
m = 1.4
m = 0.1
m = 0.1
m = 0.7
F
SEM-EDS chlorite %
m = 8.87
m = 2.18
m = 1
m = 2.92
G
SEM-EDS kaolinite %
m = 1.9
m = 0.4
m = 0.6
m = 1
H
SEM-EDS illite %
m = 0.1
m = 0.04
m = 0.04
m = 0.34
I
SEM-EDS pyrite %
m = 0.99
m = 0.32
m = 0.09
m = 0.64
J
SEM-EDS siderite %
m = 0.2
m = 0
m = 0.01
m = 0.05
K
SEM-EDS calcite %
m = 0.017
m = 0.007
m = 0
m = 0.008
L
SEM-EDS dolomite %
SF
FS
DP
BS

Figure 6

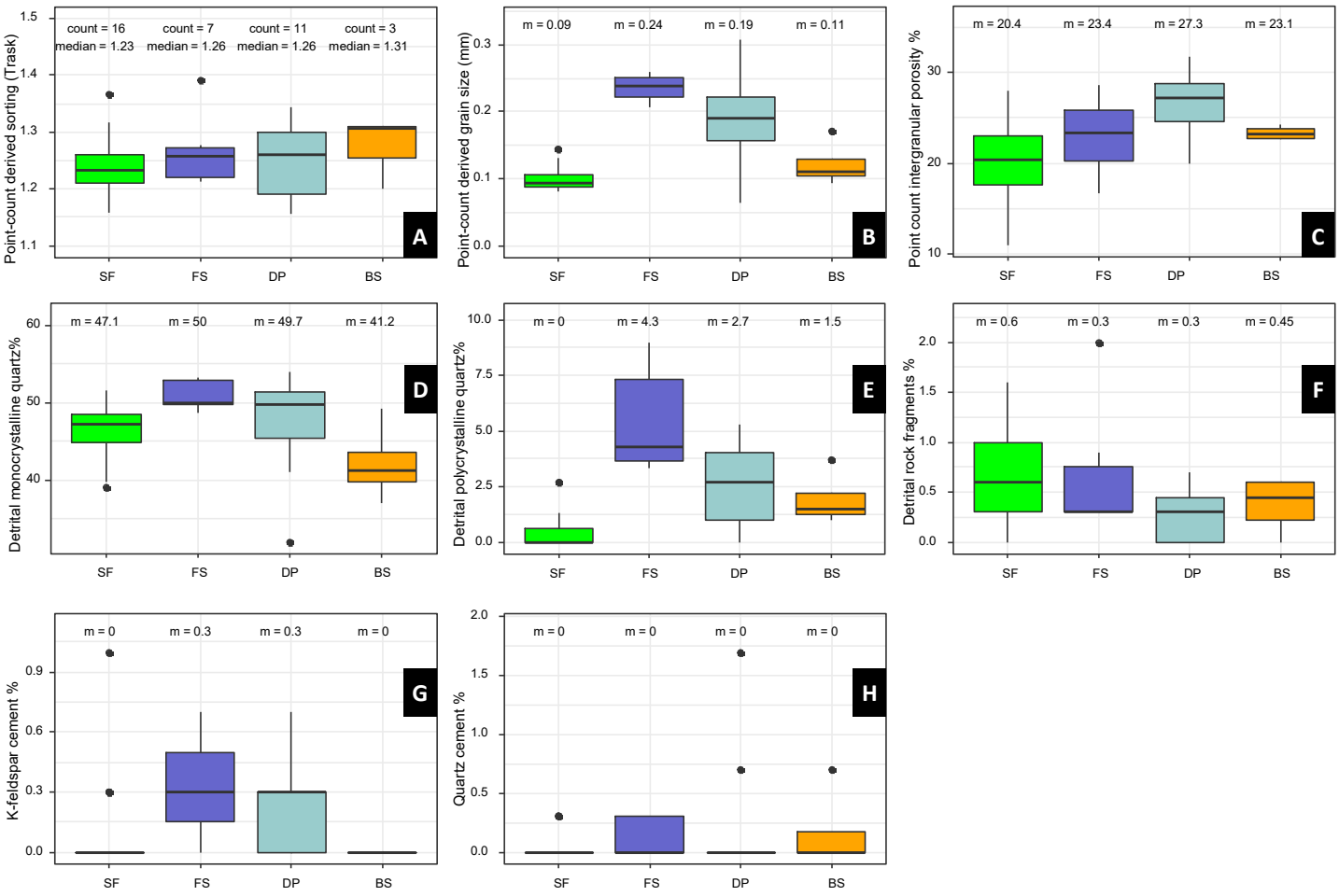
count = 16
median = 1.23
count = 7
median = 1.26
count = 11
median = 1.26
count = 3
median = 1.31
Point-count derived sorting (Trask)
A
m = 0.09
m = 0.24
m = 0.19
m = 0.11
Point-count derived grain size (mm)
B
m = 20.4
m = 23.4
m = 27.3
m = 23.1
Point count intergranular porosity %
C
m = 47.1
m = 50
m = 49.7
m = 41.2
Detrital monocrystalline quartz%
D
m = 0
m = 4.3
m = 2.7
m = 1.5
Detrital polycrystalline quartz%
E
m = 0.6
m = 0.3
m = 0.3
m = 0.45
Detrital rock fragments %
F
m = 0
m = 0.3
m = 0.3
m = 0
K-feldspar cement %
G
m = 0
m = 0
m = 0
m = 0
Quartz cement %
H
SF
FS
DP
BS

Figure 7

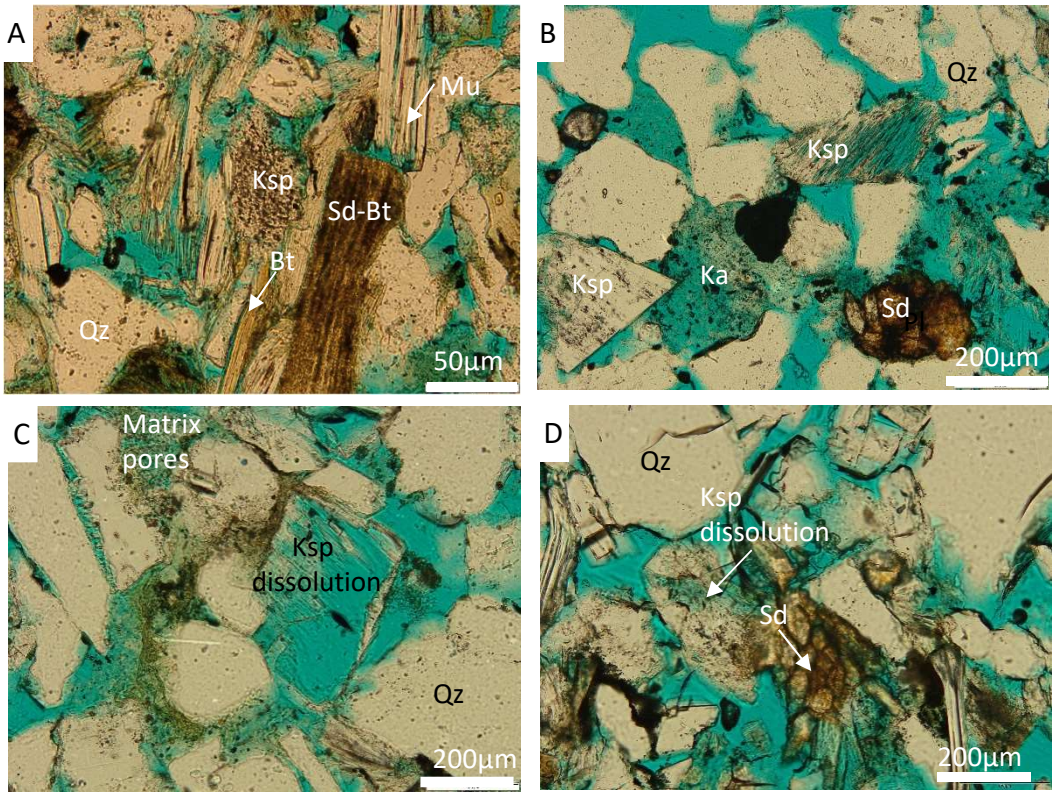
A
Mu
Ksp
Sd-Bt
Bt
Qz
50µm
B
Qz
Ksp
Ksp
Ka
Sd
200µm
C
Matrix
pores
Ksp
dissolution
Qz
200µm
D
Qz
Ksp
dissolution
Sd
200µm

Figure 8

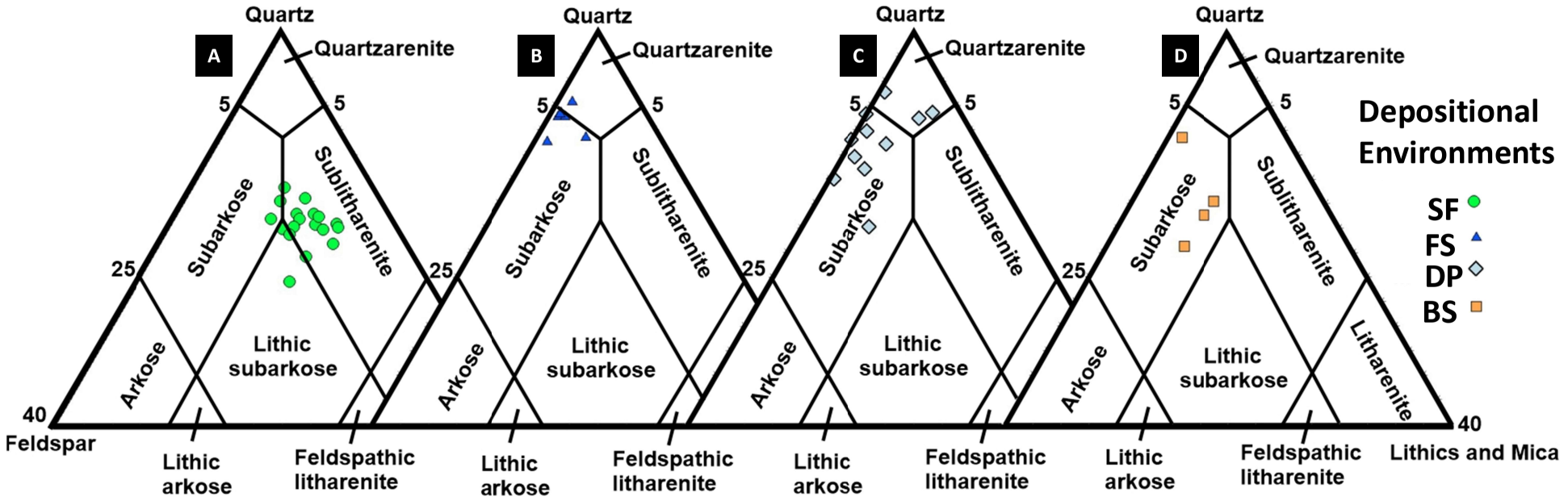
A
B
C
D
Quartz
Quartzarenite
5
5
25
40
Feldspar
Subarkose
Sublitharenite
Arkose
Lithic subarkose
Lithic arkose
Feldspathic litharenite
Litharenite
Lithics and Mica
Depositional Environments
SF
FS
DP
BS

Figure 9

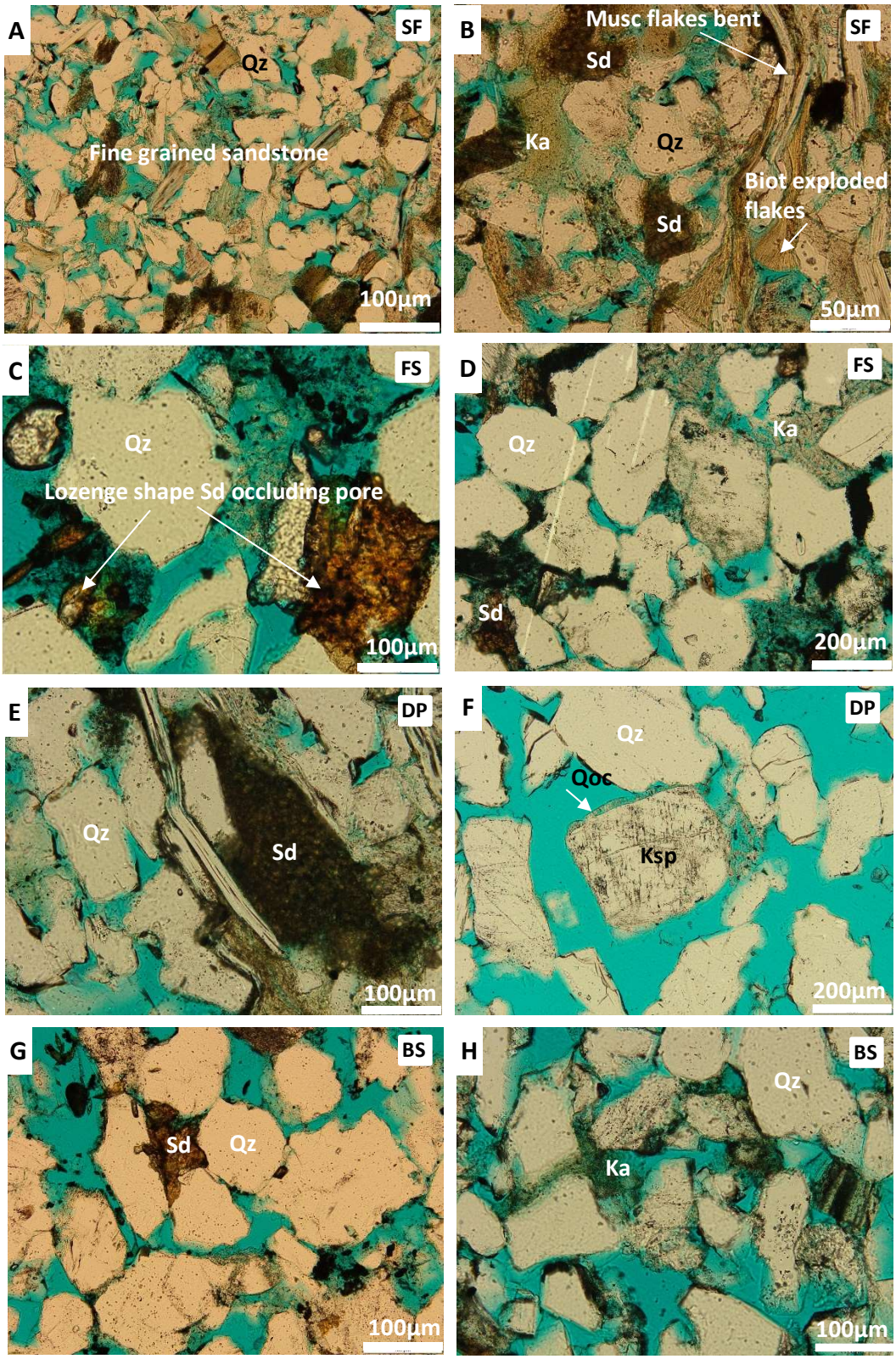
A
SF
Qz
Fine grained sandstone
100µm
B
Musc flakes bent
SF
Sd
Ka
Qz
Biot exploded flakes
Sd
50µm
C
FS
Qz
Lozenge shape Sd occluding pore
100µm
D
FS
Qz
Ka
Sd
200µm
E
DP
Qz
Sd
100µm
F
DP
Qz
Qoc
Ksp
200µm
G
BS
Sd
Qz
100µm
H
BS
Qz
Ka
100µm

Figure 10

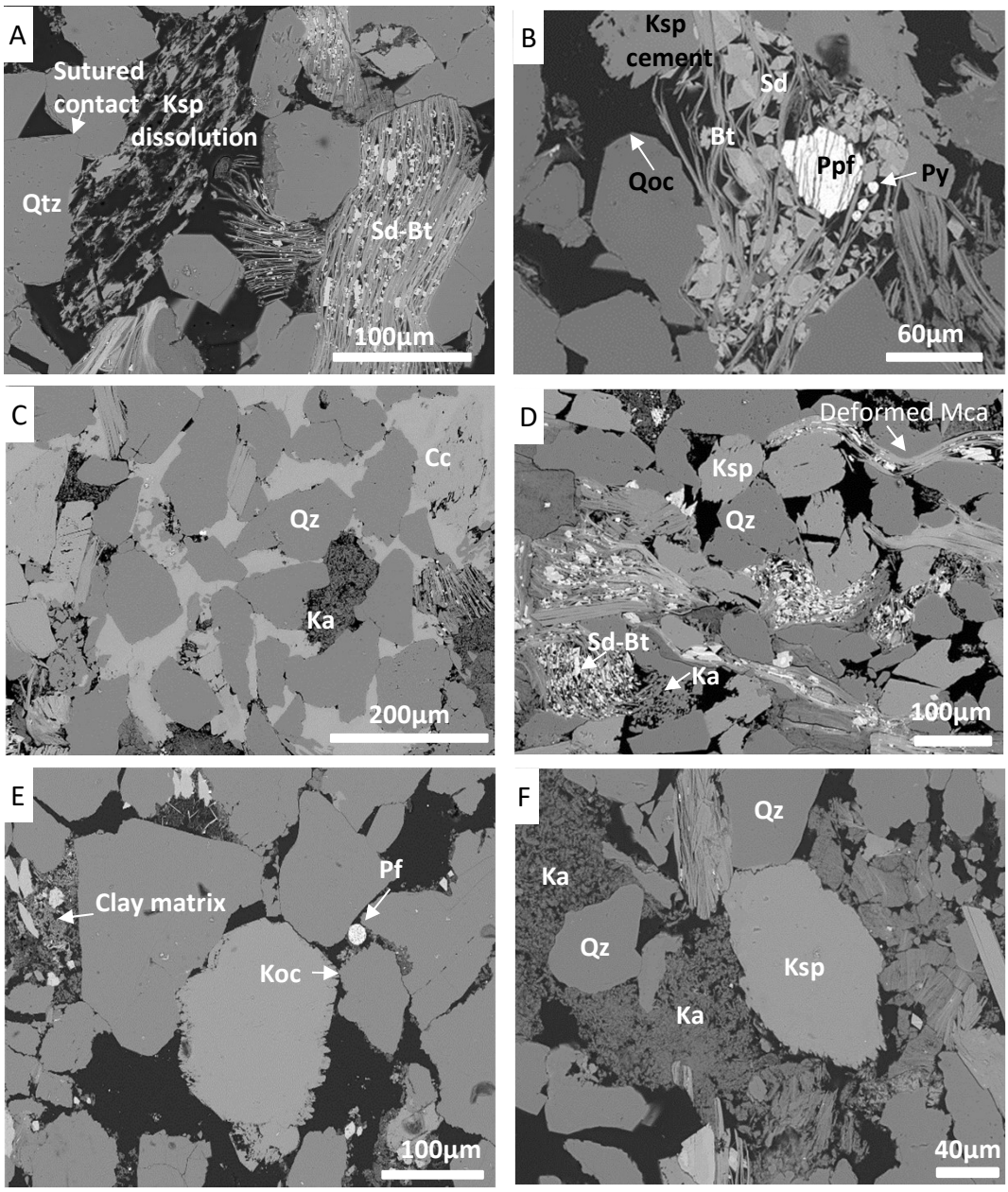
A
Sutured contact
Ksp dissolution
Qtz
Sd-Bt
100µm
B
Ksp cement
Sd
Bt
Qoc
Ppf
Py
60µm
C
Cc
Qz
Ka
200µm
D
Deformed Mca
Ksp
Qz
Sd-Bt
Ka
100µm
E
Clay matrix
Pf
Koc
100µm
F
Qz
Ka
Qz
Ksp
Ka
40µm

Figure 11

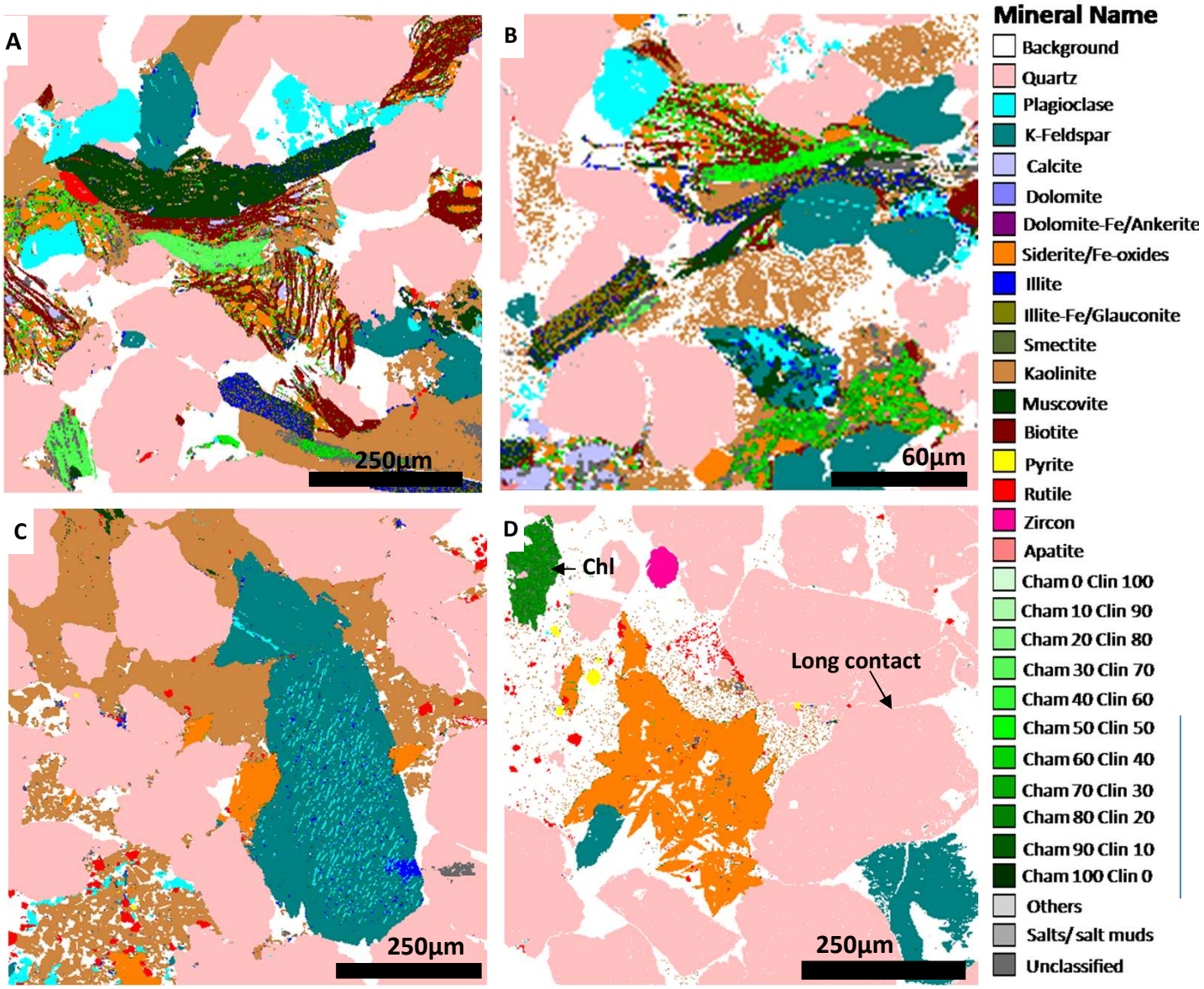
A
250µm
B
60µm
C
250µm
D
Chl
Long contact
250µm
Mineral Name
Background
Quartz
Plagioclase
K-Feldspar
Calcite
Dolomite
Dolomite-Fe/Ankerite
Siderite/Fe-oxides
Illite
Illite-Fe/Glauconite
Smectite
Kaolinite
Muscovite
Biotite
Pyrite
Rutile
Zircon
Apatite
Cham 0 Clin 100
Cham 10 Clin 90
Cham 20 Clin 80
Cham 30 Clin 70
Cham 40 Clin 60
Cham 50 Clin 50
Cham 60 Clin 40
Cham 70 Clin 30
Cham 80 Clin 20
Cham 90 Clin 10
Cham 100 Clin 0
Others
Salts/ salt muds
Unclassified

Figure 12

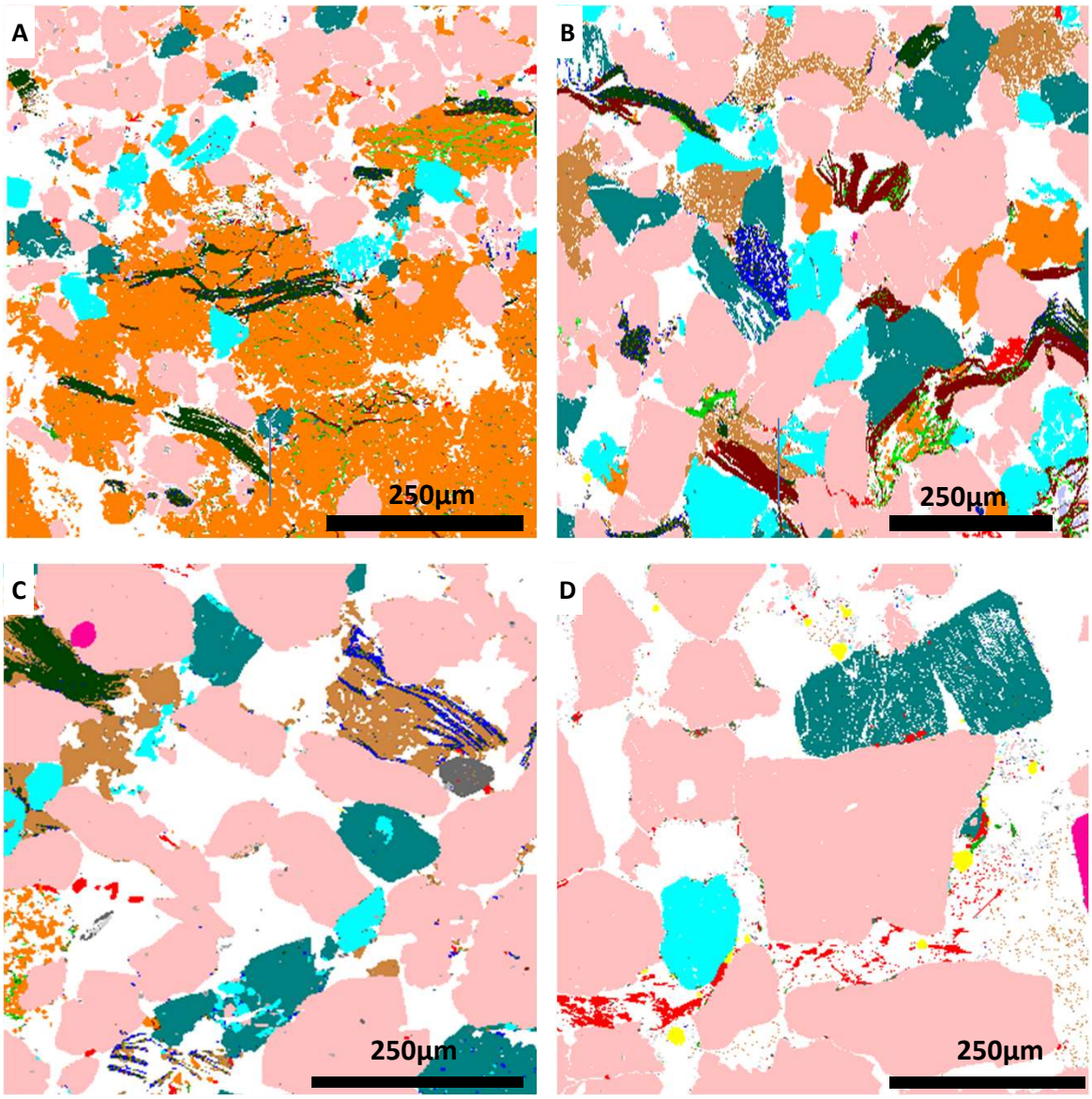


Figure 13

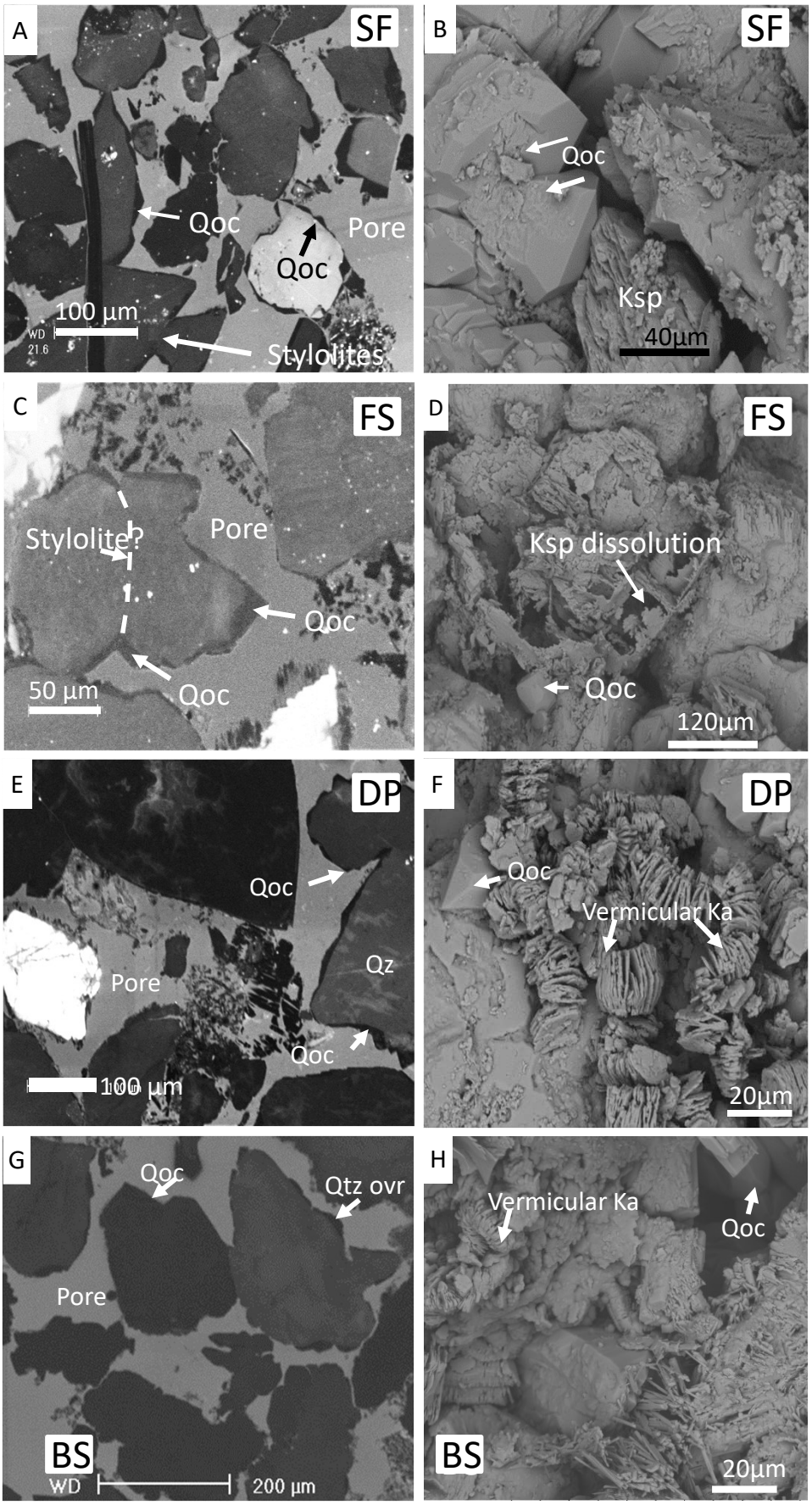
A
SF
Qoc
Pore
Qoc
100 µm
WD
21.6
Stylolites
B
SF
Qoc
Ksp
40µm
C
FS
Stylolite?
Pore
Qoc
Qoc
50 µm
D
FS
Ksp dissolution
Qoc
120µm
E
DP
Qoc
Qz
Pore
Qoc
100 µm
F
DP
Qoc
Vermicular Ka
20µm
G
Qoc
Qtz ovr
Pore
BS
WD
200 µm
H
Vermicular Ka
Qoc
BS
20µm

Figure 14

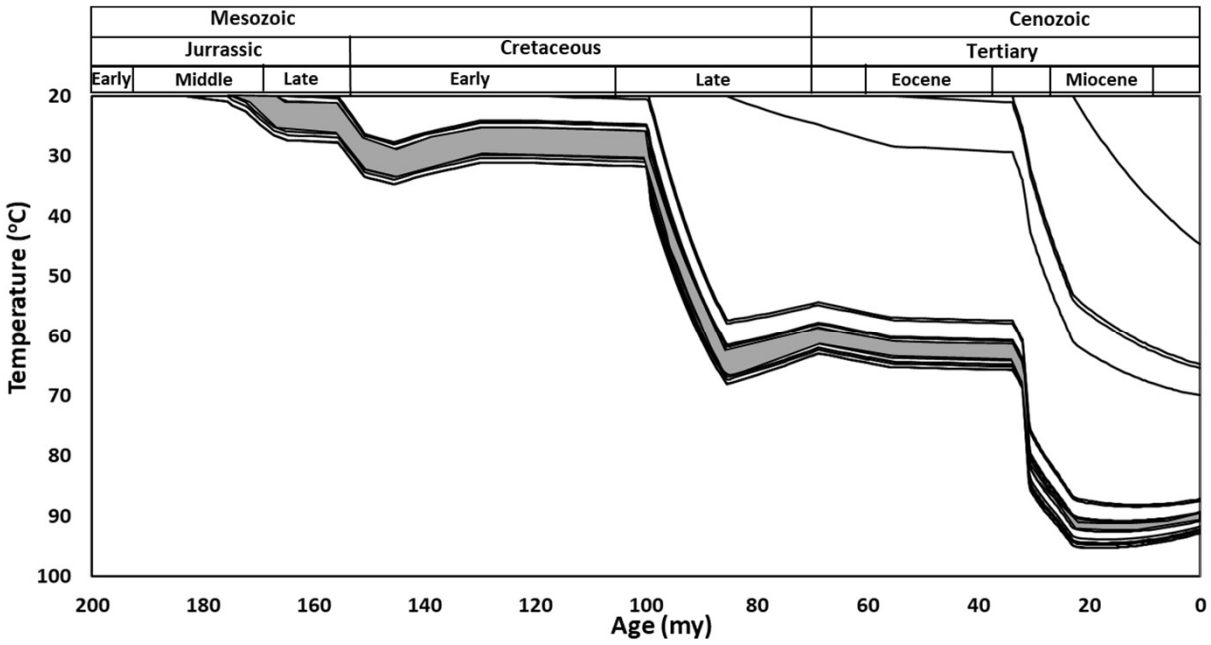
Mesozoic
Cenozoic
Jurrassic
Cretaceous
Tertiary
Early
Middle
Late
Early
Late
Eocene
Miocene
Temperature (°C)
20
30
40
50
60
70
80
90
100
200
180
160
140
120
100
80
60
40
20
0
Age (my)

Figure 15

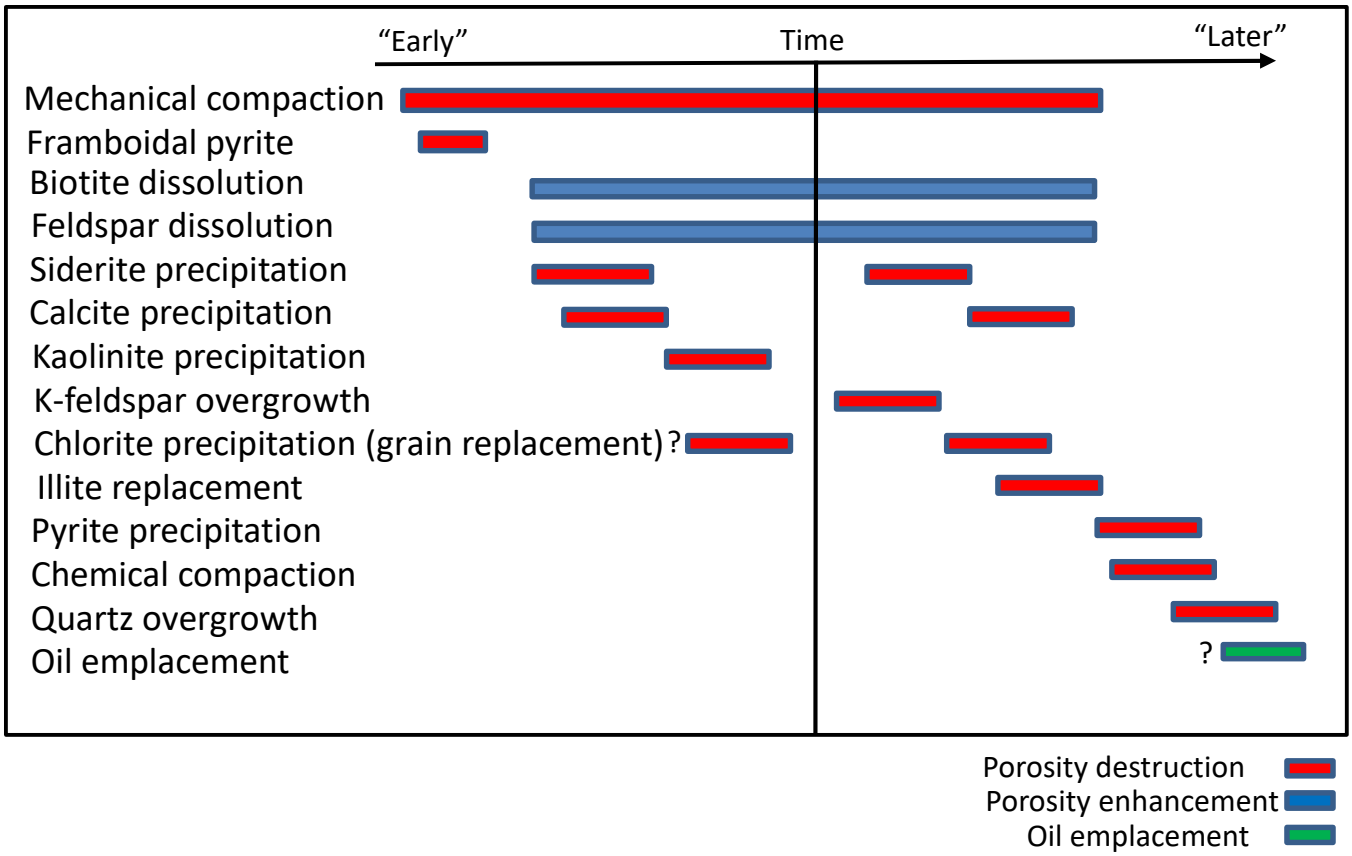
"Early"
Time
"Later"
Mechanical compaction
Framboidal pyrite
Biotite dissolution
Feldspar dissolution
Siderite precipitation
Calcite precipitation
Kaolinite precipitation
K-feldspar overgrowth
Chlorite precipitation (grain replacement)?
Illite replacement
Pyrite precipitation
Chemical compaction
Quartz overgrowth
Oil emplacement
?
Porosity destruction
Porosity enhancement
Oil emplacement

Figure 16

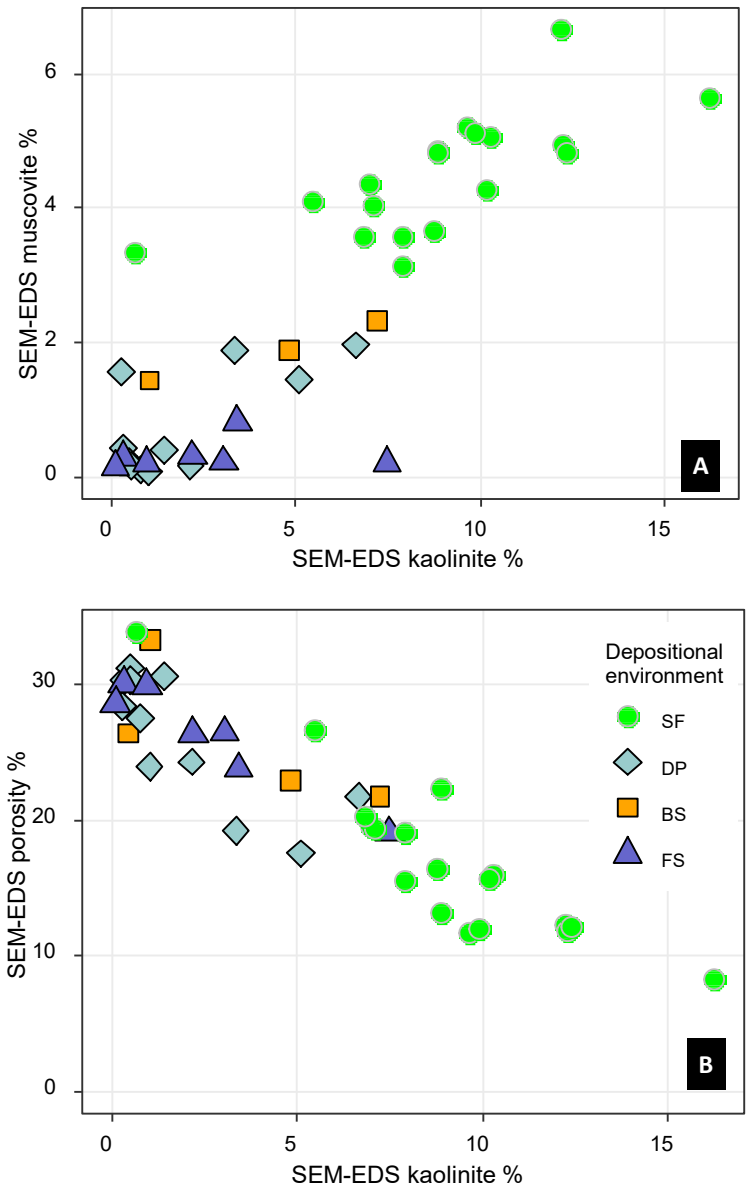
SEM-EDS muscovite %
SEM-EDS kaolinite %
A
SEM-EDS porosity %
SEM-EDS kaolinite %
B
Depositional environment
SF
DP
BS
FS

Figure 17

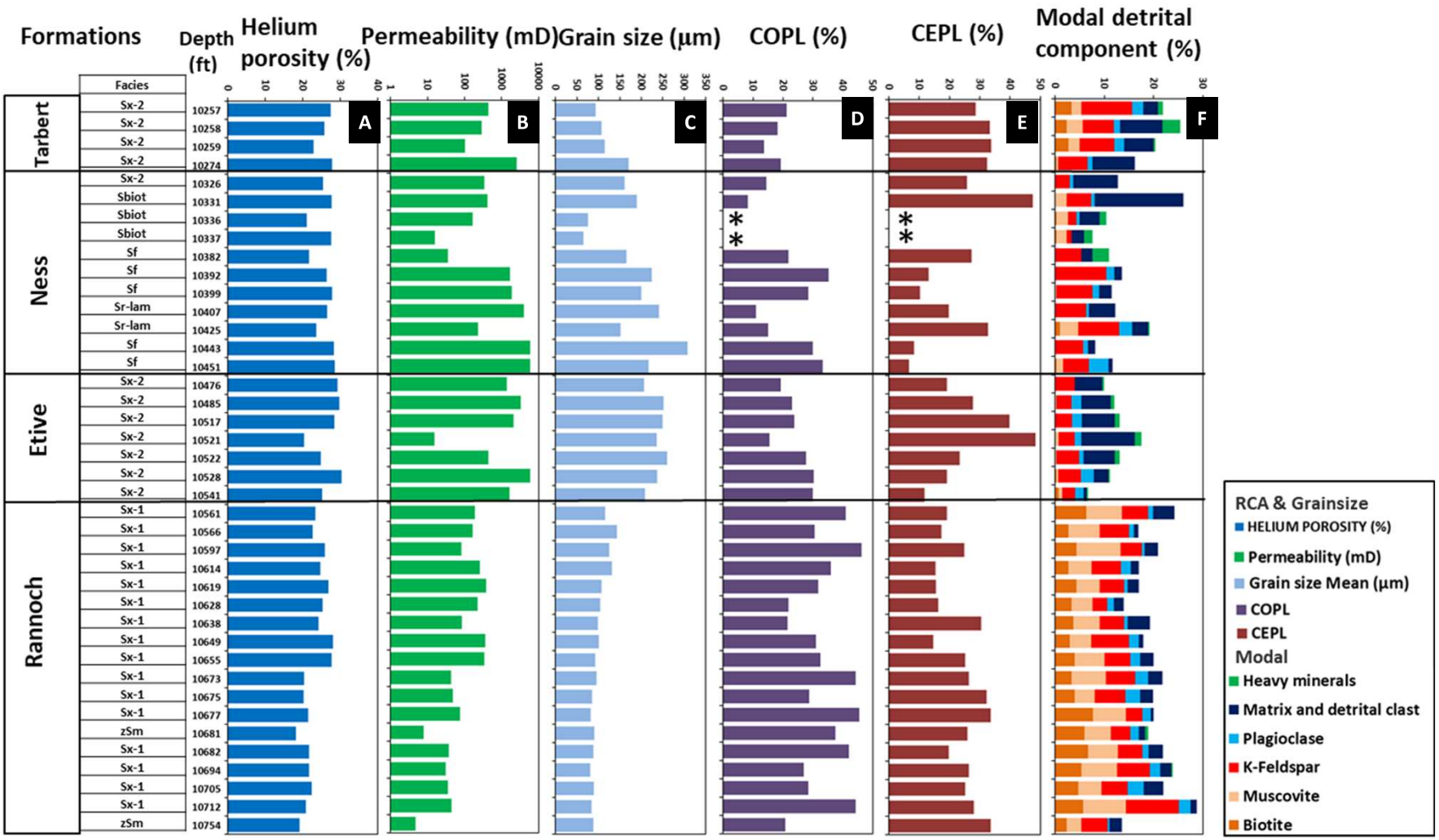
Formations
Depth (ft)
Facies
Helium porosity (%)
Permeability (mD)
Grain size (µm)
COPL (%)
CEPL (%)
Modal detrital component (%)
A
B
C
D
E
F
Tarbert
Ness
Etive
Rannoch
RCA & Grainsize
HELIUM POROSITY (%)
Permeability (mD)
Grain size Mean (µm)
COPL
CEPL
Modal
Heavy minerals
Matrix and detrital clast
Plagioclase
K-Feldspar
Muscovite
Biotite

Figure 18

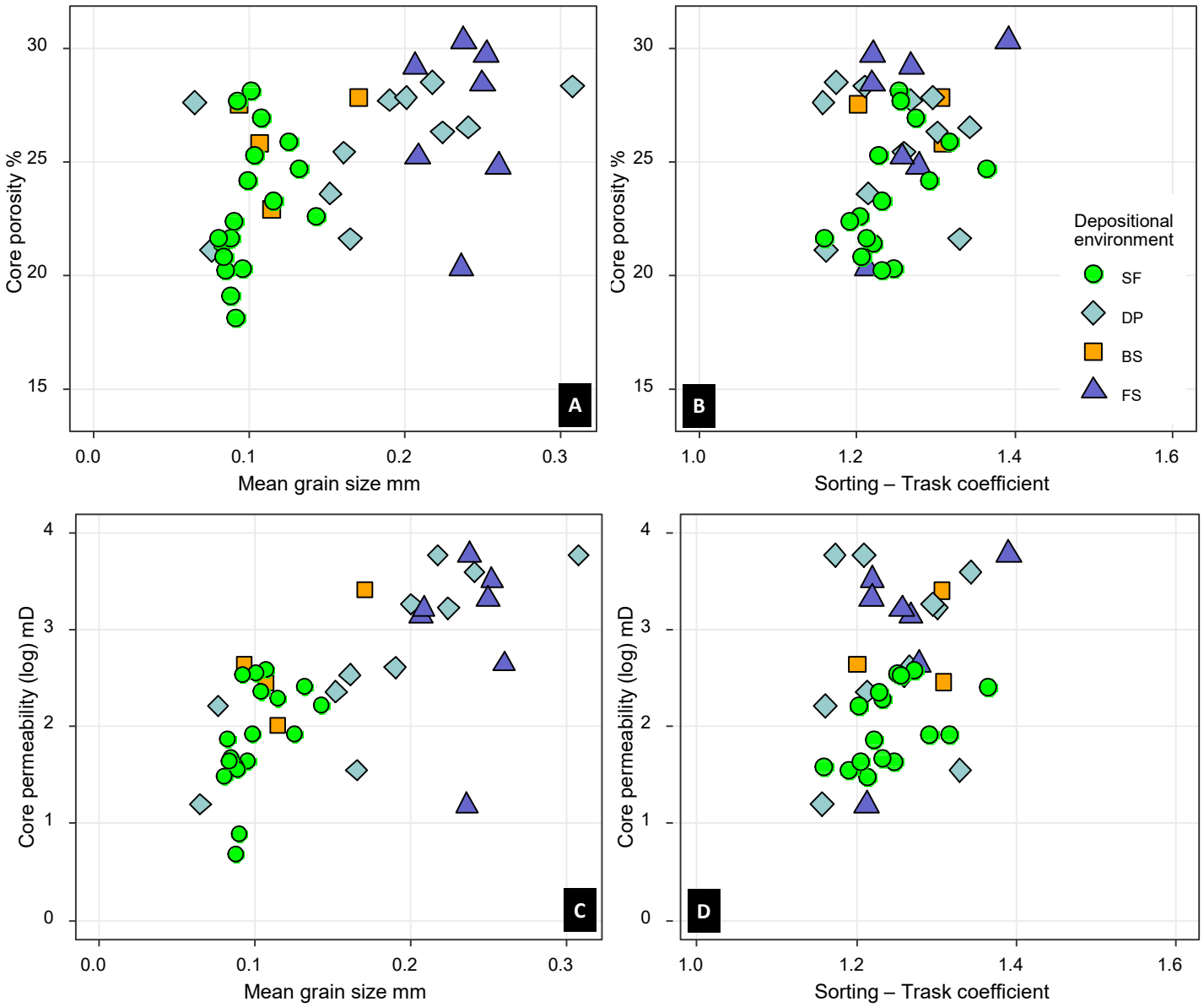
Core porosity %
30
25
20
15
0.0
0.1
0.2
0.3
Mean grain size mm
A
Core porosity %
30
25
20
15
1.0
1.2
1.4
1.6
Sorting – Trask coefficient
B
Depositional environment
SF
DP
BS
FS
Core permeability (log) mD
4
3
2
1
0
0.0
0.1
0.2
0.3
Mean grain size mm
C
Core permeability (log) mD
4
3
2
1
0
1.0
1.2
1.4
1.6
Sorting – Trask coefficient
D

Figure 19

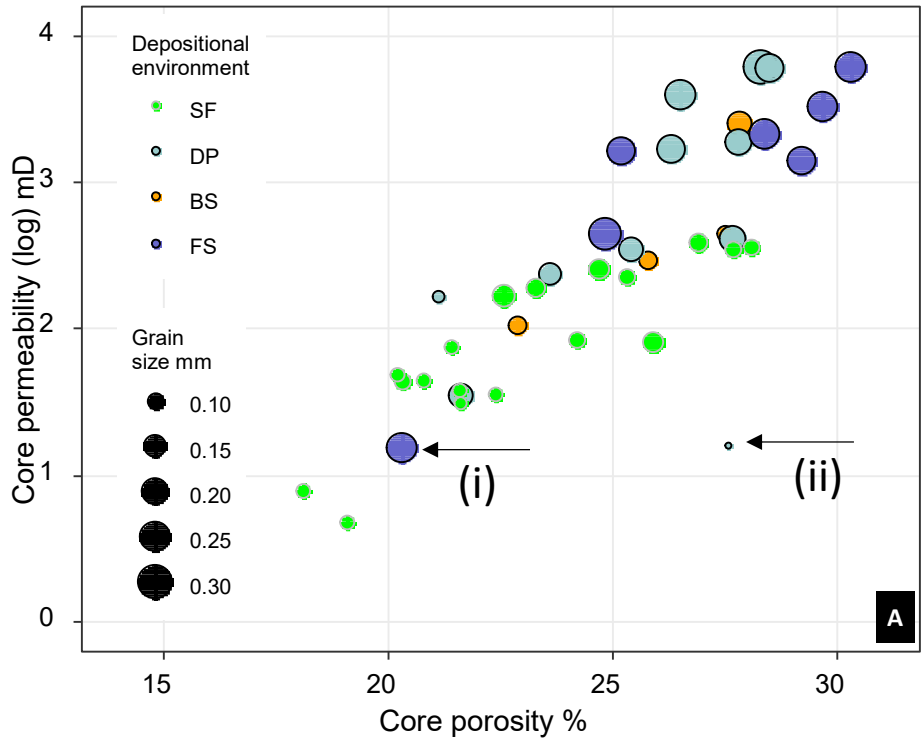
Depositional environment
SF
DP
BS
FS
Grain size mm
0.10
0.15
0.20
0.25
0.30
(i)
(ii)
A
Core permeability (log) mD
Core porosity %
0
1
2
3
4
15
20
25
30

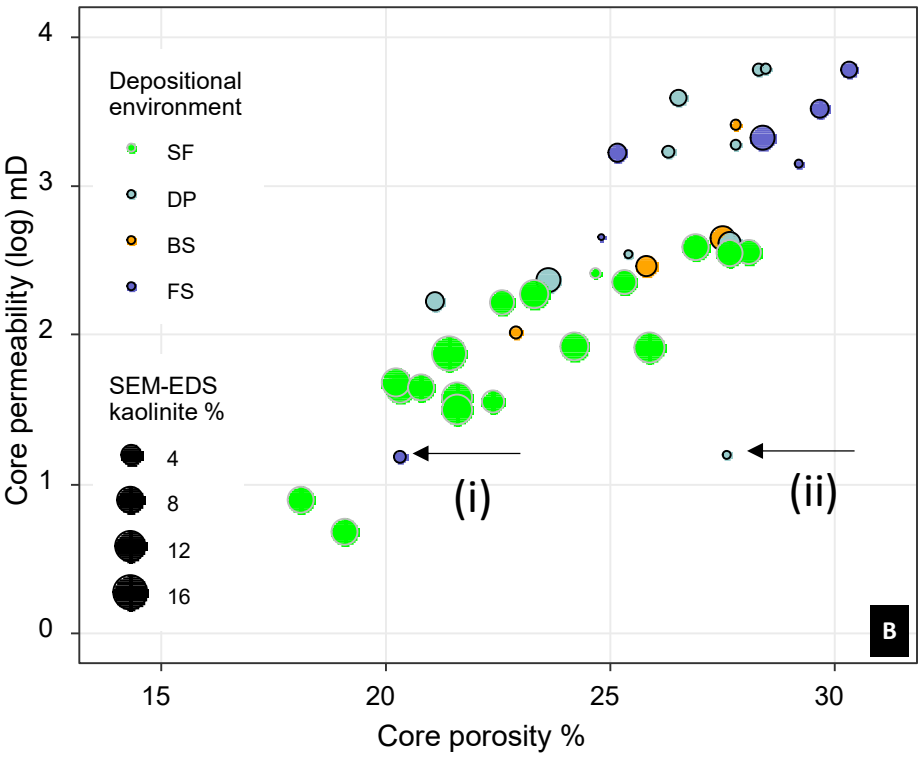
Depositional environment
SF
DP
BS
FS
SEM-EDS kaolinite %
4
8
12
16
(i)
(ii)
B
Core permeability (log) mD
Core porosity %
0
1
2
3
4
15
20
25
30

Figure 20

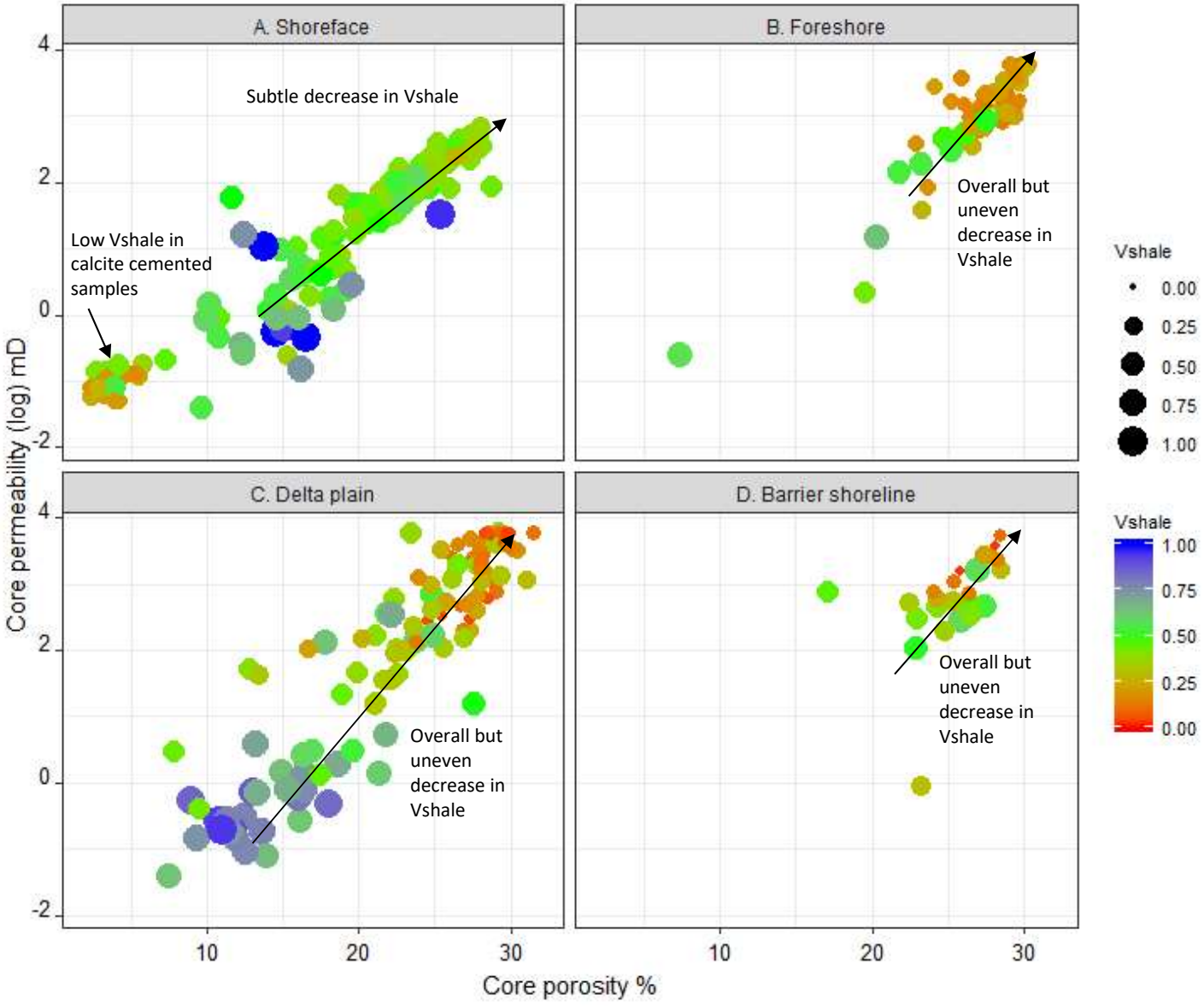
A. Shoreface
B. Foreshore
C. Delta plain
D. Barrier shoreline
Subtle decrease in Vshale
Low Vshale in calcite cemented samples
Overall but uneven decrease in Vshale
Overall but uneven decrease in Vshale
Overall but uneven decrease in Vshale
Core permeability (log) mD
Core porosity %
Vshale
0.00
0.25
0.50
0.75
1.00
Vshale
1.00
0.75
0.50
0.25
0.00

Figure 21

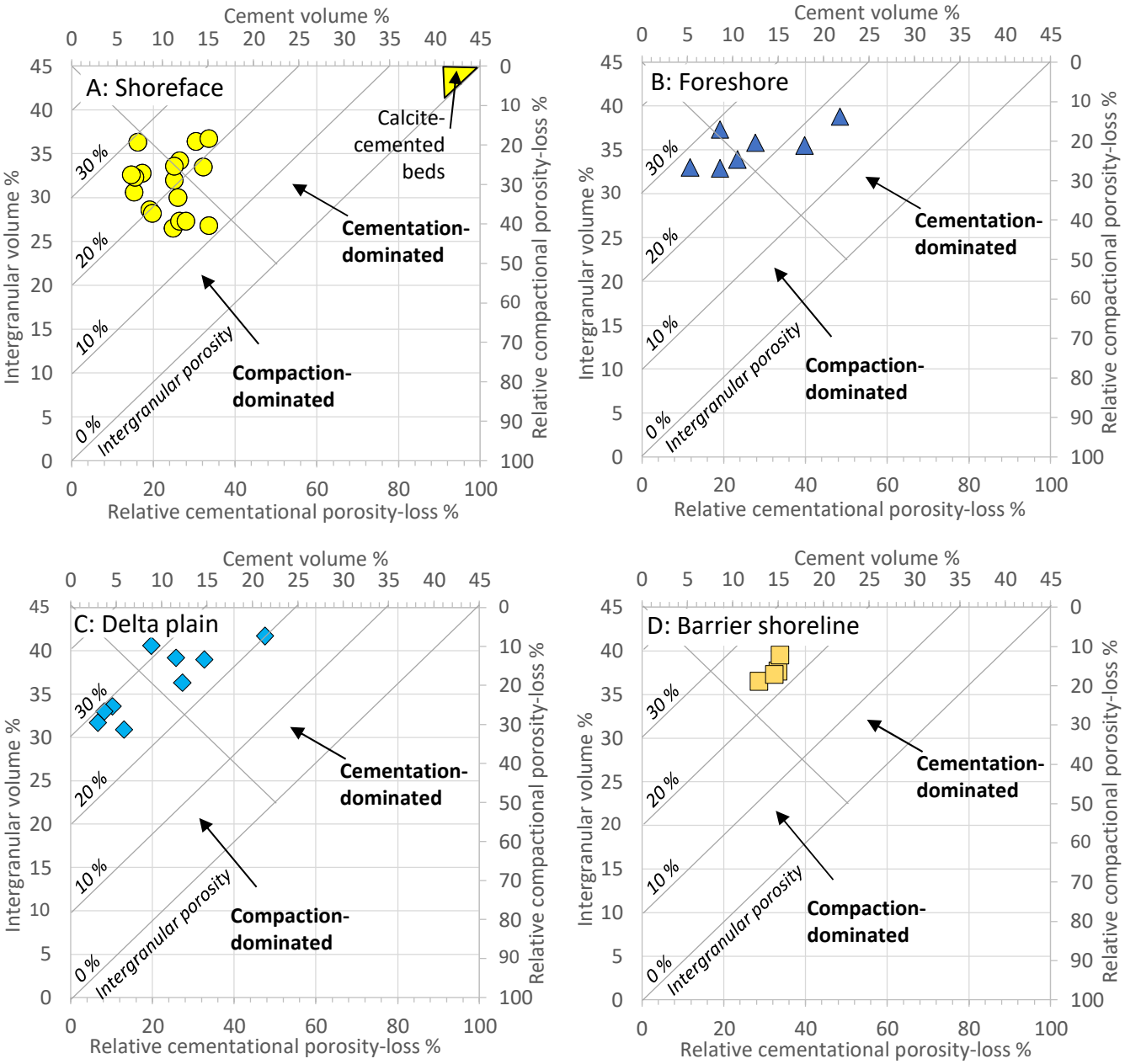
A: Shoreface
B: Foreshore
C: Delta plain
D: Barrier shoreline
Cement volume %
Intergranular volume %
Relative compactional porosity-loss %
Relative cementational porosity-loss %
Calcite-cemented beds
Cementation-dominated
Compaction-dominated
Intergranular porosity
30 %
20 %
10 %
0 %

Figure 22

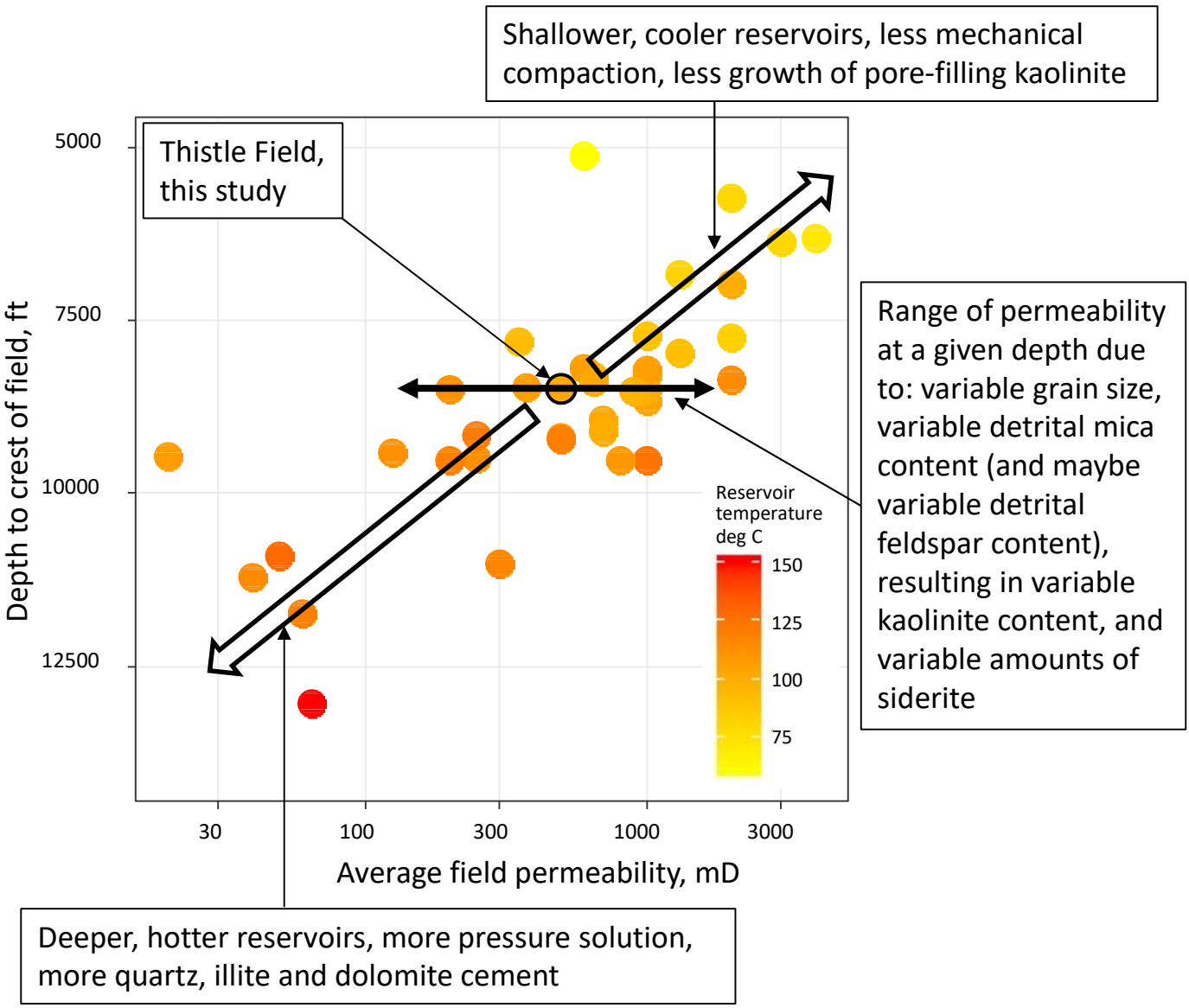
Shallower, cooler reservoirs, less mechanical compaction, less growth of pore-filling kaolinite
Thistle Field, this study
Range of permeability at a given depth due to: variable grain size, variable detrital mica content (and maybe variable detrital feldspar content), resulting in variable kaolinite content, and variable amounts of siderite
Deeper, hotter reservoirs, more pressure solution, more quartz, illite and dolomite cement
Depth to crest of field, ft
5000
7500
10000
12500
30
100
300
1000
3000
Average field permeability, mD
Reservoir temperature deg C
150
125
100
75

Figure 23

Table. 1 Brent Thistle well 211/18a-A33 sedimentary facies details description tabulated with facies code, descriptions of grain size, structures/bioturbation, interpreted depositional environment of the Brent Formations. The facies were arranged by; (a) broad group sandstone facies and (b) silty-sandstone, siltstones, mudstone and coaly bed.

| Facies type | Facies Code | Descriptions | Formation | Sedimentary structures and bed types | Trace fossils | Facies associations (FA) Depositional environments |
|---|---|---|---|---|---|---|
| Sandstones | **mSbiot** | **Bioturbated muddy sandstone.** The facies is characterised by grain size that ranges from coarse to very coarse and is highly unsorted and slightly argillaceous. This facies locally contain sideritised lithoclast and carbonaceous laminae. | Broom | Mud lenses, bioturbated. sand lenses separated by the silty shaly partings with abruptly bed-bases. | Thallasinodes, Planolites and Paleophycus | FA1-Fan delta |
| | **Sx-1** | **Planar, hummocky and swaley cross-bedded. sandstone.** This facies association is characterised by interbedded parallel laminated and hummocky cross bedded and locally massive very fine to fine micaceous sandstone. The facies occasionally has thin rippled beds and swaley sedimentary structures. | Rannoch, Etive | Lamination, hummocky beds and locally massive and swaley beds | Low bioturbated | FA2- Shoreface |
| | **Sx-2** | **Trough cross-bedded sandstone.** The facies range from fine to very coarse grained cross-bedded moderately sorted sandstone but locally becomes faintly to massive unit. The facies is non-bioturbated and non-micaceous. | Etive, Ness and Tarbert | Cross bedding. Cross-beds are characterise by moderate or low angle stratification and are defined by marked changes in grain size and/ or by truncation of underlying laminae | Non-bioturbated | FA3-Foreshore, FA4-Delta plain FA5- Barrier shoreline |
| | **Sf** | **Flaser bedded sandstone.** Non bioturbated, fine to medium grained sandstone with mud flasers and locally mud drapes. The facies is characterised by uni-directional flow ripple sedimentary structures in the mud flaser | Ness | Wave and flow ripple, mud flasers and drapes | Non-bioturbated | FA4-Delta plain |
| | **Sr-lam** | **Rippled laminated sandstone.** Characterised by combined wave and uni-directional flow rippled, fine-medium sandstone with interbedded mud and sand lenses. The mud and sand lenses show a division into a light coloured upper half and a dark coloured lower half with a horizontal separation between the two. | Ness | Ripples and cross lamination. The unit is predominantly rippled and occasionally has low angle cross beds. | Non-bioturbated | FA4-Delta plain |
| | **Sbiot** | **Bioturbated sandstone**. This facies is characterised by highly bioturbated fine-medium sandstone. Burrows are distinct; mostly U-shaped and vertical type. | Etive, Ness | The upper part of this unit is rootlets sandstone characterise by thin, subvertical, irregular, discontinues carbonaceous rods of 1mm wide and 1-4cm long. | Heavily bioturbated. Diplocraterion, Skolithos, Teichicnus and Bergaueria. | FA3- Foreshore FA4-Delta plain . |
| Silty sandstone, siltstone, mudstone and coal | **zSm** | **Massive silty sandstone.** This facies is characterised by very fine to fine grained light brown massive sandstone. The facies has a sharp based with the underlying and overlying facies. | Rannoch | Massive | Non-bioturbated | FA2- Shoreface |
| | **zScem** | **Carbonate Cemented silty sandstone**. This facies is same with facies Sx-1 in grain size and sedimentary structures but differs only in cementation. The unit is pale grey very fine to fine completely carbonate cemented and is interbedded with facies Sx1. | Rannoch | Lamination, hummocky beds and occasionally massive and swaley beds. | Non-bioturbated | FA2- Shoreface |
| | **Zlam** | **Finely laminated siltstone**. The facies is characterised by pale grey, silty to very fine, highly micaceous silty sandstone dominantly parallel laminated with minor rippled bed. This facies is interbedded with massive silty sandstone of facies zSm. | Rannoch | Parallel lamination | Non-bioturbated | FA2-Shoreface |
| | **zMbiot** | **Bioturbated silty mudstone.** This facies includes silty moderately bioturbated mudstone. The facies typically contains silty lenses within the dark grey mud. | Ness | Silty lenses, lamination | Thallasinodes, Paleophycus, Planolites and Teichichnus. | FA4-Delta plain |
| | **Mm** | **Massive mudstone.** This facies is characterised by dark colouration and is massive with a rare and very few silty streaks. The dark colouration is an indicative of high organic matter content. | Ness | Massive and few silt lenses | Non-bioturbated | FA4-Delta plain |
| | **P** | **Coaly bed**. This facies is characterised by dark colour and contains granule and pebble sized fragments of carbonaceous materials. This facies gradationally overlie the bioturbated and rooted sandstone of facies Sbiot. | Ness | Rip up clast and silt lenses | Massive | FA4-Delta plain |

Table 2. SEM-EDS normalised mineralogy data for the 40 sandstone samples selected from the Brent Group; Rannoch, Etive, Ness and Tarbert Formation of the Thistle well 211/18a-A33.

| Formation | Sample Depth (MD) | Apatite | Biotite | Calcite | Chlorite | Dolomite | Illite | Ilmenite | Kaolinite | K-Feldspar | Muscovite | Others | Plagioclase | Porosity | Pyrite | Quartz | Rutile | Siderite | Smectite | Unclassified | Zircon |
|---|---|---|---|---|---|---|---|---|---|---|---|---|---|---|---|---|---|---|---|---|---|
| Tabert | **10257** | 0.09 | 1.40 | 0.06 | 1.14 | 0.01 | 1.42 | 0.01 | 7.22 | 14.20 | 2.32 | 0.21 | 7.34 | 21.72 | 0.10 | 39.89 | 0.59 | 1.52 | 0.08 | 0.64 | 0.04 |
| | **10258** | 0.05 | 0.93 | 0.08 | 0.87 | 0.01 | 1.15 | 0.05 | 4.81 | 11.68 | 1.87 | 0.77 | 5.81 | 22.89 | 0.58 | 44.69 | 1.74 | 0.82 | 0.05 | 0.90 | 0.24 |
| | **10259** | 0.09 | 0.78 | 0.04 | 0.63 | 0.01 | 0.81 | 0.01 | 1.02 | 12.19 | 1.43 | 0.19 | 6.29 | 33.26 | 0.05 | 41.83 | 0.49 | 0.47 | 0.03 | 0.36 | 0.03 |
| | **10274** | 0.03 | 0.10 | 0.01 | 0.49 | 0.01 | 0.34 | 0.05 | 0.43 | 8.62 | 0.16 | 0.26 | 2.80 | 26.42 | 1.01 | 58.00 | 0.66 | 0.00 | 0.01 | 0.54 | 0.05 |
| Ness | **10326** | 0.03 | 0.06 | 0.00 | 0.10 | 0.00 | 0.37 | 0.02 | 0.31 | 4.10 | 0.42 | 0.19 | 6.72 | 30.35 | 0.03 | 56.84 | 0.20 | 0.03 | 0.03 | 0.18 | 0.01 |
| | **10331** | 0.19 | 0.32 | 0.02 | 0.56 | 0.00 | 2.42 | 0.01 | 5.07 | 6.29 | 1.44 | 0.40 | 6.50 | 17.52 | 0.04 | 56.68 | 0.52 | 0.58 | 0.07 | 1.37 | 0.01 |
| | **10336** | 0.23 | 0.22 | 3.52 | 0.56 | 0.01 | 1.93 | 0.02 | 3.33 | 4.49 | 1.88 | 0.36 | 5.33 | 19.18 | 0.04 | 53.11 | 0.78 | 3.94 | 0.06 | 0.91 | 0.07 |
| | **10337** | 0.12 | 0.56 | 0.55 | 0.65 | 0.00 | 0.55 | 0.04 | 0.25 | 3.65 | 1.55 | 0.16 | 3.97 | 28.38 | 0.08 | 39.86 | 0.54 | 17.85 | 0.02 | 1.17 | 0.06 |
| | **10382** | 0.06 | 0.08 | 0.00 | 0.21 | 0.01 | 0.40 | 0.01 | 1.42 | 7.28 | 0.40 | 0.06 | 3.40 | 30.66 | 0.03 | 53.33 | 1.30 | 0.51 | 0.01 | 0.71 | 0.13 |
| | **10392** | 0.01 | 0.02 | 0.01 | 0.03 | 0.00 | 0.47 | 0.00 | 0.76 | 10.09 | 0.10 | 0.35 | 3.29 | 27.47 | 0.04 | 56.96 | 0.09 | 0.08 | 0.02 | 0.20 | 0.00 |
| | **10399** | 0.02 | 0.03 | 0.01 | 0.04 | 0.00 | 0.32 | 0.00 | 0.47 | 8.65 | 0.21 | 0.12 | 3.18 | 31.27 | 0.06 | 55.32 | 0.16 | 0.01 | 0.01 | 0.11 | 0.01 |
| | **10407** | 0.01 | 0.04 | 0.02 | 0.03 | 0.00 | 0.83 | 0.01 | 2.13 | 8.31 | 0.15 | 0.49 | 2.43 | 24.30 | 0.31 | 58.94 | 0.10 | 0.02 | 0.02 | 1.85 | 0.01 |
| | **10425** | 0.07 | 0.48 | 0.01 | 0.54 | 0.01 | 1.09 | 0.01 | 6.63 | 9.71 | 1.96 | 0.24 | 5.27 | 21.75 | 0.10 | 48.43 | 0.72 | 1.53 | 0.08 | 1.32 | 0.06 |
| | **10443** | 0.00 | 0.01 | 0.00 | 0.02 | 0.00 | 0.62 | 0.00 | 1.00 | 7.24 | 0.06 | 0.29 | 1.24 | 23.93 | 0.02 | 65.27 | 0.08 | 0.06 | 0.02 | 0.13 | 0.01 |
| | **10451** | 0.00 | 0.01 | 0.00 | 0.03 | 0.00 | 0.29 | 0.01 | 0.51 | 8.95 | 0.15 | 0.10 | 2.59 | 30.29 | 0.01 | 56.81 | 0.10 | 0.10 | 0.01 | 0.05 | 0.00 |
| Etive | **10476** | 0.02 | 0.03 | 0.00 | 0.08 | 0.00 | 0.30 | 0.01 | 0.30 | 6.96 | 0.29 | 0.04 | 4.18 | 30.10 | 0.01 | 57.13 | 0.30 | 0.06 | 0.01 | 0.15 | 0.02 |
| | **10485** | 0.06 | 0.03 | 0.00 | 0.12 | 0.01 | 0.38 | 0.01 | 3.03 | 6.64 | 0.22 | 0.14 | 3.75 | 26.46 | 0.02 | 56.90 | 1.21 | 0.04 | 0.03 | 0.82 | 0.11 |
| | **10517** | 0.05 | 0.05 | 0.01 | 0.16 | 0.02 | 0.57 | 0.01 | 7.48 | 5.84 | 0.20 | 0.19 | 2.41 | 19.03 | 0.13 | 59.55 | 1.15 | 1.47 | 0.02 | 1.57 | 0.09 |
| | **10521** | 0.02 | 0.04 | 0.00 | 0.18 | 0.01 | 0.22 | 0.01 | 0.93 | 5.59 | 0.20 | 0.19 | 2.26 | 29.93 | 0.07 | 56.11 | 1.02 | 1.98 | 0.01 | 1.07 | 0.16 |
| | **10522** | 0.03 | 0.03 | 0.00 | 0.09 | 0.00 | 0.25 | 0.00 | 0.09 | 7.85 | 0.14 | 0.07 | 2.26 | 28.59 | 0.03 | 59.71 | 0.26 | 0.40 | 0.01 | 0.18 | 0.01 |
| | **10528** | 0.03 | 0.03 | 0.01 | 0.15 | 0.01 | 0.70 | 0.01 | 2.18 | 7.25 | 0.30 | 0.52 | 2.85 | 26.43 | 0.04 | 57.92 | 0.49 | 0.32 | 0.02 | 0.72 | 0.02 |
| | **10541** | 0.02 | 0.07 | 0.01 | 0.13 | 0.00 | 0.70 | 0.00 | 3.40 | 9.98 | 0.81 | 0.34 | 4.13 | 23.78 | 0.05 | 55.65 | 0.27 | 0.03 | 0.05 | 0.57 | 0.02 |
| Rannoch | **10561** | 0.11 | 2.80 | 0.08 | 1.44 | 0.01 | 1.71 | 0.00 | 10.29 | 11.56 | 5.06 | 0.32 | 6.43 | 15.90 | 0.05 | 41.15 | 0.71 | 0.86 | 0.09 | 1.39 | 0.08 |
| | **10566** | 0.05 | 1.38 | 0.04 | 0.97 | 0.02 | 1.56 | 0.00 | 7.00 | 9.69 | 4.35 | 0.13 | 5.98 | 19.47 | 0.02 | 47.00 | 0.48 | 0.59 | 0.06 | 1.18 | 0.03 |
| | **10597** | 0.16 | 3.18 | 0.23 | 1.68 | 0.04 | 2.04 | 0.00 | 12.22 | 12.67 | 6.66 | 0.28 | 6.00 | 12.29 | 0.30 | 37.74 | 0.50 | 2.32 | 0.10 | 1.58 | 0.01 |
| | **10614** | 0.05 | 0.82 | 0.05 | 0.47 | 0.00 | 0.75 | 0.00 | 0.63 | 8.45 | 3.34 | 0.07 | 5.07 | 33.86 | 0.05 | 45.28 | 0.26 | 0.50 | 0.03 | 0.31 | 0.01 |
| | **10619** | 0.07 | 1.72 | 0.09 | 0.97 | 0.02 | 1.88 | 0.00 | 7.90 | 10.65 | 3.57 | 0.19 | 6.39 | 18.99 | 0.07 | 45.46 | 0.38 | 0.54 | 0.11 | 1.00 | 0.01 |
| | **10628** | 0.07 | 1.27 | 0.07 | 0.87 | 0.01 | 1.60 | 0.00 | 7.08 | 9.75 | 4.04 | 0.24 | 5.97 | 19.41 | 0.35 | 47.36 | 0.36 | 0.61 | 0.09 | 0.83 | 0.01 |
| | **10638** | 0.13 | 2.11 | 0.18 | 1.45 | 0.02 | 1.81 | 0.00 | 10.18 | 11.51 | 4.27 | 0.40 | 7.11 | 15.70 | 0.32 | 41.57 | 0.38 | 1.63 | 0.12 | 1.10 | 0.01 |
| | **10649** | 0.10 | 0.97 | 0.15 | 0.85 | 0.02 | 1.57 | 0.00 | 6.82 | 10.96 | 3.56 | 0.27 | 6.62 | 20.19 | 0.26 | 45.17 | 0.33 | 1.15 | 0.10 | 0.93 | 0.01 |
| | **10655** | 0.10 | 1.78 | 0.23 | 1.42 | 0.03 | 2.09 | 0.00 | 8.76 | 11.86 | 3.65 | 0.38 | 7.91 | 16.39 | 0.36 | 42.15 | 0.30 | 1.48 | 0.10 | 1.01 | 0.00 |
| | **10673** | 0.13 | 1.82 | 0.19 | 1.46 | 0.02 | 2.47 | 0.00 | 9.65 | 12.37 | 5.21 | 0.33 | 8.52 | 11.59 | 0.21 | 43.59 | 0.41 | 1.03 | 0.13 | 0.88 | 0.00 |
| | **10675** | 0.13 | 1.84 | 0.29 | 1.38 | 0.02 | 2.30 | 0.00 | 9.88 | 12.36 | 5.13 | 0.30 | 8.41 | 11.99 | 0.25 | 43.05 | 0.39 | 1.27 | 0.15 | 0.87 | 0.00 |
| | **10677** | 0.17 | 3.74 | 0.36 | 2.76 | 0.05 | 2.29 | 0.00 | 16.24 | 13.27 | 5.65 | 0.56 | 8.16 | 8.23 | 0.25 | 34.72 | 0.44 | 1.56 | 0.14 | 1.42 | 0.00 |
| | **10681** | 0.11 | 1.67 | 0.17 | 1.27 | 0.02 | 2.19 | 0.00 | 8.87 | 12.49 | 4.86 | 0.27 | 8.67 | 13.14 | 0.07 | 43.92 | 0.38 | 0.96 | 0.16 | 0.79 | 0.01 |
| | **10682** | 0.14 | 2.64 | 0.43 | 1.87 | 0.04 | 2.22 | 0.00 | 12.28 | 12.44 | 4.95 | 0.32 | 8.04 | 11.75 | 0.11 | 40.08 | 0.42 | 0.94 | 0.12 | 1.20 | 0.01 |
| | **10694** | 0.19 | 2.92 | 0.45 | 2.13 | 0.04 | 2.00 | 0.00 | 12.38 | 11.96 | 4.83 | 0.41 | 7.49 | 12.09 | 0.06 | 39.76 | 0.38 | 1.19 | 0.15 | 1.57 | 0.01 |
| | **10705** | 0.10 | 1.70 | 0.37 | 1.33 | 0.03 | 1.48 | 0.00 | 5.45 | 10.50 | 4.11 | 0.21 | 7.26 | 26.56 | 0.08 | 39.15 | 0.31 | 0.50 | 0.07 | 0.79 | 0.00 |
| | **10712** | 0.23 | 2.94 | 0.47 | 2.39 | 0.03 | 1.66 | 0.00 | 8.87 | 12.04 | 4.83 | 0.20 | 7.30 | 22.30 | 0.10 | 33.23 | 0.37 | 1.74 | 0.08 | 1.22 | 0.00 |
| | **10754** | 0.13 | 1.56 | 0.21 | 1.44 | 0.01 | 2.87 | 0.00 | 7.90 | 8.93 | 3.14 | 0.27 | 9.37 | 15.48 | 0.03 | 45.98 | 0.32 | 0.40 | 0.18 | 1.78 | 0.01 |
| Tarbert | **Mininmum** | 0.03 | 0.10 | 0.01 | 0.49 | 0.01 | 0.34 | 0.01 | 0.43 | 8.62 | 0.16 | 0.19 | 2.80 | 21.72 | 0.05 | 39.89 | 0.49 | 0.00 | 0.01 | 0.36 | 0.03 |
| | **Maximum** | 0.09 | 1.40 | 0.08 | 1.14 | 0.01 | 1.42 | 0.05 | 7.22 | 14.20 | 2.32 | 0.77 | 7.34 | 33.26 | 1.01 | 58.00 | 1.74 | 1.52 | 0.08 | 0.90 | 0.24 |
| | **Average** | 0.07 | 0.80 | 0.05 | 0.78 | 0.01 | 0.93 | 0.03 | 3.37 | 11.67 | 1.45 | 0.36 | 5.56 | 26.07 | 0.43 | 46.10 | 0.87 | 0.70 | 0.04 | 0.61 | 0.09 |
| Ness | **Mininmum** | 0.00 | 0.01 | 0.00 | 0.02 | 0.00 | 0.29 | 0.00 | 0.25 | 3.65 | 0.06 | 0.06 | 1.24 | 17.52 | 0.01 | 39.86 | 0.08 | 0.01 | 0.01 | 0.05 | 0.00 |
| | **Maximum** | 0.23 | 0.56 | 3.52 | 0.65 | 0.01 | 2.42 | 0.04 | 6.63 | 10.09 | 1.96 | 0.49 | 6.72 | 31.27 | 0.31 | 65.27 | 1.30 | 17.85 | 0.08 | 1.85 | 0.13 |
| | **Average** | 0.07 | 0.17 | 0.38 | 0.25 | 0.00 | 0.84 | 0.01 | 1.99 | 7.16 | 0.76 | 0.25 | 3.99 | 25.92 | 0.07 | 54.69 | 0.42 | 2.25 | 0.03 | 0.73 | 0.03 |
| Etive | **Mininmum** | 0.02 | 0.03 | 0.00 | 0.08 | 0.00 | 0.22 | 0.00 | 0.09 | 5.59 | 0.14 | 0.04 | 2.26 | 19.03 | 0.01 | 55.65 | 0.26 | 0.03 | 0.01 | 0.15 | 0.01 |
| | **Maximum** | 0.06 | 0.07 | 0.01 | 0.18 | 0.02 | 0.70 | 0.01 | 7.48 | 9.98 | 0.81 | 0.52 | 4.18 | 30.10 | 0.13 | 59.71 | 1.21 | 1.98 | 0.05 | 1.57 | 0.16 |
| | **Average** | 0.03 | 0.04 | 0.00 | 0.13 | 0.01 | 0.45 | 0.01 | 2.49 | 7.16 | 0.31 | 0.21 | 3.12 | 26.33 | 0.05 | 57.57 | 0.67 | 0.62 | 0.02 | 0.73 | 0.06 |
| Rannoch | **Mininmum** | 0.05 | 0.82 | 0.04 | 0.47 | 0.00 | 0.75 | 0.00 | 0.63 | 8.45 | 3.14 | 0.07 | 5.07 | 8.23 | 0.02 | 33.23 | 0.26 | 0.40 | 0.03 | 0.31 | 0.00 |
| | **Maximum** | 0.23 | 3.74 | 0.47 | 2.76 | 0.05 | 2.87 | 0.00 | 16.24 | 13.27 | 6.66 | 0.56 | 9.37 | 33.86 | 0.36 | 47.36 | 0.71 | 2.32 | 0.18 | 1.78 | 0.08 |
| | **Average** | 0.12 | 2.05 | 0.23 | 1.45 | 0.02 | 1.92 | 0.00 | 9.02 | 11.30 | 4.51 | 0.29 | 7.26 | 16.96 | 0.16 | 42.02 | 0.40 | 1.07 | 0.11 | 1.10 | 0.01 |

Table 3. Pearson's Correlation Coefficient matrix calculated from the SEM-EDS mineral map and background data. For P=values <0.05[x], the correlation is statistically significant. P values of P<0.01[xx] and P<0.001[xxx] represent very and extremely significant correlations.

| | Apatite | Biotite | Calcite | Chlorite | Dolomite | Illite | Ilmenite | Kaolinite | K-Feldspar | Muscovite | Others | Plagioclase | Porosity | Pyrite | Quartz | Rutile | Siderite | Smectite | Unclassified | Zircon | Helium porosity (%) | Kh mD | Kv mD | Grainsize (µm) | Sorting (Trask-Tucker) |
|---|---|---|---|---|---|---|---|---|---|---|---|---|---|---|---|---|---|---|---|---|---|---|---|---|---|
| Biotite | 0.694 | | | | | | | | | | | | | | | | | | | | | | | | |
| | 0.000 | | | | | | | | | | | | | | | | | | | | | | | | |
| Calcite | 0.567 | 0.081 | | | | | | | | | | | | | | | | | | | | | | | |
| | 0.000 | 0.619 | | | | | | | | | | | | | | | | | | | | | | | |
| Chlorite | 0.776 | 0.967 | 0.162 | | | | | | | | | | | | | | | | | | | | | | |
| | 0.000 | 0.000 | 0.317 | | | | | | | | | | | | | | | | | | | | | | |
| Dolomite | 0.616 | 0.830 | 0.142 | 0.855 | | | | | | | | | | | | | | | | | | | | | |
| | 0.000 | 0.000 | 0.382 | 0.000 | | | | | | | | | | | | | | | | | | | | | |
| Illite | 0.773 | 0.760 | 0.284 | 0.798 | 0.588 | | | | | | | | | | | | | | | | | | | | |
| | 0.000 | 0.000 | 0.075 | 0.000 | 0.000 | | | | | | | | | | | | | | | | | | | | |
| Ilmenite | -0.100 | -0.343 | 0.180 | -0.248 | -0.234 | -0.319 | | | | | | | | | | | | | | | | | | | |
| | 0.537 | 0.030 | 0.266 | 0.123 | 0.146 | 0.045 | | | | | | | | | | | | | | | | | | | |
| Kaolinite | 0.670 | 0.900 | 0.089 | 0.888 | 0.816 | 0.832 | -0.370 | | | | | | | | | | | | | | | | | | |
| | 0.000 | 0.000 | 0.584 | 0.000 | 0.000 | 0.000 | 0.019 | | | | | | | | | | | | | | | | | | |
| K-Feldspar | 0.313 | 0.739 | -0.187 | 0.704 | 0.579 | 0.564 | -0.357 | 0.695 | | | | | | | | | | | | | | | | | |
| | 0.049 | 0.000 | 0.247 | 0.000 | 0.000 | 0.000 | 0.024 | 0.000 | | | | | | | | | | | | | | | | | |
| Muscovite | 0.691 | 0.932 | 0.144 | 0.897 | 0.740 | 0.829 | -0.377 | 0.869 | 0.703 | | | | | | | | | | | | | | | | |
| | 0.000 | 0.000 | 0.375 | 0.000 | 0.000 | 0.000 | 0.016 | 0.000 | 0.000 | | | | | | | | | | | | | | | | |
| Others | 0.260 | 0.290 | 0.148 | 0.336 | 0.281 | 0.408 | 0.246 | 0.401 | 0.312 | 0.218 | | | | | | | | | | | | | | | |
| | 0.105 | 0.070 | 0.362 | 0.034 | 0.079 | 0.009 | 0.126 | 0.010 | 0.050 | 0.176 | | | | | | | | | | | | | | | |
| Plagioclase | 0.698 | 0.759 | 0.153 | 0.807 | 0.561 | 0.862 | -0.249 | 0.743 | 0.623 | 0.816 | 0.247 | | | | | | | | | | | | | | |
| | 0.000 | 0.000 | 0.346 | 0.000 | 0.000 | 0.000 | 0.121 | 0.000 | 0.000 | 0.000 | 0.125 | | | | | | | | | | | | | | |
| Porosity | -0.647 | -0.749 | -0.201 | -0.759 | -0.675 | -0.873 | 0.273 | -0.922 | -0.552 | -0.766 | -0.494 | -0.672 | | | | | | | | | | | | | |
| | 0.000 | 0.000 | 0.213 | 0.000 | 0.000 | 0.000 | 0.088 | 0.000 | 0.000 | 0.000 | 0.001 | 0.000 | | | | | | | | | | | | | |
| Pyrite | -0.010 | 0.123 | -0.074 | 0.174 | 0.222 | 0.076 | 0.554 | 0.138 | 0.249 | 0.113 | 0.410 | 0.039 | -0.191 | | | | | | | | | | | | |
| | 0.953 | 0.451 | 0.651 | 0.282 | 0.169 | 0.642 | 0.000 | 0.397 | 0.121 | 0.488 | 0.009 | 0.812 | 0.238 | | | | | | | | | | | | |
| Quartz | -0.689 | -0.875 | -0.131 | -0.884 | -0.681 | -0.656 | 0.176 | -0.720 | -0.694 | -0.860 | -0.180 | -0.792 | 0.516 | -0.103 | | | | | | | | | | | |
| | 0.000 | 0.000 | 0.420 | 0.000 | 0.000 | 0.000 | 0.278 | 0.000 | 0.000 | 0.000 | 0.265 | 0.000 | 0.001 | 0.527 | | | | | | | | | | | |
| Rutile | 0.066 | -0.099 | 0.087 | -0.054 | 0.043 | -0.115 | 0.540 | 0.019 | -0.142 | -0.128 | 0.180 | -0.109 | 0.018 | 0.215 | 0.000 | | | | | | | | | | |
| | 0.686 | 0.545 | 0.592 | 0.741 | 0.791 | 0.480 | 0.000 | 0.905 | 0.384 | 0.430 | 0.268 | 0.502 | 0.911 | 0.182 | 0.999 | | | | | | | | | | |
| Siderite | 0.284 | 0.046 | 0.295 | 0.093 | -0.019 | -0.011 | 0.338 | -0.047 | -0.292 | 0.061 | -0.058 | -0.014 | 0.009 | -0.040 | -0.288 | 0.097 | | | | | | | | | |
| | 0.075 | 0.779 | 0.065 | 0.569 | 0.909 | 0.946 | 0.033 | 0.773 | 0.067 | 0.711 | 0.723 | 0.933 | 0.954 | 0.805 | 0.071 | 0.553 | | | | | | | | | |
| Smectite | 0.657 | 0.791 | 0.132 | 0.819 | 0.638 | 0.920 | -0.358 | 0.872 | 0.650 | 0.839 | 0.349 | 0.884 | -0.873 | 0.085 | -0.687 | -0.131 | -0.040 | | | | | | | | |
| | 0.000 | 0.000 | 0.416 | 0.000 | 0.000 | 0.000 | 0.024 | 0.000 | 0.000 | 0.000 | 0.027 | 0.000 | 0.000 | 0.601 | 0.000 | 0.419 | 0.808 | | | | | | | | |
| Unclassified | 0.547 | 0.523 | 0.132 | 0.545 | 0.519 | 0.596 | -0.074 | 0.659 | 0.183 | 0.486 | 0.408 | 0.381 | -0.654 | 0.139 | -0.424 | 0.249 | 0.213 | 0.544 | | | | | | | |
| | 0.000 | 0.001 | 0.416 | 0.000 | 0.001 | 0.000 | 0.652 | 0.000 | 0.259 | 0.001 | 0.009 | 0.015 | 0.000 | 0.392 | 0.006 | 0.121 | 0.186 | 0.000 | | | | | | | |
| Zircon | -0.162 | -0.275 | 0.047 | -0.247 | -0.162 | -0.322 | 0.610 | -0.216 | -0.264 | -0.316 | 0.162 | -0.292 | 0.232 | 0.177 | 0.151 | 0.925 | 0.117 | -0.320 | 0.093 | | | | | | |
| | 0.319 | 0.086 | 0.775 | 0.125 | 0.318 | 0.043 | 0.000 | 0.181 | 0.100 | 0.047 | 0.317 | 0.068 | 0.149 | 0.276 | 0.352 | 0.000 | 0.470 | 0.044 | 0.567 | | | | | | |
| Helium porosity | -0.505 | -0.496 | -0.293 | -0.552 | -0.434 | -0.526 | 0.253 | -0.442 | -0.334 | -0.549 | -0.055 | -0.569 | 0.411 | 0.124 | 0.488 | -0.041 | 0.023 | -0.582 | -0.317 | 0.005 | | | | | |
| | 0.001 | 0.001 | 0.067 | 0.000 | 0.005 | 0.000 | 0.115 | 0.004 | 0.035 | 0.000 | 0.738 | 0.000 | 0.008 | 0.447 | 0.001 | 0.801 | 0.889 | 0.000 | 0.046 | 0.975 | | | | | |
| Kh mD | -0.567 | -0.507 | -0.200 | -0.540 | -0.377 | -0.494 | 0.077 | -0.442 | -0.304 | -0.578 | 0.051 | -0.664 | 0.336 | -0.031 | 0.655 | -0.181 | -0.219 | -0.506 | -0.322 | -0.081 | 0.611 | | | | |
| | 0.000 | 0.001 | 0.217 | 0.000 | 0.016 | 0.001 | 0.636 | 0.004 | 0.056 | 0.000 | 0.753 | 0.000 | 0.034 | 0.852 | 0.000 | 0.263 | 0.174 | 0.001 | 0.043 | 0.620 | 0.000 | | | | |
| Kv mD | -0.514 | -0.446 | -0.181 | -0.493 | -0.373 | -0.410 | 0.015 | -0.361 | -0.266 | -0.518 | 0.079 | -0.600 | 0.235 | -0.005 | 0.611 | -0.160 | -0.197 | -0.429 | -0.112 | -0.025 | 0.482 | 0.840 | | | |
| | 0.001 | 0.006 | 0.282 | 0.002 | 0.023 | 0.012 | 0.931 | 0.028 | 0.112 | 0.001 | 0.643 | 0.000 | 0.161 | 0.975 | 0.000 | 0.343 | 0.242 | 0.008 | 0.511 | 0.885 | 0.002 | 0.000 | | | |
| Grain size (µm) | -0.728 | -0.716 | -0.367 | -0.773 | -0.535 | -0.709 | -0.017 | -0.609 | -0.517 | -0.777 | -0.192 | -0.847 | 0.510 | -0.188 | 0.888 | -0.015 | -0.331 | -0.716 | -0.362 | 0.126 | 0.530 | 0.721 | 0.705 | | |
| | 0.000 | 0.000 | 0.020 | 0.000 | 0.000 | 0.000 | 0.918 | 0.000 | 0.001 | 0.000 | 0.236 | 0.000 | 0.001 | 0.246 | 0.000 | 0.927 | 0.037 | 0.000 | 0.022 | 0.437 | 0.000 | 0.000 | 0.000 | | |
| Sorting (Trask-T | -0.126 | -0.255 | -0.355 | -0.218 | -0.175 | -0.180 | 0.100 | -0.257 | -0.176 | -0.305 | -0.102 | -0.217 | 0.254 | 0.079 | 0.293 | 0.113 | -0.267 | -0.290 | 0.054 | 0.082 | 0.189 | 0.095 | 0.050 | 0.367 | |
| | 0.439 | 0.113 | 0.024 | 0.177 | 0.281 | 0.268 | 0.537 | 0.109 | 0.276 | 0.056 | 0.531 | 0.179 | 0.114 | 0.630 | 0.067 | 0.488 | 0.095 | 0.070 | 0.742 | 0.614 | 0.242 | 0.559 | 0.769 | 0.020 | |

| Key | |
|---|---|
| | P=> 0.05 — Not significant |
| | P=< 0.05 — Statistically significant |
| | P=< 0.01 — Very significant correlation |
| | P=< 0.001 — Extremely significant correlation |